Title
Interface Properties of Functional Molecules on Au{111}: From Photoinduced Charge Transfer to Exchange Reactions

Author
Zhao, Yuxi

Publication Date
2014

UNIVERSITY OF CALIFORNIA

Los Angeles

Interface Properties of Functional Molecules on Au{111}: From Photoinduced Charge Transfer to Exchange Reactions

A dissertation submitted in partial satisfaction of the

requirements for the degree Doctor of Philosophy

in Chemistry

by

Yuxi Zhao

2014

2014

ABSTRACT OF THE DISSERTATION

Interface Properties of Functional Molecules on Au{111}:

From Photoinduced Charge Transfer to Exchange Reactions

by

Yuxi Zhao

Doctor of Philosophy in Chemistry

University of California, Los Angeles, 2014

Professor Paul S. Weiss, Chair

Understanding electron transfer at the molecular level is crucial for the rational design and performance improvement of organic optoelectronics and photovoltaics. Scanning tunneling microscope (STM) enables measurement of electronic properties with atomic precision. Here, we introduce a custom-built**,** laser-assisted STM that integrates optical excitation into the tunneling junction. The evanescent field generated by rear-incident laser light excites surface adsorbates on gold films, enabling the detection of optically induced changes in tunneling current under ambient conditions. Thin and atomically flat Au films epitaxially grown on *c*-cut sapphire prisms provide both efficient optical coupling and long-term stability to monitor optical activities of molecular donor-acceptor heterojunctions isolated in two-dimensional matrices on the surface. Our method offers a versatile platform to elucidate the involvement of individual states that affect charge generation and separation in a C_{60}-tethered 2,5-dithienylpyrrole triad, a molecular donor-acceptor heterojunction, and to correlate the particular molecular orientations and local environment with the measured photocurrent of the anthracene-terminated aromatic thiolates in the tunneling junction.

When alkanethiolate self-assembled monolayers on Au{111} are exchanged with alkaneselenols from solution, replacement of thiolates by selenols is rapid and complete, and is well described by perimeter-dependent island growth kinetics. The monolayer structures change as selenolate coverage increases, from being epitaxial and consistent with the initial thiolate structure to being characteristic of selenolate monolayer structures. At room temperature and at positive sample bias in scanning tunneling microscopy, the selenolate-gold attachment is labile, and molecules exchange positions with neighboring thiolates. The scanning tunneling microscope probe can be used to induce these place-exchange reactions.

This dissertation of Yuxi Zhao is approved.

James K. Gimzewski

Chi On Chui

Paul S. Weiss, Committee Chair

University of California, Los Angeles

2014

To my family

Table of Contents

CHAPTER 1
From the Bottom Up: Dimensional Control and Characterization in Molecular Monolayers

CHAPTER 2 Detection of Single-Molecule Optical Absorption with Ångström-Scale Precision: Chemical Specificity Revealed in Scanning Tunneling Microscopy

CHAPTER 3 Location-Controlled Incorporation of C60-Donor-C60 Triad and Donor Derivative Molecules in the Same Matrix – Towards Molecular p-n Junctions Studies

CHAPTER 4 Exchange Reactions between Alkanethiolates and Alkaneselenols on Au{111}

CHAPTER 5 Summary and Outlook

List of Figures

List of Abbreviations and Symbols

0D	zero-dimensional
1ATC9	3-mercapto-N-nonylpropionamide
2ATC9	3-mercapto-N-(N'-n-hexylacetamido) propionamide
2D	two-dimensional
5-HTP	5-hydroxytryptophan
C10	1-decanethiolate
C12	*n*-dodecanethiolate
C12Se	1-dodecaneselonolate
D12	perdeuterated dodecanethiolate
D-A	donor-acceptor
DTP	2,5-dithienylpyrrole derivative
FTIR	Fourier transform infrared spectroscopy
FWHM	full-width-half-maximum
HJ	heterojunction
HOMO	highest occupied molecular orbital
HOPG	highly oriented pyrolytic graphite
IETS	inelastic electron tunneling spectroscopy
IRRAS	infrared reflectance absorption spectroscopy
JMAK	Johnson, Mehl, Avrami, and Kolmogorov model
LEED	low-energy electron diffraction
LIA	lock-in amplifier

LUMO	lowest unoccupied molecular orbital
MPEA	9-(4-mercapto-phenylethynyl)anthracene
NEXAFS	near-edge X-ray absorption fine structure
OPE	oligo(phenylene ethynylene)
SAM	self-assembled monolayer
STM	scanning tunneling microscope
TEM	transmission electron microscopy
TTF	tetrathiafulvalene
XPS	X-ray photoelectron spectroscopy
λ	wavelength of incident light
A	absorbance of the chromophore
Å	Ångström
c	light velocity in vacuum
e	elementary charge
eV	electronvolt
h	Planck’s constant
h	hour
i	photocurrent
I	flux of photons per unit area and unit time
min	minute
mm	millimeter
mM	millimolar
mW	milliwatt

pA	picoampere
s	second
t	time
V	volt
W	light input power
κ	rate constant
φ	quantum efficiency

Acknowledgments

This dissertation is a milestone of my life and represents the majority of the research I have done in graduate school. Throughout these years, many amazing individuals have helped me in different ways. I will use this opportunity to express my gratitude to these professors, colleagues, friends and my family.

I am very lucky to be Prof. Paul Weiss's first graduate student after he moved to UCLA. Without his guidance and support, none of the work in this dissertation could have been accomplished. Paul is an extraordinary and charming advisor who has decades of experience in a wide range of research fields to offer, and a shrewd and resourceful mind to lead. He does not only help me identify important scientific problems and search for solutions, but also emphasizes the importance of exploiting the potential impact of my work and presenting it in a compelling and convincing manner. Not every researcher gets the chance to be trained towards a master of good communication, whose prudence in seemingly-trivial details makes him or her a trustworthy scientist. As an apprentice in research, I am from time to time distracted from the prime goal of the project, but Paul is always there directing me back to the main track and helping me see the bigger picture. I will benefit from Paul's advice for my career and personal development for a lifetime.

I am thankful to my thesis committee and collaborators who have guided me through all these years. Profs. James Gimzewski, Richard Kaner, and Chi On Chui, as my major advisors, offered invaluably constructive advice from different perspectives during my qualification exam and fourth year meeting. It was a pleasure collaborating with Profs. Ken Houk, Dan Neuhauser, Alex Jen and other groups. Their generous offers of expertise in theory computation, and organic synthesis are crucial for the progress I made in my graduate work. All the people from these labs I encountered inspired me to look at the scientific problems I deal with from diverse angles. Besides, I want to express my warm thanks to Profs. Louis Bouchard, Yung-Ya Lin, and Ren Sun for their precious academia and life advice.

The experts from various facilities have helped and taught me immensely: Dr. Adam Stieg (Nano & Pico Characterization Lab), Dr. Ivo Atanasov (Electron Imaging Center for NanoMachines), Hoc Ngo (Nanoelectronics Research Facility) and Shylo Stiteler (Student Machine Shop) introduced me to all the fascinating tools that have bolstered the advancement of my projects. They never hesitate to share the tips they learned through years of experience with me.

I also want to thank all the group members I have met in this five-year's of study: Dr. Nate Hohman, Dr. Bala Pathem, Dr. Shelley Claridge, Dr. Sarawut Cheunkar, Dr. Wei-ssu Liao, Dr. Amit Vaish, Huan Cao, Dr. Jay Kim, Dr. Liane Slaughter, Natcha Wattanatorn, Alex Mendoza, Andrew Guttentag, Andrew Serino, John Thomas, Nako Nakatsuka, John Abendroth, Garett Wadsworth, Harsharn Auluck, David McMillan, and everyone else for sharing their truthful and illuminating views on issues related with my projects and generous support in me.

There are two people I especially want to thank. First is my mentor, Dr. Moonhee Kim. She may not have taught me each experiment step by step, but I learned a lot of wisdom on research from her. While she was under great pressure for graduation, she managed to find time to have meetings with me every week and to revise my weekly research report. After she left the group, I still benefited tremendously by reading her well-organized lab notes. From her, I realized that maybe there is always a glass ceiling for female scientists, but we should still be ambitious and fight for what we deserve. The other person that I want to acknowledge is Jeffrey Schwartz. He was a true friend ever since we shared an office on the 6th floor of CNSI in 2009. I cannot remember how much time he has devoted to teaching me, from skills as trivial as soldering, to knowledge as complex as the working mechanism of the electronic components and each board in a scanning tunneling microscope. We had countless enlightening discussions on research among other interesting topics. As a smart physicist, he has a solid grasp of physical concepts and is able to apply the principles he learned to everyday life and research. Everyone in the lab, including me, has benefited from his vivid and accurate explanations of science. Because of him, I started to appreciate the beauty of the thinking process of physicists rationally breaking down problems.

I gratefully acknowledge the funding sources that made my graduate work possible. My research was funded by U.S. Department of Energy (DE-SC0005161), as well as the Chinese Scholarship Council. In my fourth year, I was honored to receive the DoPont Graduate Research Fellowship.

Additionally, I have so many friends who make me feel at home since the first day at UCLA. I want to thank them all, from the friends I met through CSST program, in graduate school to those dating back to my pre-UCLA days: college roommates and classmates, and high school all the way to elementary school friends. Their love and support transcends the geographic barrier between us.

I will end by acknowledging my family. I have a wonderful and happy family where everyone is tightly bound. The road of pursuing a doctorate degree is filled with smiles, sweat and tears. My parents are always there for me with their unconditional love. I will thank them in Chinese:

亲爱的爸爸妈妈，感谢你们支持我出国闯荡，即便你们是那样舍不得女儿渐行渐远，却依旧鼓励我去越飞越高。异国他乡的独立生活让我越发珍惜你们无微不至的细腻关怀。有了大洋彼岸那个温馨和睦的港湾，我才得以在此安心奋斗。读研的意义不仅仅是攀登科学的高峰，是你们的人生智慧教会了我用长远的眼光规划人生，用宽容的心善待他人，用健康积极的心态面对生活中的取舍与喜怒哀乐。女儿深知你们培养我去胜任每一个社会角色的良苦用心。谨以此文感恩你们对我无私的挚爱！

VITA

Yuxi attended Fudan University in Shanghai from 2005 to 2009, and earned her Bachelor of Science degree in macromolecular science. While pursuing this degree, she worked with Prof. Daoyong Chen to engineer multistimuli-responsive nanoparticles using block co-polymer self-assembled micelles. While at Fudan University, Yuxi was the recipient of the National People's Scholarship, 1st rank, in 2007 and 2008 for outstanding academic performance. In 2008, as part of a summer research program with an Executive Vice Chancellor Scholarship, she joined Prof. Sarah Tolbert's lab in Department of Chemistry and Biochemistry at UCLA to conduct research on inorganic/organic hybrid solar cells. After graduating with honors from Fudan University, Yuxi entered the chemistry Ph.D. program at UCLA in the fall of 2009. In recognition of her academic achievements, she received DuPont Graduate Fellowship in 2014.

List of Publications and Presentations

Zhao, Y. X.; Weiss, P. S. “Single-molecule optical spectroscopy with Ångström-scale precision.” Poster presentation at the Center for Chemistry at the Space-Time Limit (CaSTL) Conference, Irvine, California (2014, July) and Seaborg Symposium, UCLA (2013, November)

Hohman, J. N.; Thomas, J. C.; Zhao, Y. X.; Auluck, H.; Kim, M.; Vijselaar, W.; Kommeren, S.; Terfort, A.; Weiss, P. S. “Exchange reactions between alkanethiolates and alkaneselenols on Au{111}.” *J. Am. Chem. Soc.* 2014, 136, 8110-8121.

Pathem, B. K.; Zheng, Y. B.; Morton, S.; Petersen, M. A.; Zhao, Y. X.; Chung, C. H.; Yang, Y.; Jensen, L.; Nielsen, M. B.; Weiss, P. S. “Photoreaction of matrix-isolated dihydroazulene-functionalized molecules on Au{111}.” *Nano Lett.* 2013, 13, 337-343.

Claridge, S. A.; Liao, W. S.; Thomas, J. C.; Zhao, Y. X.; Cao, H. H.; Cheunkar, S.; Serino, A. C.; Andrews, A. M.; Weiss, P. S. “From the bottom up: dimensional control and characterization in molecular monolayers.” *Chem. Soc. Rev.* 2013, 42, 2725-2745.

Zheng, Y. B.; Payton, J. L.; Song, T. B.; Pathem, B. K.; Zhao, Y. X.; Ma, H.; Yang, Y.; Jensen, L.; Jen, A. K. Y.; Weiss, P. S. “Surface-enhanced raman spectroscopy to probe photoreaction pathways and kinetics of isolated reactants on surfaces: flat versus curved substrates.” *Nano Lett.* 2012, 12, 5362-5368.

Zhao, Y. X; Tolbert, S. H. (2008, September) “Nanostructured hybrid inorganic/organic photovoltaics.” Oral presentation at Cross-disciplinary Scholars in Science and Technology Summer Research Program, Final Meeting, UCLA

CHAPTER 1

From the Bottom Up: Dimensional Control and Characterization in Molecular Monolayers

1.1 Introduction

The unique chemistry of nanostructured materials involves balance between the lattice and bonding structures of the materials, the chemistries of their interfaces, the dimensionalities of their structures, and the types and distributions of defects (Figure 1.1). In comparison with other nanoscale materials, the chemistries and structures of self-assembled monolayers (SAMs) are largely determined by their interfaces, which account for a relatively high proportion of the atoms (typical monolayer thickness ranges from 1–3 nm),[1] and also frequently dominate the energetics of structure formation. For instance, in the most common synthetic SAMs, alkanethiols on gold, the enthalpy of the gold-sulfur bond formation (~50 kcal mol^{-1})[2] is several times larger than the combined interactions of the alkyl tails with surrounding molecules (1-2 kcal $mol\cdot CH_2^{-1}$).[3] Importantly, if the enthalpy of assembly at one interface provides a strong driving force for monolayer formation, it is possible to tune many other materials properties and still achieve ordered lattices.

Monolayer structures optimize both interactions with the substrate and intermolecular interactions.[1,4-6] Lattice structures in monolayers are determined by both the substrate lattice and the chemistries and structures of the molecules forming the monolayers. In alkanethiol monolayers, linear molecules are attached to gold surfaces *via* Au-S bonds; both the organization of the sulfur headgroups on the gold lattice and the packing of the alkyl tails influence molecular lattice formation.[6] For other molecules, such as adamantanethiols and carboranethiols, the tails are bulkier than the headgroups, and can play larger roles in lattice formation. In still other monolayers, such as those formed based on noncovalent interactions with graphite, molecules lie down, maximizing their interactions with the substrate.[4]

Although monolayers are typically considered to be two-dimensional (2D) structures, it is equally possible to assemble zero-dimensional (0D) molecular structures on surfaces. As with nanocrystals, the definitions of dimensionality arise from the physical properties of interest in the structure – that is, anisotropic molecules that assemble across a 2D surface. Similarly, individual functional molecules deposited on surfaces can act as 0D structures, with properties that can be controlled and measured individually.[7,8]

Defects are important in understanding and predicting the behavior of monolayers.[9] Since monolayers are often tightly coupled to solid substrates, irregularities in the substrate lattices (such as atomic step edges) can create offsets in the monolayers.[5] Defects can also arise from the molecular lattices. For instance, many classes of molecules tilt relative to the surface normal,[5] creating areas of heterogeneous structure between domains of molecules oriented in different azimuthal directions. Still other defects can be created as monolayers are formed. When alkanethiols are assembled on gold from solution, thiols can extract gold atoms from the surface, resulting in one-atom-deep 'etch pits' in the Au{111} substrate surface that disrupt monolayer structures.[5] These and other defects can be selectively removed by subsequent monolayer and substrate dynamics and processing.[10]

Importantly, as with other nanostructured materials, defects are often the most reactive sites in the materials, and dominate both access of additional molecules to the substrates and the dynamics of the systems. In the context of monolayers, this reactivity can be exploited to design 0D structures within 2D monolayers, or to nucleate processes such as molecular exchange.[11-16]

Characterization of lattice structures and defects in SAMs and related structures relies on surface-sensitive tools that provide chemical, electronic, and/or topographic information.[9,17] Typical analytical techniques providing chemical information about surfaces and adsorbates include grazing angle Fourier transform infrared (FTIR) spectroscopy, Raman spectroscopy, electron diffraction (transmission electron microscopy, TEM, and low energy electron diffraction, LEED), near-edge X-ray absorption fine structure (NEXAFS), and neutron scattering.[1] Scanning probe techniques – atomic force microscopy and scanning tunneling microscopy[17] – provide more localized information, down to the single-molecule scale.

In this chapter, we discuss the physical properties and applications of SAMs as nanostructured materials, with a focus on assembled structures ranging from 2D (full monolayers) down to 0D (single molecules), including methods for top-down patterning of monolayer structures. Throughout, we select examples highlighting the breadth of molecular functions available through these materials, and specialized characterization techniques and methods that enable quantitative measurements of these properties down to the single-molecule scale.

1.2 Two-Dimensional Structure and Function

Studies of 2D monolayers on solid surfaces began as early as the 1940s,[18] and now encompass systems ranging from alkanes and aromatic molecules to much larger macromolecules, and substrates from glass to single-crystalline metal surfaces. [1,4,19-21] Self-assembled monolayer structure is influenced by the substrate lattice, the interface between the molecular head group functionality and the substrate, the molecular lattice formed based on head group and backbone chemistries, and the exposed interface dominated by the chemical functionality of the tail group (Figure 1.2). Monolayers of alkanethiols on

Au{111} are the most common and most studied;[1] thus, we discuss many aspects of monolayer formation and structure in relation to these systems. The strategies developed for controlling monolayers of thiols on Au{111} will, over time, be translated to other molecule–substrate systems.[6,22]

1.2.1 Substrate Lattices

Monolayers have been formed on metals including Au,[1,9,23] Ag,[23-25] Cu,[23,26,27] Pd,[26,28] Pt,[29,30] Ni,[26,31] Fe,[26] Ti,[32] Te,[33] Hg,[34] and GaIn.[35,36] Since bonding with the substrate is often a critical driving force for monolayer formation, the substrate atomic lattice and electronic structure are key. The Au{111} crystal face is often used in monolayer formation for a number of reasons – gold readily forms bonds with thiols, and such surfaces are easily prepared, commercially available, and stable under normal atmospheric conditions. Other metal surfaces (such as Ag, Cu, Pt, and Pd) are more easily oxidized; these substrates are often used in studies of monolayers in vacuum, in which molecules are evaporated onto the surface rather than deposited from solution.

Semiconductors such as Si, Ge, GaAs, and InP can also be used as substrates for monolayer formation.[37-42] Silicon is particularly widely used due to its electronic applications; however, silicon forms a native oxide under normal atmospheric conditions. Thus, chemistry has developed to interface with both silicon and its oxide.[43-45] Other semiconductors have also been explored as monolayer substrates, including GaN[46] and ZnSe.[47]

Highly oriented pyrolytic graphite (HOPG) is a semimetal and forms atomically flat surfaces over relatively large areas (>1 μm^2). Although the surface does not readily form covalent bonds to common functional groups such as thiols or amines, it can be used as a substrate for monolayers in which aromatic groups in the monolayers form π-stacking interactions with graphite (or graphene) surfaces.[4,48-51]

1.2.2 Substrate–Head-Group Interfaces

The substrate–molecule interface both influences monolayer structures and serves as the electronic connection to the substrate. Thus, understanding these interfaces is important in predicting structures, stabilities, and physical properties (such as conductance) of SAMs, as well as of molecules matrix isolated within them.

Although there are many possible pairings of substrate and molecular head group chemistries, the substrate–molecule interface is more complex than would be predicted based solely on bonding between substrates and the functional head groups. The substrate lattice presents multiple chemically non-equivalent binding sites, involving one or more atoms. Further, substrate surfaces often reconstruct to minimize energy; these changes create lower symmetry surface structures that also influence the interfaces. Binding of the functional head group can lead to additional surface structural changes, and restrictions on orbital hybridization can influence the angle between molecular backbones and surfaces.

Surface reconstruction is widely observed for metal and semiconductor surfaces.[52,53] Here, we briefly discuss the relationship between surface reconstruction and alkanethiol SAM formation on Au{111} as an illustrative example of the complexities of these rearrangements.

Substrate atoms on bare Au{111} surfaces compact slightly, forming a reconstruction with both face-centered-cubic- and hexagonally close-packed-stacked zones and a (22 × √3) unit cell relative to the Au{111} lattice, referred to as the herringbone reconstruction. When sulfur-containing molecules (including thiols, disulfides, and thioethers) bind to Au{111}, the formation of Au–S bonds removes the reconstruction, a phenomenon that is possible to visualize by STM. The nominal strength of Au–S bonds (~50 kcal mol^{-1}) is greater than that of Au–Au bonds,[24,54] and the ability to remove the reconstruction can be used as a qualitative descriptor of molecule–substrate bond strengths. For instance, thioethers have weaker molecule–substrate bonds than thiols; however, SAMs of thioethers nonetheless lift the Au{111} herringbone reconstruction.[55-58] In contrast, adsorbed benzene does not lift the native Au{111} reconstruction.[59]

The growing consensus is that thiols lift selected atoms to sit at a subset of sites on the restored Au{111} lattice; these are referred to as Au adatoms.[60] It has been known for some time that thiolates move as a Au-thiolate complex at defect sites such as step edges.[61] Recent calculations show that there are multiple stable surface reconstructions (similar to within 0.2 eV): one sulfur bound to a three-fold hollow site, one sulfur bound to a bridge site, one sulfur bound to one Au adatom, and two sulfur atoms bound to one Au adatom.[62-67] Thiols on Ag{111} exhibit different binding properties than those on Au{111},[68] typically binding at bridge and three-fold hollow sites, and are tilted at angles closer to the surface normal.[25] Selenols on Au{111} have more promiscuous binding, and as a result Moiré patterns are observed in STM images.[69]

The multiplicity of possible binding structures highlights the importance of techniques for characterizing the buried interfaces. Some chemical properties can be characterized at large (micron to millimeter) scales using techniques such as FTIR spectroscopy and X-ray photoelectron spectroscopy (XPS), or at intermediate scales by measuring reductive desorption electrochemically.[16] Characterization at the sub-nanometer scale with STM-based techniques provides complementary information about heterogeneous structure important for understanding reconstructions. Weiss and coworkers found that the largest buried dipole in a SAM can be mapped by varying the tunneling gap distance in STM imaging. For alkanethiols on Au{111}, this locates the Au–S bond; thus, correlating buried dipoles (head groups) with topography (tail groups) enabled the first single-molecule tilt angle measurements.[70] A similar spectroscopy technique applied to cyclohexanethiol on Au{111} distinguishes between binding at bridge and atop sites.[2,20,23]

In addition to the molecules with head groups based on sulfur, discussed above,[1,21,24] many other head groups are available, including isocyanides,[71] Si,[72-74] P,[46,75-77] Se,[25,50,78,79] carboxylic acids,[80,81] and head groups that allow noncovalent π-stacking interactions on highly oriented graphite, such as cyclodextrins,[82-85] pentacene,[86] and peptides.[87-89] While these surface connectors are less explored, comparisons between molecule–substrate systems provide insight into how to translate surface attachment and patterning strategies from one system to another, and will ultimately lead to the identification of new strategies.

Selenols provide a useful comparison with thiols since they come from the same group in the periodic table.[79,90-92] In contrast to the hexagonal lattices formed by alkanethiols, alkaneselenols form either densely packed distorted hexagonal lattices incommensurate with the underlying Au{111} substrate, or commensurate linear missing-row structures.[69] These differences in bonding likely contribute to the differences in conductance observed between alkaneselenol and alkanethiol SAMs.[93] Short (n = 2-6) *n*-alkaneselenols follow the odd/even rule for stability (even chain lengths are more stable), as do alkanethiols. However, selenols are more stable toward exchange than alkanethiols of equivalent length,[94] which has been attributed to differences in bonding configurations (sp^3 and sp).[25] Polyfunctional head groups increase binding strength; for instance, diselenides and dithiols displace monothiolate monolayers on Au, similar to chelating effects found for other molecules.[90]

Silanes and silanols are typically used to form monolayers on silica (SiO_2) surfaces.[21,95,96] Head groups based on phosphorus (including phosphonates, phosphines, and phosphonic acids) are also common. Phosphorus headgroup binding to metals, such as Au, is generally weaker than thiol binding, but strong enough (in the case of trimethylphosphine) to lift the Au reconstruction.[75] Phosphonic acids form stable monolayers on Ti and Au substrates,[32] and phosphonates and alkylphosphonic acids assemble on GaN and nitinol (NiTi), respectively.[46,97] Alkylphosphonates assemble on Al_2O_3, TiO_2, ZrO_2, planar mica, TiO_2, and SiO_2;[76] however, monolayer structures are typically found to be less regular, and largely based on backbone and tailgroup interactions.

Monolayers can also form based on noncovalent interactions with substrates. Noncovalently bound molecular monolayers have been studied by STM, in many cases at low temperature, to stabilize the self-assembled structures sufficiently for imaging.[98,99] Many conjugated molecules can form 2D assemblies on surfaces, including styrene,[98] pentacene,[86] pyrene,[21] and larger graphitic molecules.[100,101]

1.2.3 Molecular Lattices

Molecular lattice structures are influenced by both molecule–substrate interfaces and the packing of the molecular backbones. The relative influence of these contributions can vary due to factors including interfacial bond strengths and sizes of the molecular backbones. Molecular interactions within lattices include van der Waals, dipole–dipole, and hydrogenbonding interactions. van der Waals interactions between molecules in lattices contribute to stability. In alkanethiol–Au SAMs, this contribution increases with alkyl chain length, as each methylene (–CH_2–) unit contributes approximately 1 kcal mol^{-1}.[26] Alkanethiolates on Au{111} tilt roughly 30° relative to the surface normal, to maintain nominally all-*trans* configurations that maximize van der Waals interactions.[21,70] As chain lengths increase in alkanethiols, the range of accessible backbone tilt angles is constrained due to steric effects.[102] Monolayers on other substrates have different tilt angles, again determined by the substrate lattice and maximizing intermolecular interactions. [5,103]

Chemical functional groups incorporated into the molecular backbone can influence molecular lattice structures. For instance, 3-mercapto-N-nonylpropionamide (**1ATC9**) is chemically similar to the more commonly used decanethiol, with an amide functional group replacing a methylene unit near the thiol headgroup. Two phases have been observed, one normal to the surface, the other tilted[104] relative to the surface normal.[105] The amide groups enable hydrogen bonding between molecules in the monolayer in the tilted conformation, increasing intermolecular interaction strength by ~6 kcal mol^{-1}, and increasing the electronic polarizability of the monolayer.[87,105,106] Such interactions can cause phase segregation, creating monolayers with two distinct types of domains: **1ATC9** monolayers phase separate from *n*-alkanethiols of equivalent length based on their hydrogen-bonding networks.[107] Amide-bonding networks in SAMs have also been used for charge transport across Ag/SAM//Ga_2O_3/EGaIn (Eutectic Gallium–Indium) junctions.[108]

Even functional groups that introduce relatively strong interactions such as hydrogen bonding can disrupt monolayer formation if they interfere with molecular packing. The di-amide and tri-amide counterparts of the system described above, 3-mercapto-N-(N'-*n*-hexylacetamido) propionamide (**2ATC9**) and 3-mercapto-N-(N'-(N''-*n*-propylacetamido) acetamido) propionamide, do not form ordered monolayers, at least in the terminal zone of the alkyl layers measured with STM.[107,109]

Other chemical functional groups can be added within the molecular backbones to impact monolayer formation, including alkenes, alkynes, diacetylene, aryl groups, oligo(phenylene ethynylene), oligo(ethylene glycol), sulfones, and azobenzenes.[11,21,110-112] Functional groups can be used to create a wide variety of properties in monolayers, including switchable conductivity,[15] targeted capture of biological molecules,[113] or the ability to crosslink under an electron beam[114] or restructure under an ion beam[115] to act as a molecular resist.

Cage molecules such as adamantanes and carboranes are classes of SAM substituents in which the cage serves as a short, sterically bulky backbone.[6,78,116,117] Thiolated cage molecules thus have large molecular lattice constants relative to alkanethiols (~0.7 nm *vs.* 0.5 nm), and weaker intermolecular interactions,[118] meaning they are easily displaced from Au{111} surfaces by alkanethiols. [6,117] Adamantane cages can be engineered to orient normal or tilted relative to the surface, by thiolating at either a primary (2-adamantanethiol) or tertiary (1-adamantanethiol) carbon, making it possible to create or to eliminate tilt defects based on small changes in molecular structure.[117] Larger diamondoid structures also form monolayers with a variety of interesting structures and properties.[6,119,120]

As with alkanethiols, carboranethiols have been designed to have molecular dipoles that contribute to molecular lattice interactions;[6,121] carboranethiols with strong lateral dipole-dipole interactions dominate surface coverage when codeposited with carboranethiols that lack such interactions.[121] Dipole effects can also be important in noncovalently bound monolayers. For instance, styrene, under vacuum and low temperature, forms dipole-organized assemblies on Au{111}.[98]

1.2.4 Molecule–Environment Interfaces

Terminal functional groups determine the physical properties at environmental interfaces. Terminal group chemistries can vary widely, including methyl groups, amines, nitriles, carboxylic acids, sulfides, alcohols, ferrocenes, pyrroles, fullerenes, and biomolecules.[1,113,122-131]

Interface physical properties can be changed dramatically based on relatively straightforward chemical changes to terminal groups. The conventionally used methyl terminal group for alkanethiolates produces hydrophobic SAMs, whereas hydroxyl terminated alkanethiols assemble into hydrophilic SAMs, even though the bulk of the backbone is hydrophobic. Similarly, SAMs can present large numbers of aligned dipoles at the interface, which can be reversed based on terminal substituents, for instance electron-rich amines vs. electron-poor nitriles.[124]

Specialized terminal groups create additional possibilities for monolayer function. Azobenzene terminal groups isomerize on exposure to UV (365 nm) and blue (450 nm) light, respectively.[11,110,132] Pyrrole-terminated SAMs polymerize upon plasma exposure, forming conductive and mechanically active polymers.[128] Hydroxyl-terminated SAMs have also been used to immobilize Au nanoparticles on surfaces.[133]

Simple functional groups displayed at SAM-environment interfaces can be used for further reactions to display more complex molecules on surfaces. Common functional groups incorporated into SAMs for reactions to create biological interfaces include carboxylic acids, amines, and azides.[113,134-139] Care is needed in further functionalization of SAMs as the reaction exothermicity of vigorous surface reactions can disrupt the assemblies and nanostructures previously formed.[10,136,140,141]

Carboxylic acids can be used in standard synthetic reactions (such as *N*-hydroxy-succinimide-ethylenediaminecarbodiimide, NHS-EDC, coupling) to create amide linkages – such reactions have been used to attach benzenesulfonamide ligands for enzymes,[142] as well as for attachment of small-molecule neurotransmitters, their precursors, proteins, and other molecules.[113,130,131] Interactions with large molecules such as receptor proteins are in some cases more specific when ligands are distributed several nanometers apart on the surface; this is discussed further in the section below on 0D assemblies. Amines, similarly, can be used for coupling reactions, which have been used to display functional groups including nitrophenyl phosphonates[76,97] and neurotransmitters[143] on surfaces, to interact with molecules in solution.

Azides displayed on surfaces can be used for a copper(I)-catalyzed azide–alkyne cycloaddition known as the ‘click’ reaction due to its high reaction efficiency.[144] This approach has been used, for instance, to attach peptides to surfaces to study cell adhesion.[145,146] This reaction has also been carried out using a copper atomic force microscope tip to create localized molecular patterns.[147]

1.3 Zero-Dimensional Assemblies

Zero-dimensional molecular features consisting of individual molecules or small molecular clusters have been studied for their electronic, mechanical, magnetic, optical, biological, and chemical properties.[17] Studies at this level illuminate unique properties that otherwise are lost through averaging in ensemble measurements. Here, we select illustrative examples, classified based on molecular function (Figure 1.3).

Single-molecule electronic properties in particular have been extensively investigated with the goal of producing single-molecule devices performing the functions of macroscale circuit components.[148,149] Such studies began in 1974 with a theoretical proposal of a molecular rectifier by Aviram and Ratner,[150] and now encompass both theoretical and experimental work on molecular resistors, rectifiers, electronic and photochromic switches, and other devices.[151-153]

Just as decreasing the size of macro- and microscale circuit components increases the importance of interface issues such as line edge roughness, the interface between a molecular device and its environment (including electrodes and surrounding molecules) is critical. Electrode–molecule coupling, determined by band alignment, contact bonding, and contact geometry, plays a critical role in electron transport properties. Thus, with proper control over electrode interfaces, electronic properties of contacts can be tuned.[93,148,149,152]

1.3.1 Characterization

Scanning probe microscopes are widely used for molecular device characterization, since they can both image target molecules in their environments and position one electrode (the scanning probe tip) with sub-nanometer precision in three dimensions.[154-156] In addition to interfaces with the substrate, nearby conductive molecules can influence the electronic properties of target molecules. To reduce the effects of such interactions, active molecules can be distributed in less conducting monolayer matrices.[7,17] One method for doing this is solution deposition of conductive molecules inserted into existing ordered alkanethiolate (or other) SAMs (Figure 1.3).[7,8] Target molecules have high probabilities of deposition at domain boundaries and other defects in SAMs, typically resulting in few-nm spacings between molecules, adequate for electrical isolation. This method was used by Weiss and co-workers to test the conductance switching mechanism of isolated oligo(phenylene ethynyl) (OPE) thiolate molecules inserted into self-assembled dodecanthiolate monolayers.[7,13,15]

Active molecules can also be co-deposited at low concentration with alkanethiolates, dispersing them within the alkanethiolate domains; however, high-temperature (~80 °C) annealing after deposition can cause the active molecules to phase segregate.[157]

Single molecules can also be suspended between contacts in break junctions.[156,158,159] In this configuration, one electrode is initially in contact with or in close proximity to the other, and is slowly drawn away to break contact. If bi-functional (for instance, α, ω-dithiol) conductive molecules are present in the junction, quantized conductance decreases are observed as the number of molecules bridging the junction decreases. Junction lengths can be controlled to ±1 Å, and the junction is typically broken and reformed repeatedly to test reproducibility. Alternatively, controlled junction lengths can be achieved in static conformations using techniques such as on-wire lithography.[160]

Further molecular measurements can be made using scanning tunneling spectroscopy.[155] Inelastic electron tunneling spectroscopy (IETS) is performed using STM by holding the tip stationary over a molecule (i.e., without varying the tip–sample separation or the lateral position), and varying the voltage while monitoring the current at low temperature (4 K). This yields current–voltage curves dependent on the vibrational spectrum of the molecule, providing both structural and electronic information about the single-molecule junction.[161,162] Comparable measurements have been made in break junctions.[163,164]

1.3.2 Molecular Function

1.3.2.1 Resistors

Single-molecule conductance is sensitive to several factors, in addition to the chemical structures of molecules. These include the chemistry, geometry, and electronic properties of the contacts with the electrode (thiol, amine, etc.), as well as interactions with surrounding molecules.[93,165-167]

Conductance measurements based on repeated break-junction formation can generate histograms of values for thousands of Au–molecule–Au junctions, which are important due to variations in conductance with electrode geometry.[168] Conductance is often reported in relation to the quantum point contact value G_0 = 77.4 μS, which is the ideal conductance value for two metal electrodes bridged by a single atom of the same metal.[165] Conjugated molecules with extended π systems have higher conductances than unconjugated molecules such as alkanethiols.[169] Conductance also varies with the chemistry of the contacts, with reported conductance orders of R–P > R–S > $R–NH_2$ > R–COOH for saturated alkanes,[170,171] and differences between thiolates and selenolates.[93] Again, values and relative order depend on the specific backbones and electrodes, as band alignment effects dominate.[172]

Molecular energy levels (particularly the highest occupied molecular orbital, HOMO, and lowest unoccupied molecular orbital, LUMO) shift on binding to the electrodes. This shift determines the difference between molecular energy levels and the Fermi levels of the electrodes; alignment of either the HOMO or LUMO with the Fermi level typically increases conductivity.[166,167]

1.3.2.2 Rectifiers and Diodes

Certain molecules with two conjugated groups having donor-bridge-acceptor structures exhibit asymmetric conduction, or rectification.[173,174] Several factors contribute to rectification. One is the magnitude of the Schottky barrier at each interface, which depends on the mismatch between the molecular HOMO or LUMO and the substrate Fermi level.[174,175] Another is the placement of the donor-bridge-acceptor structure relative to the two electrodes. Asymmetric placement (often achieved using alkyl spacers with different lengths) increases rectification.[115,176] Rectification also occurs due to differences in energy levels between the donor and acceptor groups.[176] Distinguishing this contribution from the formation of a Schottky barrier requires the use of the same metal for both electrodes, first achieved by Metzger and coworkers.[177] Rectification ratios (ratio of conductances at positive and negative voltages of the same magnitude) of up to 3000 at ±1 V have been measured in a cationic donor-bridge-acceptor dye.[178] Experimentally, the same challenges described above for resistors apply here; for instance, rectification depends on the structure of the junction between the electrodes. In addition, the rectification ratio has been observed to decrease with successive measurements, complicating quantification.

1.3.2.3 Switches

Molecular switches transition between two (or more) electronic, structural, or optical states in response to external stimuli. The behavior of most such molecules is initially characterized in solution. Surface-bound switching is of interest because it creates the possibility of using switch states in devices; however, surface attachment often impacts switching, meaning careful characterization is important.

Certain classes of molecules undergo switching between high and low conductance states. Oligo(phenylene ethynylene)s are widely studied examples, in which switching occurs due to hybridization changes at the metal-molecule contact.[13,15] As with the molecules discussed above, switching behavior depends on the local environment. For instance, placing OPE molecules in well-ordered alkanethiol SAM matrices increases stability and reduces stochastic switching frequency. Hydrogen-bonding interactions with appropriately designed amide- containing alkanethiol SAMs have been used to stabilize one or both switch states.[14,179]

Photochromic molecules switch between conformational states upon exposure to light of characteristic wavelengths, with switching behavior that is often different on surfaces vs. in solution. For instance, azobenzene molecules, containing two benzene rings linked through an N═N double bond, undergo photoisomerization from a lower-energy *trans* conformation to a higher-energy *cis* conformation when irradiated at ~365 nm.[180] Isomerization on surfaces introduces additional considerations. If molecules lie flat on bare metal surfaces, isomerization is typically quenched due to electronic coupling with the surface.[180,181] If molecules are elevated off the surface on bulky legs to decouple them from the substrate, switching is again observed;[181] however, the photon absorption cross-section is reduced relative to that in solution,[182] and the reaction can proceed *via* a different mechanism.[183] Switching can also be achieved by depositing the molecules at defects in background SAM matrices, linked to the surface through tethers long enough to place the azo functionality protruding beyond the matrix.[110] In this case, the structure of the tether plays a key role in mediating switching.[172,181,184] Placing functional molecules on surfaces also opens new possibilities for controlling switching. For instance, azobenzene switching on surfaces can be initiated using electric fields or tunneling electrons from a STM probe tip.[172]

Mechanically interlocked molecules such as catenanes and rotaxanes operate based on the motion of two or more noncovalently linked molecules relative to each other.[185-188] Rotaxanes are comprised of dumbbell-shaped molecules with a ring-shaped molecule threaded on the shaft. The ring can move between two stations on the shaft based on the oxidation state of the preferred tetrathiafulvalene (TTF) station. Tethering these molecules to solid surfaces enables them to perform work,[189] but also raises the possibility that interactions with the surface or neighboring molecules may affect their function.

The motion of individual rings can be tracked using electrochemical STM (with solution covering the surface), as the potential is raised and lowered (from ~0.1 to ~0.5 V), reversibly changing the oxidation state of the TTF station. Since the shafts are much less conductive than the rings, only the rings are visible in STM images. Observing the motions of ~100 rings as the potential is cycled reveals a distribution of ring displacements around the ~3 nm distance between stations of the fully extended molecule, with an average displacement of ~2 nm.[190] This suggests that the shaft binds to the surface without the ends fully extended. Direct measurements such as those described inform strategies for optimizing molecular function for devices, such as development of rotaxane switches with more rigid shafts. Rigid shafts would have the further advantage of being able to transmit greater force in assembled, cooperative devices.[147,189]

1.3.2.4 Single-Molecule Reactions

Isolating individual molecules or pairs of molecules on surfaces as 0D structures enables chemical reactions to be initiated and monitored at the single molecule level. Again, STM is a useful tool, since electronic excitation can trigger chemical reactions, which can then be observed with the microscope; many STM measurements are performed at low temperature (4 K) under ultrahigh vacuum conditions (pressures $< 10^{-10}$ torr), both reducing the likelihood of unwanted side reactions with gas-phase molecules, and slowing reaction kinetics.[191]

Such single-molecule chemistry was pioneered by Ho,[192] and Meyer and Rieder.[193] Ho and coworkers performed single molecule dissociation of pyridine and benzene molecules on Cu(001).[192] Meyer, Rieder, and coworkers induced Ullmann coupling (formation of biphenyl from two iodobenzene molecules) on Cu{111}.[193] Weiss and coworkers later extended single-molecule reaction studies, inducing Ullman coupling with a scanning tunneling microscope and differentiating reactive intermediates from products based on IETS measurements.[194] Reaction mechanisms for catalytic chemistry on metal surfaces are technologically important, and often difficult to monitor using standard characterization techniques under reaction conditions.

In addition to observing important and normally short-lived reaction intermediates, 0D molecular assemblies on surfaces can be used to control reaction pathways to select for paths that would be unfavorable in solution. Pairs of thiolated anthracene phenylene ethynylene derivatives deposited at defects in alkanethiolate SAMs are confined in head-to-head arrangements.[195] When photoexcited, the molecules dimerize *via* cycloaddition, since they cannot access the head-to-tail conformation that would otherwise be sterically favored in solution.

1.3.2.5 Biological applications of 0D assembly

Isolating individual biomolecules on surfaces provides unique opportunities for understanding their structure and function,[17,196-198] although many systems benefit from careful selection of passivating monolayers to control interactions between the target molecules and the substrates.[1] Proteins are relatively large (~4 nm diameter for a 50 kD globular protein[199]) and can interact with other nearby proteins on surfaces, meaning that if proteins are targeted to surfaces by ligands, it is useful to have the ligands distributed several nanometers apart on surfaces. This is possible using the defect-based insertion strategy discussed previously.[131,200] For instance, 5-hydroxytryptophan (5-HTP), a serotonin precursor, has been covalently bound to tethers via its additional carboxyl group. The use of insertion-directed self-assembly distributes 5-HTP at defects in SAM matrices, effectively spacing these molecules far apart. The use of the precursor molecule, instead of the neurotransmitter serotonin (5-hydroxytryptamine) itself, leaves all epitopes of serotonin accessible for molecular recognition. These surfaces have been used to capture native serotonin receptor proteins.[113,143] Substrates capable of biomolecule-specific recognition can ultimately be used in tandem with other methods, such as surface mass spectrometry, to identify new target molecules.[139]

1.4 Perspectives

Molecular monolayers represent one of the limits of nanostructured materials, and, in some cases, enable control of structure and environment down to the single-molecule level. In 2D monolayers, the molecular lattice structures and physical properties can be tuned based on substrate structures, and the steric and chemical functionalities of the molecules making up the monolayers. Combining monolayer strategies with top-down patterning enables 2D monolayer structures to be created with features from below 100 nm to the wafer scale.[141] The self- and directed-assembly strategies described above enable control down to the sub-nanometer scale.

To date, the properties of 2D monolayers have been explored extensively; however, restricting additional dimensions can provide even greater control over function and provide insight into molecular processes. For instance, 0D structures allow the course of individual molecular reactions to be controlled and monitored.

Studying molecular structures and processes at the sub-nanometer scale in real space makes it uniquely possible to understand how nanoscale properties change based on interactions with the environment, particularly defects and neighboring molecules. Since interfaces, defects, and heterogeneous structures are critical in applications from device performance to biological function, characterization tools that provide additional information about interfaces will open new fields of study and new means of control.

1.5 Dissertation Overview

This dissertation is organized as follows, Chapter 1 has discussed monolayer structures ranging from surface down to single molecules, with a focus on applications of each type of structure, and on techniques that enable characterization of monolayer physical properties down to the single-molecule scale. In Chaper 2, we introduce the design of custom-built laser-assisted STM that has eliminated heating at tunneling junction and is capable of detecting photocurrent originated from single anthrancene derivatives adsorbed on gold at ambient condition. Chapter 3 demonstrates that C_{60}-donor-C_{60} and its chromophore control are positioned at well-controlled environment in the same two-dimensional matrix to test the chemical specificity of our laser-assisted STM and elucidate the photoinduced charge transfer process within the molecular p-n junction. Chapter 4 describes a study of study of exchange reactions between alkaneselenolates and alkanethiolates bound to gold surfaces. The outlook for work in these areas based on this dissertation is summarized in Chapter 5.

Previous publications:

Chapter 1 is based on the following invited review and adapted with permission.

Claridge, S. A.; Liao, W.-S.; Thomas, J. C.; Zhao, Y.; Cao, H. H.; Cheunkar, S.; Serino, A. C.; Andrews, A. M.; Weiss, P. S. From the bottom up: dimensional control and characterization in molecular monolayers. *Chem. Soc. Rev.* 2013, 42, 2725-2745.

Chapter 2 is based on two manuscripts in preparation. Currently, they are as follows: Zhao, Y; Kim, M.; Hohman, J. N.; Schwartz, J. J.; Wadsworth, G. A.; Weiss, P. S. Single-Molecule Optical Spectroscopy with Ångström-Scale Precision. *TBD* 2015 and Zhao, Y; Kim, M.; Wattanatorn, N.; Ma, H.; Jen, A. K.–Y.; Weiss P. S. Photoconductance of Single Organic Molecules Dictated by Image Potential Surface States of Gold Substrate. *TBD* 2015.

Chapter 3 is a manuscript in preparation. Currently, the paper is as follows: Zhao, Y; Kim, M.; Wattanatorn, N.; Ma, H.; Jen, A. K.–Y.; Weiss P. S. Direct Measurement of Photoinduced Charge Creation in Single C_{60}-tethered Triad Molecule. *TBD* 2015.

Chapter 4 has been published and is adapted with permission. The paper is:

Hohman, J. N.; Thomas, J. C.; Zhao, Y. X.; Auluck, H.; Kim, M.; Vijselaar, W.; Kommeren, S.; Terfort, A.; Weiss, P. S. Exchange Reactions between Alkanethiolates and Alkaneselenols on Au{111}. J. Am. Chem. Soc. 2014, 136, 8110-8121.

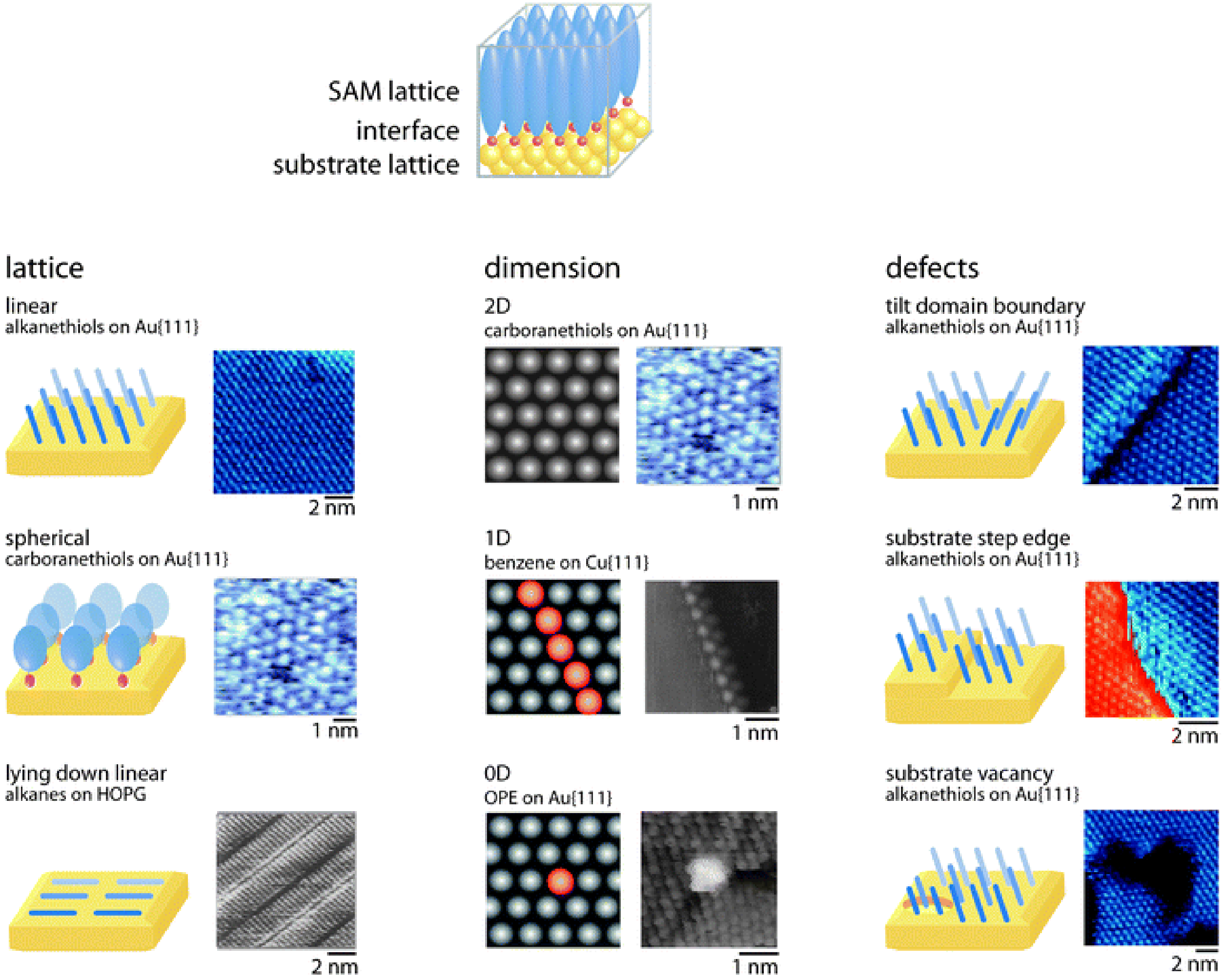

Figure 1.1 Self-assembled monolayers have molecular lattices that optimize interactions both with substrate lattices and between molecules in the monolayers, leading to a variety of lattice structures. Molecular structures in monolayers exhibit restricted dimensionality, similar to other nanostructured materials, which changes molecular behavior through directional coupling and other effects. Adapted with permission from ref. 15, 121, and 201. Defects in monolayer structure arise from substrate structure or molecular interactions, and create reactive sites in materials that can be used to control and to characterize molecular properties. Adapted with permission from ref. 8.

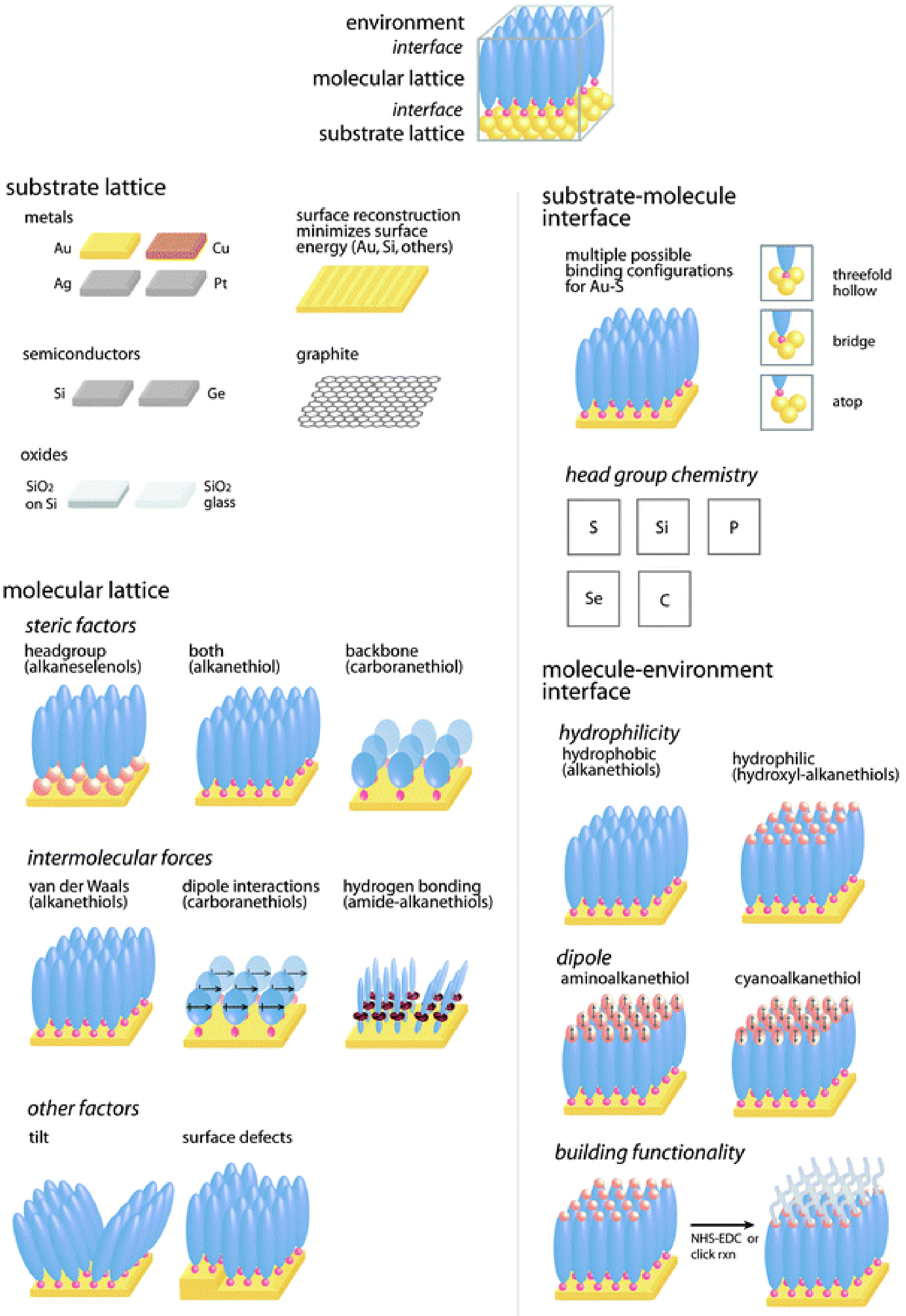

Figure 1.2 Two-dimensional molecular structures on surfaces form via the interplay between substrates and molecular lattices, and interactions at interfaces.

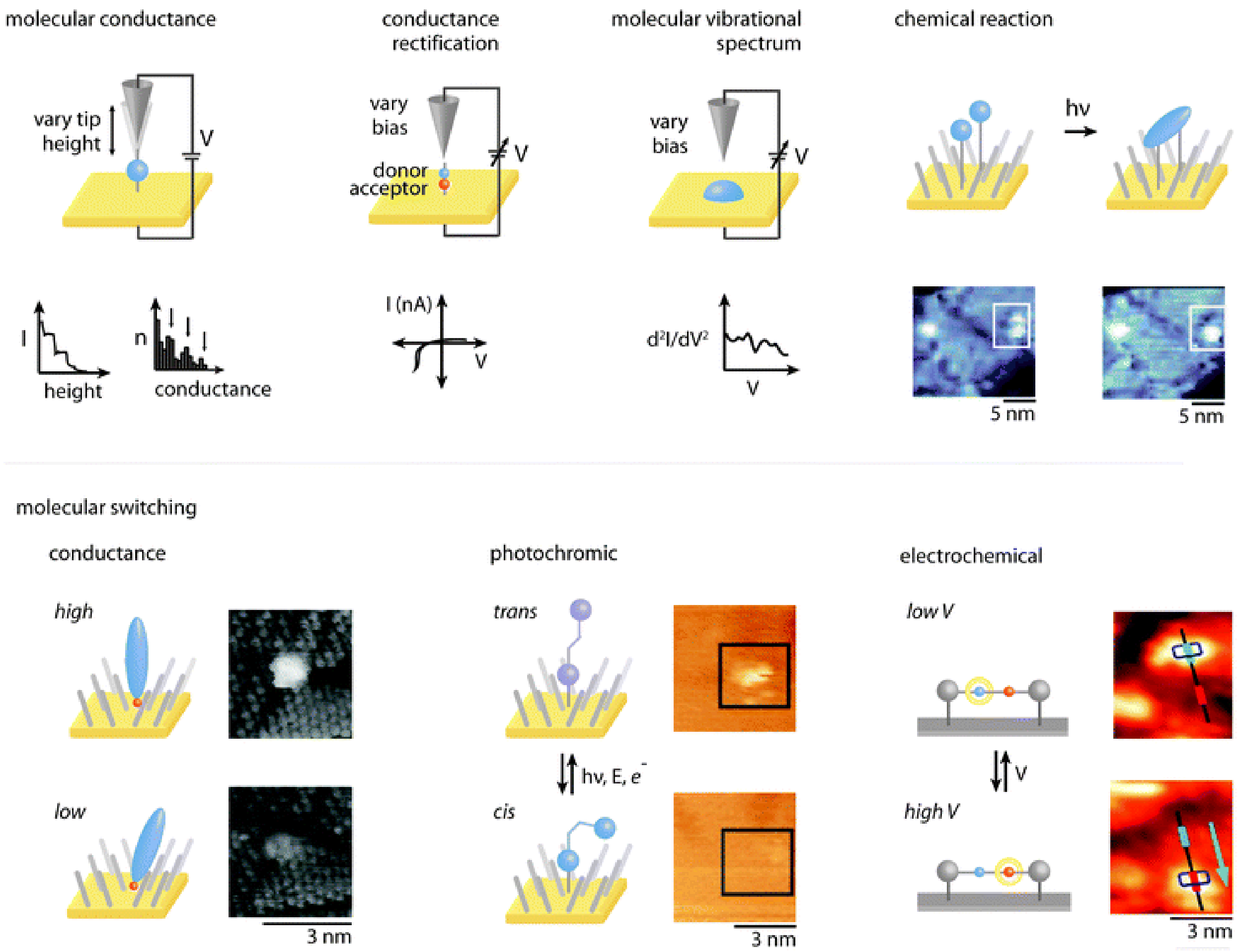

Figure 1.3 Molecular conductance is measured in a STM break junction by monitoring current as the STM probe tip is moved away from the surface (top left). A donor–bridge–acceptor molecular rectifier exhibits an asymmetric I–V curve, also measured with STM (top center). Photodimerization of paired anthracene phenylene ethynylene derivatives isolated in a SAM is visualized with STM (top right). Adapted with permission from ref. 195. An isolated oligo(phenylene ethynylene) molecule inserted in a dodecanethiolate SAM on Au{111} undergoes reversible conductance switching (bottom left). Adapted with permission from ref. 15. Azobenzene inserted in a dodecanethiolate SAM undergoes reversible photoisomerization (bottom middle). Adapted with permission from ref. 110. The ring of a surface-bound rotaxane

shuttles between two stations as the electrochemical potential in the cell is cycled from 0.1 to 0.5 V (bottom right). Adapted with permission from ref. 190.

References

1. Love, J. C.; Estroff, L. A.; Kriebel, J. K.; Nuzzo, R. G.; Whitesides, G. M. Self-assembled monolayers of thiolates on metals as a form of nanotechnology. *Chem. Rev.* 2005, 105, 1103-1169.

2. Nuzzo, R. G.; Zegarski, B. R.; Dubois, L. H. Fundamental studies of the chemisorption of organosulfur compounds on gold(111). Implications for molecular self-assembly on gold surfaces. *J. Am. Chem. Soc.* 1987, 109, 733-40.

3. Dubois, L. H.; Nuzzo, R. G. Synthesis, structure, and properties of model organic surfaces. *Annu. Rev. Phys. Chem.* 1992, 43, 437-63.

4. De Feyter, S.; De Schryver, F. C. Two-dimensional supramolecular self-assembly probed by scanning tunneling microscopy. *Chem. Soc. Rev.* 2003, 32, 139-150.

5. Poirier, G. E. Characterization of organosulfur molecular monolayers on Au(111) using scanning tunneling microscopy. *Chem. Rev.* 1997, 97, 1117-1127.

6. Hohman, J. N.; Claridge, S. A.; Kim, M.; Weiss, P. S. Cage molecules for self-assembly. *Mat. Sci. Eng. R* 2010, 70, 188-208.

7. Bumm, L. A.; Arnold, J. J.; Cygan, M. T.; Dunbar, T. D.; Burgin, T. P.; Jones, L., II; Allara, D. L.; Tour, J. M.; Weiss, P. S. Are single molecular wires conducting? *Science* 1996, 271, 1705-07.

8. Cygan, M. T.; Dunbar, T. D.; Arnold, J. J.; Bumm, L. A.; Shedlock, N. F.; Burgin, T. P.; Jones, L., II; Allara, D. L.; Tour, J. M.; Weiss, P. S. Insertion, conductivity, and structures of conjugated organic oligomers in self-assembled alkanethiol aonolayers on Au{111}. *J. Am. Chem. Soc.* 1998, 120, 2721-2732.

9. Weiss, P. S. Functional molecules and assemblies in controlled environments: formation and measurements. *Acc. Chem. Res.* 2008, 41, 1772-1781.

10. Bumm, L. A.; Arnold, J. J.; Charles, L. F.; Dunbar, T. D.; Allara, D. L.; Weiss, P. S. Directed self-assembly to create molecular terraces with molecularly sharp boundaries in organic monolayers. *J. Am. Chem. Soc.* 1999, 121, 8017-8021.

11. Zheng, Y. B.; Payton, J. L.; Chung, C.-H.; Liu, R.; Cheunkar, S.; Pathem, B. K.; Yang, Y.; Jensen, L.; Weiss, P. S. Surface-enhanced raman spectroscopy to probe reversibly photoswitchable azobenzene in controlled nanoscale environments. *Nano Lett.* 2011, 11, 3447-3452.

12. Moore, A. M.; Dameron, A. A.; Mantooth, B. A.; Smith, R. K.; Fuchs, D. J.; Ciszek, J. W.; Maya, F.; Yao, Y.; Tour, J. M.; Weiss, P. S. Molecular engineering and measurements to test hypothesized mechanisms in single molecule conductance switching. *J. Am. Chem. Soc.* 2006, 128, 1959-1967.

13. Lewis, P. A.; Inman, C. E.; Yao, Y. X.; Tour, J. M.; Hutchison, J. E.; Weiss, P. S. Mediating stochastic switching of single molecules using chemical functionality. *J. Am. Chem. Soc.* 2004, 126, 12214-12215.

14. Lewis, P. A.; Inman, C. E.; Maya, F.; Tour, J. M.; Hutchison, J. E.; Weiss, P. S. Molecular engineering of the polarity and interactions of molecular electronic switches. *J. Am. Chem. Soc.* 2005, 127, 17421-17426.

15. Donhauser, Z. J.; Mantooth, B. A.; Kelly, K. F.; Bumm, L. A.; Monnell, J. D.; Stapleton, J. J.; Price, D. W.; Rawlett, A. M.; Allara, D. L.; Tour, J. M.; Weiss, P. S. Conductance switching in single molecules through conformational changes. *Science* 2001, 292, 2303-2307.

16. Saavedra, H. M.; Barbu, C. M.; Dameron, A. A.; Mullen, T. J.; Crespi, V. H.; Weiss, P. S. 1-Adamantanethiolate Monolayer Displacement Kinetics Follow a Universal Form. *J. Am. Chem. Soc.* 2007, 129, 10741-10746.

17. Claridge, S. A.; Schwartz, J. J.; Weiss, P. S. Electrons, Photons, and Force: Quantitative single-molecule measurements from physics to biology. *ACS Nano* 2011, 5, 693-729.

18. Bigelow, W. C.; Pickett, D. L.; Zisman, W. A. Oleophobic monolayers: I. Films adsorbed from solution in nonpolar liquids. *J. Colloid Sci.* 1946, 1, 513-38.

19. Sagiv, J. Organized monolayers by adsorption. 1. Formation and structure of oleophobic mixed monolayers on solid surfaces. *J. Am. Chem. Soc.* 1980, 102, 92-8.

20. Nuzzo, R. G.; Allara, D. L. Adsorption of bifunctional organic disulfides on gold surfaces. *J. Am. Chem. Soc.* 1983, 105, 4481-3.

21. Smith, R. K.; Lewis, P. A.; Weiss, P. S. Patterning self-assembled monolayers. *Prog. Surf. Sci.* 2004, 75, 1-68.

22. Bent, S. F. Heads or Tails: which is more important in molecular self-assembly? *ACS Nano* 2007, 1, 10-12.

23. Laibinis, P. E.; Whitesides, G. M.; Allara, D. L.; Tao, Y. T.; Parikh, A. N.; Nuzzo, R. G. Comparison of the structures and wetting properties of self-assembled monolayers of n-alkanethiols on the coinage metal surfaces, copper, silver, and gold. *J. Am. Chem. Soc.* 1991, 113, 7152-67.

24. Ulman, A. Formation and structure of self-assembled monolayers. *Chem. Rev.* 1996, 96, 1533-1554.

25. Shaporenko, A.; Ulman, A.; Terfort, A.; Zharnikov, A. Self-assembled monolayers of alkaneselenolates on (111) gold and silver. *J. Phys. Chem. B* 2005, 109, 3898-3906.

26. Vericat, C.; Vela, M. E.; Benitez, G.; Carro, P.; Salvarezza, R. C. Self-assembled monolayers of thiols and dithiols on gold: new challenges for a well-known system. *Chem. Soc. Rev.* 2010, 39, 1805-1834.

27. Azzaroni, O.; Vela, M. E.; Fonticelli, M.; Benitez, G.; Carro, P.; Blum, B.; Salvarezza, R. C. Electrodesorption potentials of self-assembled alkanethiolate monolayers on copper electrodes. an experimental and theoretical study. *J. Phys. Chem. B* 2003, 107, 13446-13454.

28. Love, J. C.; Wolfe, D. B.; Haasch, R.; Chabinyc, M. L.; Paul, K. E.; Whitesides, G. M.; Nuzzo, R. G. Formation and structure of self-assembled monolayers of alkanethiolates on palladium. *J. Am. Chem. Soc.* 2003, 125, 2597-2609.

29. Floridia Addato, M. A.; Rubert, A. A.; Benitez, G. A.; Fonticelli, M. H.; Carrasco, J.; Carro, P.; Salvarezza, R. C. Alkanethiol adsorption on platinum: chain length effects on the quality of self-assembled monolayers. *J. Phys. Chem. C* 2011, 115, 17788-17798.

30. Zangmeister, C. D.; Picraux, L. B.; Van Zee, R. D.; Yao, Y.; Tour, J. M. Energy-level alignment and work function shifts for thiol-bound monolayers of conjugated molecules self-assembled on Ag, Cu, Au, and Pt. *Chem. Phys. Lett.* 2007, 442, 390-393.

31. Bengio, S.; Fonticelli, M.; Benitez, G.; Creus, A. H.; Carro, P.; Ascolani, H.; Zampieri, G.; Blum, B.; Salvarezza, R. C. Electrochemical self-assembly of alkanethiolate molecules on Ni(111) and polycrystalline Ni surfaces. *J. Phys. Chem. B* 2005, 109, 23450-23460.

32. Mani, G.; Johnson, D. M.; Marton, D.; Dougherty, V. L.; Feldman, M. D.; Patel, D.; Ayon, A. A.; Agrawal, C. M. Stability of self-assembled monolayers on titanium and gold. *Langmuir* 2008, 24, 6774-6784.

33. Nakamura, T.; Miyamae, T.; Nakai, I.; Kondoh, H.; Kawamoto, T.; Kobayashi, N.; Yasuda, S.; Yoshimura, D.; Ohta, T.; Nozoye, H.; Matsumoto, M. Adsorption states of dialkyl ditelluride autooxidized monolayers on Au(111). *Langmuir* 2005, 21, 3344-3353.

34. Rampi, M. A.; Schueller, O. J. A.; Whitesides, G. M. Alkanethiol self-assembled monolayers as the dielectric of capacitors with nanoscale thickness. *Appl. Phys. Lett.* 1998, 72, 1781-1783.

35. Chiechi, R. C.; Weiss, E. A.; Dickey, M. D.; Whitesides, G. M. Eutectic gallium-indium (EGaIn): a moldable liquid metal for electrical characterization of self-assembled monolayers. *Angew. Chem., Int. Ed.* 2008, 47, 142-144.

36. Hohman, J. N.; Kim, M.; Wadsworth, G. A.; Bednar, H. R.; Jiang, J.; LeThai, M. A.; Weiss, P. S. Directing substrate morphology via self-assembly: ligand-mediated scission of gallium-indium microspheres to the nanoscale. *Nano Lett.* 2011, 11, 5104-5110.

37. Buriak, J. M. Organometallic chemistry on silicon and germanium surfaces. *Chem. Rev.* 2002, 102, 1271-1308.

38. Bent, S. F. Organic functionalization of group IV semiconductor surfaces: Principles, examples, applications, and prospects. *Surf. Sci.* 2002, 500, 879-903.

39. Kachian, J. S.; Wong, K. T.; Bent, S. F. Periodic trends in organic functionalization of group iv semiconductor surfaces. *Acc. Chem. Res.* 2010, 43, 346-355.

40. Hohman, J. N.; Kim, M.; Bednar, H. R.; Lawrence, J. A.; McClanahan, P. D.; Weiss, P. S. Simple, robust molecular self-assembly on germanium. *Chem. Sci.* 2011, 2, 1334-1343.

41. McGuiness, C. L.; Shaporenko, A.; Mars, C. K.; Uppili, S.; Zharnikov, M.; Allara, D. L. Molecular self-assembly at bare semiconductor surfaces: preparation and characterization of highly organized octadecanethiolate monolayers on GaAs(001). *J. Am. Chem. Soc.* 2006, 128, 5231-5243.

42. Lim, H.; Carraro, C.; Maboudian, R.; Pruessner, M. W.; Ghodssi, R. Chemical and thermal stability of alkanethiol and sulfur passivated InP(100). *Langmuir* 2004, 20, 743-747.

43. Wasserman, S. R.; Tao, Y. T.; Whitesides, G. M. Structure and reactivity of alkylsiloxane monolayers formed by reaction of alkyltrichlorosilanes on silicon substrates. *Langmuir* 1989, 5, 1074-87.

44. Schreiber, F. Structure and growth of self-assembling monolayers. *Prog. Surf. Sci.* 2000, 65, 151-256.

45. Maury, P.; Peter, M.; Mahalingam, V.; Reinhoudt, D. N.; Huskens, J. Patterned self-assembled monolayers on silicon oxide prepared by nanoimprint lithography and their applications in nanofabrication. *Adv. Funct. Mater.* 2005, 15, 451-457.

46. Ito, T.; Forman, S. M.; Cao, C.; Li, F.; Eddy, C. R.; Mastro, M. A.; Holm, R. T.; Henry, R. L.; Hohn, K. L.; Edgar, J. H. Self-assembled monolayers of alkylphosphonic acid on GaN substrates. *Langmuir* 2008, 24, 6630-6635.

47. Noble-Luginbuhl, A. R.; Nuzzo, R. G. Assembly and characterization of sams formed by the adsorption of alkanethiols on zinc selenide substrates. *Langmuir* 2001, 17, 3937-3944.

48. Elemans, J. A. A. W.; Lei, S.; De Feyter, S. Molecular and supramolecular networks on surfaces: from two-dimensional crystal engineering to reactivity. *Angew. Chem., Int. Ed.* 2009, 48, 7298-7332.

49. De Feyter, S.; De Schryver, F. C. Self-assembly at the liquid/solid interface: STM reveals. *J. Phys. Chem. B* 2005, 109, 4290-4302.

50. Xu, L.; Miao, X.; Ying, X.; Deng, W. Two-dimensional self-assembled molecular structures formed by the competition of van der waals forces and dipole-dipole interactions. *J. Phys. Chem. C* 2012, 116, 1061-1069.

51. Xue, Y.; Zimmt, M. B. Patterned monolayer self-assembly programmed by side chain shape: four-component gratings. *J. Am. Chem. Soc.* 2012, 134, 4513-4516.

52. Somorjai, G. A.; Li, Y. *Introduction to Surface Chemistry and Catalysis*. John Wiley and Sons, Inc.: New Jersey, 2010.

53. Duke, C. B. Semiconductor surface reconstruction: the structural chemistry of two-dimensional surface compounds. *Chem. Rev.* 1996, 96, 1237-1259.

54. Liao, W.-S.; Cheunkar, S.; Cao, H. H.; Bednar, H. R.; Weiss, P. S.; Andrews, A. M. Subtractive patterning via chemical lift-off lithography. *Science* 2012, 337, 1517-1521.

55. Tierney, H. L.; Han, J. W.; Jewell, A. D.; Iski, E. V.; Baber, A. E.; Sholl, D. S.; Sykes, E. C. H. Chirality and rotation of asymmetric surface-bound thioethers. *J. Phys. Chem. C* 2011, 115, 897-901.

56. Bellisario, D. O.; Jewell, A. D.; Tierney, H. L.; Baber, A. E.; Sykes, E. C. H. Adsorption, assembly, and dynamics of dibutyl sulfide on Au{111}. *J. Phys. Chem. C* 2010, 114, 14583-14589.

57. Tierney, H. L.; Baber, A. E.; Sykes, E. C. H.; Akimov, A.; Kolomeisky, A. B. Dynamics of thioether molecular rotors: effects of surface interactions and chain flexibility. *J. Phys. Chem. C* 2009, 113, 10913-10920.

58. Jensen, S. C.; Baber, A. E.; Tierney, H. L.; Sykes, E. C. H. Adsorption, interaction, and manipulation of dibutyl sulfide on Cu{111}. *ACS Nano* 2007, 1, 22-29.

59. Han, P.; Mantooth, B. A.; Sykes, E. C. H.; Donhauser, Z. J.; Weiss, P. S. Benzene on Au{111} at 4 K. Monolayer growth and tip-induced molecular cascades. *J. Am. Chem. Soc.* 2004, 126, 10787-10793.

60. Yu, M.; Bovet, N.; Satterley, C. J.; Bengio, S.; Lovelock, K. R. J.; Milligan, P. K.; Jones, R. G.; Woodruff, D. P.; Dhanak, V. True nature of an archetypal self-assembly system: Mobile Au-thiolate species on Au(111). *Phys. Rev. Lett.* 2006, 97.

61. Stranick, S. J.; Parikh, A. N.; Allara, D. L.; Weiss, P. S. A new mechanism for surface diffusion: motion of a substrate-adsorbate complex. *J. Phys. Chem.* 1994, 98, 11136-42.

62. Hakkinen, H. The gold-sulfur interface at the nanoscale. *Nat. Chem.* 2012, 4, 443-455.

63. Maksymovych, P.; Voznyy, O.; Dougherty, D. B.; Sorescu, D. C.; Yates, J. T., Jr. Gold adatom as a key structural component in self-assembled monolayers of organosulfur molecules on Au(111). *Prog. Surf. Sci.* 2010, 85, 206-240.

64. Cossaro, A.; Mazzarello, R.; Rousseau, R.; Casalis, L.; Verdini, A.; Kohlmeyer, A.; Floreano, L.; Scandolo, S.; Morgante, A.; Klein, M. L.; Scoles, G. X-ray diffraction and computation yield the structure of alkanethiols on gold(111). *Science* 2008, 321, 943-946.

65. Chaudhuri, A.; Lerotholi, T. J.; Jackson, D. C.; Woodruff, D. P.; Dhanak, V. R. The local adsorption structure of methylthiolate and butylthiolate on Au(111). A photoemission core-level shift investigation. *Surf. Sci.* 2010, 604, 227-234.

66. Mazzarello, R.; Cossaro, A.; Verdini, A.; Rousseau, R.; Casalis, L.; Danisman, M. F.; Floreano, L.; Scandolo, S.; Morgante, A.; Scoles, G. Structure of a CH_3S monolayer on Au(111)

solved by the interplay between molecular dynamics calculations and diffraction measurements. *Phys. Rev. Lett.* 2007, 98, 016102.

67. Otalvaro, D.; Veening, T.; Brocks, G. Self-assembled monolayer induced Au(111) and Ag(111) reconstructions: work functions and interface dipole formation. *J. Phys. Chem. C* 2012, 116, 7826-7837.

68. Iski, E. V.; El-Kouedi, M.; Calderon, C.; Wang, F.; Bellisario, D. O.; Ye, T.; Sykes, E. C. H. The extraordinary stability imparted to silver monolayers by chloride. *Electrochim. Acta* 2010, 56, 1652-1661.

69. Monnell, J. D.; Stapleton, J. J.; Jackiw, J. J.; Dunbar, T.; Reinerth, W. A.; Dirk, S. M.; Tour, J. M.; Allara, D. L.; Weiss, P. S. ordered local domain structures of decaneselenolate and dodecaneselenolate monolayers on Au{111}. *J. Phys. Chem. B* 2004, 108, 9834-9841.

70. Han, P.; Kurland, A. R.; Giordano, A. N.; Nanayakkara, S. U.; Blake, M. M.; Pochas, C. M.; Weiss, P. S. Heads and tails: simultaneous exposed and buried interface imaging of monolayers. *ACS Nano* 2009, 3, 3115-3121.

71. Murphy, K. L.; Tysoe, W. T.; Bennett, D. W. A Comparative investigation of aryl isocyanides chemisorbed to palladium and gold: An ATR-IR Spectroscopic Study. *Langmuir* 2004, 20, 1732-1738.

72. Lio, A.; Charych, D. H.; Salmeron, M. Comparative atomic force microscopy study of the chain length dependence of frictional properties of alkanethiols on gold and alkylsilanes on mica. *J. Phys. Chem. B* 1997, 101, 3800-3805.

73. Allara, D. L.; Parikh, A. N.; Rondelez, F. Evidence for a unique chain organization in long chain silane monolayers deposited on two widely different solid substrates. *Langmuir* 1995, 11, 2357-60.

74. Bourgeat-Lami, E. Organic-inorganic nanostructured colloids. *J. Nanosci. Nanotechnol.* 2002, 2, 1-24.

75. Jewell, A. D.; Tierney, H. L.; Sykes, E. C. H. Gently lifting gold's herringbone reconstruction: Trimethylphosphine on Au(111). *Phys. Rev. B* 2010, 82.

76. Gouzman, I.; Dubey, M.; Carolus, M. D.; Schwartz, J.; Bernasek, S. L. Monolayer *vs.* multilayer self-assembled alkylphosphonate films: X-ray photoelectron spectroscopy studies. *Surf. Sci.* 2006, 600, 773-781.

77. Jewell, A. D.; Kyran, S. J.; Rabinovich, D.; Sykes, E. C. H. Effect of Head-group chemistry on surface-mediated molecular self-assembly. *Chem. - Eur. J.* 2012, 18, 7169-7178.

78. Hohman, J. N.; Kim, M.; Schupbach, B.; Kind, M.; Thomas, J. C.; Terfort, A.; Weiss, P. S. Dynamic double lattice of 1-adamantaneselenolate self-assembled monolayers on Au{111}. *J. Am. Chem. Soc.* 2011, 133, 19422-19431.

79. Huang, F. K.; Horton, R. C., Jr.; Myles, D. C.; Garrell, R. L. Selenolates as alternatives to thiolates for self-assembled monolayers: A SERS study. *Langmuir* 1998, 14, 4802-4808.

80. Taylor, C. E.; Schwartz, D. K. Octadecanoic acid self-assembled monolayer growth at sapphire surfaces. *Langmuir* 2003, 19, 2665-2672.

81. Lim, M. S.; Feng, K.; Chen, X.; Wu, N.; Raman, A.; Nightingale, J.; Gawalt, E. S.; Korakakis, D.; Hornak, L. A.; Timperman, A. T. Adsorption and desorption of stearic acid self-assembled monolayers on aluminum oxide. *Langmuir* 2007, 23, 2444-2452.

82. Li, J.; Li, X.; Ni, X.; Wang, X.; Li, H.; Leong, K. W. Self-assembled supramolecular hydrogels formed by biodegradable PEO-PHB-PEO triblock copolymers and α-cyclodextrin for controlled drug delivery. *Biomaterials* 2006, 27, 4132-4140.

83. Uemura, S.; Tanoue, R.; Yilmaz, N.; Ohira, A.; Kunitake, M. Molecular dynamics in two-dimensional supramolecular systems observed by STM. *Materials* 2010, 3, 4252-4276.

84. Dorokhin, D.; Hsu, S.-H.; Tomczak, N.; Reinhoudt, D. N.; Huskens, J.; Velders, A. H.; Vancso, G. J. Fabrication and luminescence of designer surface patterns with β-Cyclodextrin functionalized quantum dots via multivalent supramolecular coupling. *ACS Nano* 2010, 4, 137-142.

85. Gonzalez-Campo, A.; Hsu, S.-H.; Puig, L.; Huskens, J.; Reinhoudt, D. N.; Velders, A. H. Orthogonal covalent and noncovalent functionalization of cyclodextrin-alkyne patterned surfaces. *J. Am. Chem. Soc.* 2010, 132, 11434-11436.

86. Hu, W. S.; Tao, Y. T.; Hsu, Y. J.; Wei, D. H.; Wu, Y. S. Molecular orientation of evaporated pentacene films on gold: Alignment effect of self-assembled monolayer. *Langmuir* 2005, 21, 2260-2266.

87. Clegg, R. S.; Reed, S. M.; Hutchison, J. E. Self-assembled monolayers stabilized by three-dimensional networks of hydrogen bonds. *J. Am. Chem. Soc.* 1998, 120, 2486-2487.

88. Mao, X.; Wang, Y.; Liu, L.; Niu, L.; Yang, Y.; Wang, C. Molecular-level evidence of the surface-induced transformation of peptide structures revealed by scanning tunneling microscopy. *Langmuir* 2009, 25, 8849-8853.

89. Nowinski, A. K.; Sun, F.; White, A. D.; Keefe, A. J.; Jiang, S. Sequence, structure, and function of peptide self-assembled monolayers. *J. Am. Chem. Soc.* 2012, 134, 6000-6005.

90. Prato, M.; Toccafondi, C.; Maidecchi, G.; Chaudhari, V.; Harish, M. N. K.; Sampath, S.; Parodi, R.; Esaulov, V. A.; Canepa, M. Mercury segregation and diselenide self-assembly on gold. *J. Phys. Chem. C* 2012, 116, 2431-2437.

91. Chaudhari, V.; Kotresh, H. M. N.; Srinivasan, S.; Esaulov, V. A. Substitutional Self-assembly of alkanethiol and selenol sams from a lying-down doubly tethered butanedithiol SAM on gold. *J. Phys. Chem. C* 2011, 115, 16518-16523.

92. Choi, J.; Kang, H.; Ito, E.; Hara, M.; Noh, J. Phase transition of octaneselenolate self-assembled monolayers on Au(111) studied by scanning tunneling microscopy. *Bull. Korean Chem. Soc.* 2011, 32, 2623-2627.

93. Monnell, J. D.; Stapleton, J. J.; Dirk, S. M.; Reinerth, W. A.; Tour, J. M.; Allara, D. L.; Weiss, P. S. Relative conductances of alkaneselenolate and alkanethiolate monolayers on Au{111}. *J. Phys. Chem. B* 2005, 109, 20343-20349.

94. Szelagowska-Kunstman, K.; Cyganik, P.; Schuepbach, B.; Terfort, A. Relative stability of thiol and selenol based SAMs on Au(111) - exchange experiments. *Phys. Chem. Chem. Phys.* 2010, 12, 4400-4406.

95. Livage, J. The gel route to transition metal oxides. *J. Solid State Chem.* 1986, 64, 322-30.

96. Sanchez, C.; Boissiere, C.; Grosso, D.; Laberty, C.; Nicole, L. Design, synthesis, and properties of inorganic and hybrid thin films having periodically organized nanoporosity. *Chem. Mater.* 2008, 20, 682-737.

97. Petrovic, Z.; Katic, J.; Metikos-Hukovic, M.; Dadafarin, H.; Omanovic, S. Modification of a nitinol surface by phosphonate self-assembled monolayers. *J. Electrochem. Soc.* 2011, 158, F159-F165.

98. Baber, A. E.; Lawton, T. J.; Sykes, E. C. H. Hydrogen-bonded networks in surface-bound methanol. *J. Phys. Chem. C* 2011, 115, 9157-9163.

99. Otero, R.; Rosei, F.; Besenbacher, F. Scanning tunneling microscopy manipulation of complex organic molecules on solid surfaces. *Annu. Rev. Phys. Chem.* 2006, 57, 497-525.

100. Han, P.; Weiss, P. S. Electronic substrate-mediated interactions. *Surf. Sci. Rep.* 2012, 67, 19-81.

101. Arakawa, H.; Umemura, K.; Ikai, A. Protein images obtained by STM, AFM and TEM. *Nature* 1992, 358, 171-3.

102. Torres, E.; Blumenau, A. T.; Biedermann, P. U. Steric and chain length effects in the ($\sqrt{(3)} \times \sqrt{(3)}$)R30° structures of alkanethiol self-assembled monolayers on Au(111). *ChemPhysChem* 2011, 12, 999-1009.

103. Poirier, G. E. Butanethiol self-assembly on Au(001): the 1×4 Au missing row, c(2×8) molecular lattice. *J. Vac. Sci. Technol., B* 1996, 14, 1453-1460.

104. Okawa, Y.; Aono, M. Linear chain polymerization initiated by a scanning tunneling microscope tip at designated positions. *J. Chem. Phys.* 2001, 115, 2317-2322.

105. Moore, A. M.; Yeganeh, S.; Yao, Y.; Claridge, S. A.; Tour, J. M.; Ratner, M. A.; Weiss, P. S. Polarizabilities of adsorbed and assembled molecules: measuring the conductance through buried contacts. *ACS Nano* 2010, 4, 7630-7636.

106. Clegg, R. S.; Hutchison, J. E. Control of monolayer assembly structure by hydrogen bonding rather than by adsorbate-substrate templating. *J. Am. Chem. Soc.* 1999, 121, 5319-5327.

107. Lewis, P. A.; Smith, R. K.; Kelly, K. F.; Bumm, L. A.; Reed, S. M.; Clegg, R. S.; Gunderson, J. D.; Hutchison, J. E.; Weiss, P. S. The role of buried hydrogen bonds in self-assembled mixed composition thiols on Au{111}. *J. Phys. Chem. B* 2001, 105, 10630-10636.

108. Yoon, H. J.; Shapiro, N. D.; Park, K. M.; Thuo, M. M.; Soh, S.; Whitesides, G. M. The rate of charge tunneling through self-assembled monolayers is insensitive to many functional group substitutions. *Angew. Chem., Int. Ed.* 2012, 51, 4658-4661, S4658/1-S4658/23.

109. Smith, R. K.; Reed, S. M.; Lewis, P. A.; Monnell, J. D.; Clegg, R. S.; Kelly, K. F.; Bumm, L. A.; Hutchison, J. E.; Weiss, P. S. Phase separation within a binary self-assembled monolayer on Au{111} driven by an amide-containing alkanethiol. *J. Phys. Chem. B* 2001, 105, 1119-1122.

110. Kumar, A. S.; Ye, T.; Takami, T.; Yu, B. C.; Flatt, A. K.; Tour, J. M.; Weiss, P. S. Reversible photo-switching of single azobenzene molecules in controlled nanoscale environments. *Nano Lett.* 2008, 8, 1644-1648.

111. Kim, M.; Hohman, J. N.; Serino, A. C.; Weiss, P. S. Structural manipulation of hydrogen-bonding networks in amide-containing alkanethiolate monolayers *via* electrochemical processing. *J. Phys. Chem. C* 2010, 114, 19744-19751.

112. Grave, C.; Risko, C.; Shaporenko, A.; Wang, Y.; Nuckolls, C.; Ratner, M. A.; Rampi, M. A.; Zharnikov, M. Charge transport through oligoarylene self-assembled monolayers: interplay of molecular organization, metal-molecule interactions, and electronic structure. *Adv. Funct. Mater.* 2007, 17, 3816-3828.

113. Vaish, A.; Shuster, M. J.; Cheunkar, S.; Singh, Y. S.; Weiss, P. S.; Andrews, A. M. Native serotonin membrane receptors recognize 5-hydroxytryptophan-functionalized substrates: enabling small-molecule recognition. *ACS Chem. Neurosci.* 2010, 1, 495-504.

114. Geyer, W.; Stadler, V.; Eck, W.; Zharnikov, M.; Golzhauser, A.; Grunze, M. Electron-induced crosslinking of aromatic self-assembled monolayers: Negative resists for nanolithography. *Appl. Phys. Lett.* 1999, 75, 2401-2403.

115. Chabinyc, M. L.; Chen, X. X.; Holmlin, R. E.; Jacobs, H.; Skulason, H.; Frisbie, C. D.; Mujica, V.; Ratner, M. A.; Rampi, M. A.; Whitesides, G. M. Molecular rectification in a metal-insulator-metal junction based on self-assembled monolayers. *J. Am. Chem. Soc.* 2002, 124, 11730-11736.

116. Bould, J.; Machacek, J.; Londesborough, M. G. S.; Macias, R.; Kennedy, J. D.; Bastl, Z.; Rupper, P.; Base, T. Decaborane thiols as building blocks for self-assembled monolayers on metal surfaces. *Inorg. Chem.* 2012, 51, 1685-1694.

117. Kim, M.; Hohman, J. N.; Morin, E. I.; Daniel, T. A.; Weiss, P. S. Self-assembled monolayers of 2-adamantanethiol on Au{111}: Control of structure and displacement. *J. Phys. Chem. A* 2009, 113, 3895-3903.

118. Jobbins, M. M.; Raigoza, A. F.; Kandel, S. A. Adatoms at the sulfur-gold interface in 1-adamantanethiolate monolayers, studied using reaction with hydrogen atoms and scanning tunneling microscopy. *J. Phys. Chem. C* 2011, 115, 25437-25441.

119. Willey, T. M.; Fabbri, J. D.; Lee, J. R. I.; Schreiner, P. R.; Fokin, A. A.; Tkachenko, B. A.; Fokina, N. A.; Dahl, J. E. P.; Carlson, R. M. K.; Vance, A. L.; Yang, W.; Terminello, L. J.; van Buuren, T.; Melosh, N. A. Near-edge X-ray absorption fine structure spectroscopy of diamondoid thiol monolayers on gold. *J. Am. Chem. Soc.* 2008, 130, 10536-10544.

120. Wang, Y.; Kioupakis, E.; Lu, X.; Wegner, D.; Yamachika, R.; Dahl, J. E.; Carlson, R. M. K.; Louie, S. G.; Crommie, M. F. Spatially resolved electronic and vibronic properties of single diamondoid molecules. *Nat. Mater.* 2008, 7, 38-42.

121. Hohman, J. N.; Zhang, P.; Morin, E. I.; Han, P.; Kim, M.; Kurland, A. R.; McClanahan, P. D.; Balema, V. P.; Weiss, P. S. Self-assembly of carboranethiol isomers on au{111}: intermolecular interactions determined by molecular dipole orientations. *ACS Nano* 2009, 3, 527-536.

122. Wang, H.; He, Y.; Ratner, B. D.; Jiang, S. Y. Modulating cell adhesion and spreading by control of FnIII(7×10) orientation on charged self-assembled monolayers (SAMs) of alkanethiolates. *J. Biomed. Mater. Res. A* 2006, 77A, 672-678.

123. Lee, S.-H.; Lin, W.-C.; Chang, C.-J.; Huang, C.-C.; Liu, C.-P.; Kuo, C.-H.; Chang, H.-Y.; You, Y.-W.; Kao, W.-L.; Yen, G.-J.; Kuo, D.-Y.; Kuo, Y.-T.; Tsai, M.-H.; Shyue, J.-J. Effect of the chemical composition on the work function of gold substrates modified by binary self-assembled monolayers. *Phys. Chem. Chem. Phys.* 2011, 13, 4335-4339.

124. Romaner, L.; Heimel, G.; Zojer, E. Electronic structure of thiol-bonded self-assembled monolayers: Impact of coverage. *Phys. Rev. B* 2008, 77.

125. Carot, M. L.; Macagno, V. A.; Paredes-Olivera, P.; Patrito, E. M. Structure of mixed carboxylic acid terminated self-assembled monolayers: experimental and theoretical investigation. *J. Phys. Chem. C* 2007, 111, 4294-4304.

126. Watcharinyanon, S.; Moons, E.; Johansson, L. S. O. Mixed self-assembled monolayers of ferrocene-terminated and unsubstituted alkanethiols on gold: surface structure and work function. *J. Phys. Chem. C* 2009, 113, 1972-1979.

127. Chambers, R. C.; Inman, C. E.; Hutchison, J. E. Electrochemical detection of nanoscale phase separation in binary self-assembled monolayers. *Langmuir* 2005, 21, 4615-4621.

128. Yague, J. L.; Agullo, N.; Fonder, G.; Delhalle, J.; Mekhalif, Z.; Borros, S. Thiol versus selenol SAMs as nucleation enhancers and adhesion promoters for plasma polymerized pyrrole on copper substrates. *Plasma Process. Polym.* 2010, 7, 601-609.

129. Patnaik, A.; Setoyama, H.; Ueno, N. Surface/interface electronic structure in C_{60} anchored aminothiolate self-assembled monolayer. An approach to molecular electronics. *J. Chem. Phys.* 2004, 120, 6214-6221.

130. Shuster, M. J.; Vaish, A.; Szapacs, M. E.; Anderson, M. E.; Weiss, P. S.; Andrews, A. M. Biospecific recognition of tethered small molecules diluted in self-assembled monolayers. *Adv. Mater.* 2008, 20, 164-167.

131. Shuster, M. J.; Vaish, A.; Cao, H. H.; Guttentag, A. I.; McManigle, J. E.; Gibb, A. L.; Martinez, M. M.; Nezarati, R. M.; Hinds, J. M.; Liao, W. S.; Weiss, P. S.; Andrews, A. M. Patterning small-molecule biocapture surfaces: microcontact insertion printing vs. photolithography. *Chem. Commun.* 2011, 47, 10641-10643.

132. Cho, J.; Berbil-Bautista, L.; Levy, N.; Poulsen, D.; Frechet, J. M. J.; Crommie, M. F. Functionalization, self-assembly, and photoswitching quenching for azobenzene derivatives adsorbed on Au(111). *J. Chem. Phys.* 2010, 133.

133. Smith, R. K.; Nanayakkara, S. U.; Woehrle, G. H.; Pearl, T. P.; Blake, M. M.; Hutchison, J. E.; Weiss, P. S. Spectral diffusion in the tunneling spectra of ligand-stabilized undecagold clusters. *J. Am. Chem. Soc.* 2006, 128, 9266-9267.

134. Vaish, A.; Liao, W.-S.; Shuster, M. J.; Hinds, J. M.; Weiss, P. S.; Andrews, A. M. Thin gold film-assisted fluorescence spectroscopy for biomolecule sensing. *Anal. Chem.* 2011, 83, 7451-7456.

135. Shuster, M. J.; Vaish, A.; Gilbert, M. L.; Martinez-Rivera, M.; Nezarati, R. M.; Weiss, P. S.; Andrews, A. M. Comparison of oligo(ethylene glycol)alkanethiols versus *n*-alkanethiols: self-assembly, insertion, and functionalization. *J. Phys. Chem. C* 2011, 115, 24778-24787.

136. Saavedra, H. M.; Thompson, C. M.; Hohman, J. N.; Crespi, V. H.; Weiss, P. S. Reversible lability by in situ reaction of self-assembled monolayers. *J. Am. Chem. Soc.* 2009, 131, 2252-2259.

137. Perez-Luna, V. H.; O'Brien, M. J.; Opperman, K. A.; Hampton, P. D.; Lopez, G. P.; Klumb, L. A.; Stayton, P. S. Molecular recognition between genetically engineered streptavidin and surface-bound biotin. *J. Am. Chem. Soc.* 1999, 121, 6469-6478.

138. Lahiri, J.; Ostuni, E.; Whitesides, G. M. Patterning ligands on reactive SAMs by microcontact printing. *Langmuir* 1999, 15, 2055-2060.

139. Mrksich, M. Mass spectrometry of self-assembled monolayers: A new tool for molecular surface science. *ACS Nano* 2008, 2, 7-18.

140. Weck, M.; Jackiw, J. J.; Rossi, R. R.; Weiss, P. S.; Grubbs, R. H. Ring-opening metathesis polymerization from surfaces. *J. Am. Chem. Soc.* 1999, 121, 4088-4089.

141. Saavedra, H. M.; Mullen, T. J.; Zhang, P. P.; Dewey, D. C.; Claridge, S. A.; Weiss, P. S. Hybrid strategies in nanolithography. *Rep. Prog. Phys.* 2010, 73.

142. Lahiri, J.; Isaacs, L.; Tien, J.; Whitesides, G. M. a strategy for the generation of surfaces presenting ligands for studies of binding based on an active ester as a common reactive intermediate: A surface plasmon resonance study. *Anal. Chem.* 1999, 71, 777-790.

143. Vaish, A.; Shuster, M. J.; Cheunkar, S.; Weiss, P. S.; Andrews, A. M. Tuning stamp surface energy for soft lithography of polar molecules to fabricate bioactive small-molecule microarrays. *Small* 2011, 7, 1471-1479.

144. Kolb, H. C.; Finn, M. G.; Sharpless, K. B. Click chemistry: diverse chemical function from a few good reactions. *Angew. Chem., Int. Ed.* 2001, 40, 2004-2021.

145. Sun, X.-L.; Stabler, C. L.; Cazalis, C. S.; Chaikof, E. L. Carbohydrate and protein immobilization onto solid surfaces by sequential diels-alder and azide-alkyne cycloadditions. *Bioconjugate Chem.* 2006, 17, 52-57.

146. Qin, G.; Santos, C.; Zhang, W.; Li, Y.; Kumar, A.; Erasquin, U. J.; Liu, K.; Muradov, P.; Trautner, B. W.; Cai, C. Biofunctionalization on alkylated silicon substrate surfaces *via* "click" chemistry. *J. Am. Chem. Soc.* 2010, 132, 16432-16441.

147. Paxton, W. F.; Spruell, J. M.; Stoddart, J. F. Heterogeneous catalysis of a copper-coated atomic force microscopy tip for direct-write click chemistry. *J. Am. Chem. Soc.* 2009, 131, 6692-6694.

148. Joachim, C.; Gimzewski, J. K.; Aviram, A. Electronics using hybrid-molecular and mono-molecular devices. *Nature* 2000, 408, 541-548.

149. Moth-Poulsen, K.; Bjornholm, T. Molecular electronics with single molecules in solid-state devices. *Nat. Nanotechnol.* 2009, 4, 551-556.

150. Aviram, A.; Ratner, M. A. Molecular rectifiers. *Chem. Phys. Lett.* 1974, 29, 277-283.

151. Metzger, R. M. Unimolecular electronics. *J. Mater. Chem.* 2008, 18, 4364-4396.

152. McCreery, R. L.; Bergren, A. J. Progress with molecular electronic junctions: meeting experimental challenges in design and fabrication. *Adv. Mater.* 2009, 21, 4303-4322.

153. Heath, J. R.; Ratner, M. A. Molecular electronics. *Phys. Today* 2003, 56, 43-49.

154. Gimzewski, J. K.; Joachim, C. Nanoscale science of single molecules using local probes. *Science* 1999, 283, 1683-1688.

155. Moore, A. M.; Weiss, P. S. Functional and spectroscopic measurements with scanning tunneling microscopy. *Annu. Rev. Anal. Chem.* 2008, 1, 857-882.

156. Chen, F.; Tao, N. J. Electron transport in single molecules: from benzene to graphene. *Acc. Chem. Res.* 2009, 42, 429-438.

157. Donhauser, Z. J.; Price, D. W.; Tour, J. M.; Weiss, P. S. Control of alkanethiolate monolayer structure using vapor-phase annealing. *J. Am. Chem. Soc.* 2003, 125, 11462-11463.

158. Krans, J. M.; Vanruitenbeek, J. M.; Fisun, V. V.; Yanson, I. K.; Dejongh, L. J. The signature of conductance quantization in metallic point contacts. *Nature* 1995, 375, 767-769.

159. Nielsen, S. K.; Noat, Y.; Brandbyge, M.; Smit, R. H. M.; Hansen, K.; Chen, L. Y.; Yanson, A. I.; Besenbacher, F.; van Ruitenbeek, J. M. Conductance of single-atom platinum contacts: Voltage dependence of the conductance histogram. *Phys. Rev. B* 2003, 67.

160. Qin, L. D.; Park, S.; Huang, L.; Mirkin, C. A. On-wire lithography. *Science* 2005, 309, 113-115.

161. Lorente, N.; Persson, M.; Lauhon, L. J.; Ho, W. Symmetry selection rules for vibrationally inelastic tunneling. *Phys. Rev. Lett.* 2001, 86, 2593-2596.

162. Lauhon, L. J.; Ho, W. Single-molecule vibrational spectroscopy and microscopy: CO on Cu(001) and Cu(110). *Phys. Rev. B* 1999, 60, R8525-R8528.

163. Reed, M. A.; Zhou, C.; Muller, C. J.; Burgin, T. P.; Tour, J. M. Conductance of a molecular junction. *Science* 1997, 278, 252-254.

164. Selzer, Y.; Cabassi, M. A.; Mayer, T. S.; Allara, D. L. Thermally activated conduction in molecular junctions. *J. Am. Chem. Soc.* 2004, 126, 4052-4053.

165. Chen, F.; Hihath, J.; Huang, Z.; Li, X.; Tao, N. J. Measurement of single-molecule conductance. *Annu. Rev. Phys. Chem.* 2007, 58, 535-564.

166. Xue, Y. Q.; Datta, S.; Ratner, M. A. Charge transfer and "band lineup" in molecular electronic devices: A chemical and numerical interpretation. *J. Chem. Phys.* 2001, 115, 4292-4299.

167. Xue, Y. Q.; Ratner, M. A. Microscopic study of electrical transport through individual molecules with metallic contacts. I. Band lineup, voltage drop, and high-field transport. *Phys. Rev. B* 2003, 68.

168. Xu, B. Q.; Tao, N. J. J. Measurement of single-molecule resistance by repeated formation of molecular junctions. *Science* 2003, 301, 1221-1223.

169. Lindsay, S. M.; Ratner, M. A. Molecular transport junctions: Clearing mists. *Adv. Mater.* 2007, 19, 23-31.

170. Park, Y. S.; Whalley, A. C.; Kamenetska, M.; Steigerwald, M. L.; Hybertsen, M. S.; Nuckolls, C.; Venkataraman, L. Contact chemistry and single-molecule conductance: a comparison of phosphines, methyl sulfides, and amines. *J. Am. Chem. Soc.* 2007, 129, 15768-15769.

171. Chen, F.; Li, X.; Hihath, J.; Huang, Z.; Tao, N. Effect of anchoring groups on single-molecule conductance: comparative study of thiol-, amine-, and carboxylic-acid-terminated molecules. *J. Am. Chem. Soc.* 2006, 128, 15874-15881.

172. Pathem, B. K.; Claridge, S. A.; Zheng, Y. B.; Weiss, P. S. Molecular switches and motors on surfaces. *Annu. Rev. Phys. Chem.* 2013, 64, 605-630.

173. Metzger, R. M. Unimolecular electrical rectifiers. *Chem. Rev.* 2003, 103, 3803-3834.

174. Geddes, N. J.; Sambles, J. R.; Jarvis, D. J.; Parker, W. G.; Sandman, D. J. Fabrication and investigation of asymmetric current-voltage characteristics of a metal/Langmuir-Blodgett monolayer/metal structure. *Appl. Phys. Lett.* 1990, 56, 1916-18.

175. Geddes, N. J.; Sambles, J. R.; Jarvis, D. J.; Parker, W. G.; Sandman, D. J. The electrical properties of metal-sandwiched Langmuir-Blodgett multilayers and monolayers of a redox-active organic molecular compound. *J. Appl. Phys.* 1992, 71, 756-68.

176. Krzeminski, C.; Delerue, C.; Allan, G.; Vuillaume, D.; Metzger, R. M. Theory of electrical rectification in a molecular monolayer. *Phys. Rev. B* 2001, 64.

177. Metzger, R. M.; Xu, T.; Peterson, I. R. Electrical rectification by a monolayer of hexadecylquinolinium tricyanoquinodimethanide measured between macroscopic gold electrodes. *J. Phys. Chem. B* 2001, 105, 7280-7290.

178. Ashwell, G. J.; Urasinska, B.; Tyrrell, W. D. Molecules that mimic Schottky diodes. *Phys. Chem. Chem. Phys.* 2006, 8, 3314-3319.

179. Donhauser, Z. J.; Mantooth, B. A.; Pearl, T. P.; Kelly, K. F.; Nanayakkara, S. U.; Weiss, P. S. Matrix-mediated control of stochastic single molecule conductance switching. *Jpn. J. Appl. Phys., Part 1.* 2002, 41, 4871-4877.

180. Zhou, X. L.; Zhu, X. Y.; White, J. M. Photochemistry at adsorbate/metal interfaces. *Surf. Sci. Rep.* 1991, 13, 73-220.

181. Comstock, M. J.; Levy, N.; Kirakosian, A.; Cho, J.; Lauterwasser, F.; Harvey, J. H.; Strubbe, D. A.; Frechet, J. M. J.; Trauner, D.; Louie, S. G.; Crommie, M. F. Reversible photomechanical switching of individual engineered molecules at a metallic surface. *Phys. Rev. Lett.* 2007, 99.

182. Comstock, M. J.; Levy, N.; Cho, J.; Berbil-Bautista, L.; Crommie, M. F.; Poulsen, D. A.; Frechet, J. M. J. Measuring reversible photomechanical switching rates for a molecule at a surface. *Appl. Phys. Lett.* 2008, 92.

183. Hagen, S.; Kate, P.; Leyssner, F.; Nandi, D.; Wolf, M.; Tegeder, P. Excitation mechanism in the photoisomerization of a surface-bound azobenzene derivative: Role of the metallic substrate. *J. Chem. Phys.* 2008, 129.

184. Pathem, B. K.; Zheng, Y. B.; Payton, J. L.; Song, T.-B.; Yu, B.-C.; Tour, J. M.; Yang, Y.; Jensen, L.; Weiss, P. S. Effect of tether conductivity on the efficiency of photoisomerization of azobenzene-functionalized molecules on Au{111}. *J. Phys. Chem. Lett.* 2012, 3, 2388-2394.

185. Davis, J. J.; Orlowski, G. A.; Rahman, H.; Beer, P. D. Mechanically interlocked and switchable molecules at surfaces. *Chem. Commun.* 2010, 46, 54-63.

186. Collier, C. P.; Mattersteig, G.; Wong, E. W.; Luo, Y.; Beverly, K.; Sampaio, J.; Raymo, F. M.; Stoddart, J. F.; Heath, J. R. A [2]catenane-based solid state electronically reconfigurable switch. *Science* 2000, 289, 1172-1175.

187. Stoddart, J. F. The chemistry of the mechanical bond. *Chem. Soc. Rev.* 2009, 38, 1802-1820.

188. Coskun, A.; Spruell, J. M.; Barin, G.; Dichtel, W. R.; Flood, A. H.; Botros, Y. Y.; Stoddart, J. F. High hopes: Can molecular electronics realize its potential? *Chem. Soc. Rev.* 2012, 41, 4827-4859.

189. Juluri, B. K.; Kumar, A. S.; Liu, Y.; Ye, T.; Yang, Y.-W.; Flood, A. H.; Fang, L.; Stoddart, J. F.; Weiss, P. S.; Huang, T. J. A mechanical actuator driven electrochemically by artificial molecular muscles. *ACS Nano* 2009, 3, 291-300.

190. Ye, T.; Kumar, A. S.; Saha, S.; Takami, T.; Huang, T. J.; Stoddart, J. F.; Weiss, P. S. Changing stations in single bistable rotaxane molecules under electrochemical control. *ACS Nano* 2010, 4, 3697-3701.

191. Mayne, A. J.; Dujardin, G.; Comtet, G.; Riedel, D. Electronic control of single-molecule dynamics. *Chem. Rev.* 2006, 106, 4355-4378.

192. Lauhon, L. J.; Ho, W. Single-molecule chemistry and vibrational spectroscopy: pyridine and benzene on Cu(001). *J. Phys. Chem. A* 2000, 104, 2463-2467.

193. Hla, S. W.; Bartels, L.; Meyer, G.; Rieder, K. H. Inducing all steps of a chemical reaction with the scanning tunneling microscope tip: Towards single molecule engineering. *Phys. Rev. Lett.* 2000, 85, 2777-2780.

194. Blake, M. M.; Nanayakkara, S. U.; Claridge, S. A.; Fernandez-Torres, L. C.; Sykes, E. C. H.; Weiss, P. S. Identifying reactive intermediates in the ullmann coupling reaction by scanning tunneling microscopy and spectroscopy. *J. Phys. Chem. A* 2009, 113, 13167-13172.

195. Kim, M.; Hohman, J. N.; Cao, Y.; Houk, K. N.; Ma, H.; Jen, A. K. Y.; Weiss, P. S. Creating favorable geometries for directing organic photoreactions in alkanethiolate monolayers. *Science* 2011, 331, 1312-1315.

196. Bustamante, C.; Macosko, J. C.; Wuite, G. J. L. Grabbing the cat by the tail: manipulating molecules one by one. *Nat. Rev. Mol. Cell Biol.* 2000, 1, 130-136.

197. Kelley, A. M.; Michalet, X.; Weiss, S. Perspectives: Chemical physics: Single-molecule spectroscopy comes of age. *Science* 2001, 292, 1671-1672.

198. Greenleaf, W. J.; Woodside, M. T.; Block, S. M. High-resolution, single-molecule measurements of biomolecular motion. *Annu. Rev. Biophys. Biomol. Struct.* 2007, 36, 171-190.

199. Harpaz, Y.; Gerstein, M.; Chothia, C. Volume changes on protein folding. *Structure* 1994, 2, 641-9.

200. Srinivasan, C.; Mullen, T. J.; Hohman, J. N.; Anderson, M. E.; Dameron, A. A.; Andrews, A. M.; Dickey, E. C.; Horn, M. W.; Weiss, P. S. Scanning electron microscopy of nanoscale chemical patterns. *ACS Nano* 2007, 1, 191-201.

201. Stranick, S. J.; Kamna, M. M.; Weiss, P. S. Atomic-scale dynamics of a two-dimensional gas-solid interface. *Science* 1994, 266, 99-102.

CHAPTER 2

Detection of Single-Molecule Optical Absorption with Ångström-Scale Precision:

Chemical Specificity Revealed in Scanning Tunneling Microscopy

2.1 Introduction

The interaction of light with a molecular junction is an interesting and challenging scientific problem in many respects. Techniques such as tip-enhanced Raman spectroscopy,[1,2] inelastic electron tunneling spectroscopy,[3] and ultrafast optical excitation[4-6] use photons as a characterization tool and have revealed unprecedented spatial and temporal details of surface adsorbates and their interactions with substrates. At the same time, there is a growing effort in exploiting the control afforded by electromagnetic waves at molecular junctions. The radiation field can induce photophysical and photochemical transitions that alter the electronic structure and conformation at the molecular scale.[7,8] Compared with controlling by a gate potential, whose efficiency reduces in systems of nanoscale dimensions, using light has the advantages of speed and selectivity in governing junction conduction

Scanning tunneling microscopy offers highly localized, real-space information, and substantially better spatial resolution than optical methods,[9] enabling the study of atoms, molecules, and nanomaterials in real time and space. However, the lack of chemical specificity is a trade-off for the otherwise extraordinary resolution. Chemical identification is interpretive, and it is challenging to treat a chemically complex sample quantitatively. From a technical standpoint, numerous problems stem from the application of light to a molecular tunneling junction, including the need to discern genuine optical effects from those associated with thermal effects, such as lateral tip drift, thermal expansion, etc.[10-12] Most of the available techniques require ultrahigh vacuum and/or low temperature.[12-14] They have achieved high stability and resolution, but the compromise is that observations are time-consuming and complicated. Therefore, a STM that measures photoinduced electrical signal from single molecule with little junction heating and functions at ambient condition proves to be a versatile tool in molecular optoelectronics research. Here, we introduce our custom-built laser-assisted STM (photon STM) that eliminates the effects of laser heating by evanescent field excitation of the tunneling junction using Kretschmann-Raether geometry,[15,16] establishing stable imaging conditions with long-duration illumination at room temperature. This configuration was first described and used by Scherer and co-workers.[20]

We investigate the optical response of single organic molecules with Ångström-scale precision with the photon STM. Thin Au{111} films on *c*-cut sapphire prisms serves as the substrate of *n*-alkanethiolate monolayer, which isolates and stabilizes organic molecules[8,17,18] for single-molecule optical spectroscopy. Light modulation, combined with phase-sensitive detection, improves the photoresponse registry. The STM tip, as a near-field detector, collects both spatial and optical information of the excited molecules.[19,20] Under illumination, photoconductive anthracene derivatives undergo strong charge-transfer transitions into their excited states and the produced current is detected.

2.2 Methods

2.2.1 System Design

The custom-built photon STM (Figure 2.1) operates under ambient environmental conditions. The incident light, coming from the back of the sample, undergoes total internal reflection at the half-cylindrical sapphire prism surface and forms evanescent field that excites the molecules adsorbed on the Au film. The field intensity in the immediate vicinity of the Au/air interface decays exponentially normal to the surface, and its penetration depth is on the order of a fraction of the input light wavelength (Figure 2.2).[21] As a result, the bulk of the tip is not illuminated in this configuration. Due to their high surface specificity, evanescent optical modes enable us to monitor sensitive electrical signals created by the molecular bridge.

The expected laser-induced tunneling current that reflects the fast surface dynamics is only a small contribution to the total tunneling current. It is because this current flows only during the short lifetime of the surface excitation, whereas the total tunneling current flows continuously. Therefore, rapid amplitude modulation of laser light with a mechanical chopper, combined with photo-sensitive detection facilitates photoresponse registration.

Vibrational and Electrical Noise Reduction

The acoustic enclosure (Herzan LLC, NanoVault) housing the STM and optical system are isolated from floor vibrations by bolting them to an optical table top (Newport SmartTable®) with pneumatic legs and active damping cancellation. In order to avoid mechanical disturbances from the cables passing through the wall of acoustic chamber, they are clamped tightly with foam. The STM is placed on a vibration isolation platform (Minus K Technology Inc., 100BM) that has a 1.5 Hz horizontal and 0.5 Hz vertical natural frequency. The temperature inside the enclosure fluctuates 1-2 ºC when its door is opened and closed. We measure the temperature using a thermocouple near tunneling junction with an Ethernet data acquisition interface (NI ENET-9163). Light-induced current measurements are only taken when thermal equilibrium is reached inside the chamber. To reduce 60 Hz line signal, ground connection of all electronic devices are joined into a separate master ground. Extra precaution has been taken to minimize electromagnetic noise: covering the tunneling junction with a μ-metal Faraday cage, having all the electronic devices in the acoustic enclosure shut off, and eliminating ground loops.

Scanning Tunneling Microscope

The STM scanner (Figure 2.3C) is a piezoelectric tube, on which the probe tip is fixed, mounted on two sets of approach micro slides (Omicron MS-5, 40-400 nm movement per step in 5 mm distance) employed for coarse tip positioning in the X (parallel to the ground beneath the microscope) and Z (sample surface normal) directions, so that the STM tip can be brought within tunneling range and reach an area of ~5 mm × 2.4 μm on the surface. We use mechanically cut Pt/Ir wire (80/20%) of 250 μm diameter (Goodfellow Cambridge Ltd.) as tips. The piezoelectric tube (EBL Products Inc.) has hollow cylindrical shape. Four divided quadrants are used for XY (surface plane) motion while inner electrode controls the Z motion. The piezo-tube is electrically isolated from micro slides through Macor base, which is glued to the tube to reduce differential thermal expansion. The tunneling current is detected using preamplifier (RHK Technology, Inc., Stage I: IVP-300, 10^9 V/A gain and Stage II: IVP-PGA, ×10 gain selected) configured to 10^{10} V/A gain and 5 kHz bandwidth.

Sample Holder

The custom-built sample holder made of stainless steel is shown in Figure 2.3B. A half-cylindrical prism is fixed in position by screwing a cap with a hole in the center. The gold foil on the cap makes direct contact with the top surface of the sample and provides electrical contact to the current preamplifier via a gold spring. To prevent the spring from being shorted with electrically grounded sample holder, the stainless steel surface surrounding the spring is insulated with nail polish. The slit at the rear of the sample holder offers passage to incident and reflected laser beams.

Light Coupling

The laser beam (*p*-polarized, 405 ± 5 nm, Coherent Inc. CUBE diode laser) is transmitted through a broadband window on the wall of the acoustic enclosure and focused onto the Au/air interface by a converging lens (focal length = 75 mm). The alignment of the focusing lens in the XYZ directions is accomplished by stepper motor actuator (Newport Corporation, TRA25PPD). We have installed a motorized continuous rotation stage (Thorlabs Inc., CR1Z7) to align the lens focal plane perpendicular to the propagation direction of the incident beam. The light incident angle at Au/sapphire interface can be varied by revolving the scanner and prism holder with the rotating stage (Newport Corporation, RV160PE-F) underneath. We analyze the light reflected off the interface at discrete incident angles via a CCD camera beam profiler (Thorlabs Inc., BC106-VIS) that orbits around the tip/sample junction.

One crucial part of the photon STM is to have the probe tip scan the area that the laser beam illuminates. We adjust the tip height (Y direction, perpendicular to the ground beneath the microscope) relative to incident beam via the vibration stage. For the X direction, the tip is positioned by moving the micro slide on which it resides, according to the view of tip/sample junction (Figure 2.3D) through a digital camera (Thorlabs Inc., DCU223C) that has XYZ motion with respect to the junction fully controlled by motorized translation stages (Newport Corporation, ILS200CC and Thorlabs Inc., MTS Series).

The incident field is modulated by a chopper wheel (Thorlabs Inc., MC1F60) at 4.5 kHz. Hence, the laser on/off switching rate is faster than the responsive time (approximately 1 ms) of the tip height control loop. With the chopper frequency reference signal connected to the lock-in amplifier (LIA) reference input, light-triggered current is recorded phase sensitively.

2.2.2 Substrate Preparation

Thin (45 nm), flat (roughness 0.3-1 nm) epitaxial Au {111} films are deposited on *c*-cut sapphire cylindrical prisms (Figure 2.4A). Half-cylindrical sapphire prisms (1 cm × 1 cm, 1 cm diameter) with *epi*-polished *c*-cut planes, Al_2O_3(0001) were purchased from Meller Optics (Providence, RI). These substrates were annealed in air at 1100 and 1400 ºC for 24 h and 18 h, respectively, in consecutive cycles.

Thin Au{111} films were grown on *c*-cut plane sapphire prisms with a Nb seed layer.[22] The annealed sapphire substrates were introduced to the ultrahigh vacuum evaporator chamber with a base pressure in the 10^{-10} mbar range, and were outgassed for 1 h at 150 °C to remove adsorbed water. A 2-nm-thick Nb seed layer was evaporated at a rate of 0.15 Å/s at room temperature.[23] The pressure increased to $\sim 5 \times 10^{-9}$ mbar during evaporation. Room temperature deposition favors the Nb{110} orientation over Nb{111}, while elevated temperatures (over 800 °C) yield Nb{111}.[24] The orientation of Au{111} is parallel to Nb{110} with the epitaxial relationship as follows:[23,25,26] $Au(111)[0\bar{1}1]\|Nb\{111\}[001]\|Al_2O_3/0001/[1\ 0\ \bar{1}0]$.

Thin Au films (45 nm, Figure 2.5A) were then deposited at a substrate temperature of 300 ºC and an evaporation rate of 0.50 Å/s. The surface temperature should not exceed 300 ºC, to avoid inter-diffusion and intermetallic compounds (primarily $AuNb_3$ and Au_2Nb_3) that occur above 325 ºC.[27]

Sapphire prisms can be recycled by etching off the metal. The Au film is removed by immersing the substrate in *aqua regia* solution for approximately 30 s. After the prisms are rinsed with copious deionized water, they are submerged into chemical etchant (70% HNO_3 : 49%

HF = 1:1) for three days to remove Nb and subsequently washed with water and blown dry. Complete removal of Nb is critical for atomically flat gold film growth, and Nb residue aggregates during annealing, roughening the surface.

A *n*-dodecanethiolate (**C12**) monolayer was assembled from the vapor phase on the Au{111}/Al_2O_3(0001) substrate with 1 mM *n*-dodecanethiol (Sigma Aldrich, St. Louis, MO) ethanolic solution. 9-(4-Mercaptophenylethynyl)anthracene (**MPEA**) molecules were inserted into a **C12** monolayer by placing the substrate into a 10 µM **MPEA** ethanolic solution for 10 min. Single-molecule insertion is highly sensitive to temperature, concentration, and time during assembly.

2.3 Results and Discussion

2.3.1 Substrate Quality

The thermal annealing of sapphire substrates at high temperatures is a crucial step to obtain atomically flat substrates for high-quality thin film fabrication.[28,29] Atomically flat sapphire substrates are expected to enhance epitaxial growth of films with sharp interfaces.[30] Among commercially available sapphire substrates with various crystallographic faces, the Al_2O_3 (0001) basal plane is a good candidate substrate for metal and semiconductor thin film growth.

The as-supplied Al_2O_3(0001) substrates show surface irregularity and are contaminated with grease from the commercial epi-polishing procedure (Figure 2.4B). Chemical cleaning with strong acids removes surface contaminants, however, such procedures attack surface defects faster, further roughening the surfaces.[31]

After thermal annealing, *c*-cut sapphire substrates exhibit a dramatic increase in the prevalence of fine, smooth surfaces with atomically flat terraces (~100 nm wide) and uniform atomic steps (~0.2 nm in height). Longer annealing (more than 24 h) at 1100 °C improves the step edge straightness (Figure 2.4C). However, the terrace sizes increase more slowly with the annealing time. Further annealing at 1400 °C doubles the terrace sizes (Figure 2.4D). Several repeated cycles of annealing at both 1100 and 1400 ºC substantially improves the overall substrate quality. Ultimately, the annealed substrates are air stable until metal deposition.

The $Al_2O_3(0001)$ terraces are no longer visible after Au deposition. Grains are discontinuous and are smaller than those observed for Au{111} evaporated on a mica substrate (Figure 2.5C). Substantial improvement of the Au film quality was observed after thermal and hydrogen flame annealing. Thermal annealing of metal films causes diffusion at grain boundaries, allowing them to merge, producing larger grains. Au atoms diffuse during heat treatments between 100 and 400 ºC.[32] Evaporated Au layers become smoother, even after annealing at 200 ºC in air for 24 h. This smoothing effect can be maximized by long-duration annealing at 400 ºC (Figure 2.5B).

Hydrogen flame annealing is another effective way to improve Au film quality.[33, 34] Flame annealing removes contaminants from the Au surface and increases the grain size. Flame annealing Au{111}/mica produces contaminant-free Au surfaces with terrace widths increased by a factor of 25 relative to the unannealed films.[35] After Au deposition, Au{111}/$Al_2O_3(0001)$ substrates were routinely annealed at 400 ºC for 24 h, and flame annealed immediately prior to self-assembly.

2.3.2 Scanning Tunneling Microscope Stability

In order to obtain a surface topography with high resolution or to perform tunneling spectroscopy while the tunneling junction is under illumination, the tip length has to be constant during the time required to record one image or one spectroscopic curve. Figure 2.6 shows that the tip displacement required to keep the distance between tip apex and surface constant is not affected by the laser. The tunneling junction is stable with laser power up to 10 mW, which is much higher than the power used for direct illumination (< 1 mW). However, at 20 mW, heating from the laser causes the tip length change and a heat-induced current.

We utilize *n*-alkanethiolate monolayers on Au/{111}Al_2O_3(0001) as a background matrix for single-molecule optical absorption measurements. The height of the matrix can be tuned by altering the alkyl chain length to support light-absorbing organic molecules such that the matrix is slightly shorter than the inserted photosensitive molecules. The stability of the SAM matrix is critical to resolve the intrinsic photoinduced activities of the inserted molecules, excluding any outside systematic effects such as heating, electric field, and non-linear harmonic oscillation.

n-Dodecanethiolate (**C12**) SAMs on sapphire-prism-supported Au{111} films display standard SAM features and hexagonally close packing, identical to those on Au{111}/mica. Terrace sizes on the sapphire-supported films are smaller (~500 Å) than observed for high-quality Au on mica (~1500 Å). Small terraces with many steps are frequently observed (Figure 2.7A), which reduces the tunneling junction stability. Substrate vacancy islands (red arrows), step edges (blue arrows), and domain boundaries (yellow arrows), shown in Figure 2.7B indicates no systematic difference from **C12** monolayer on Au{111}/mica. A molecularly resolved STM image, Figure 2.7C, shows the **C12** molecules arrange in $(\sqrt{3}\times\sqrt{3})R30^\circ$ hexagonal lattice.

2.3.3 Optical Sensitivity and Chemical Selectivity

While the STM probe tip is scanning over the surface, the junction is illuminated by a laser at an incident angle of 37°. The topography and light-induced current were obtained simultaneously with modulated laser illumination (Figure 2.8). The anthracene derivative, 9-(4-mercapto-phenylethynyl)anthracene (**MPEA**) was selected for photocurrent mapping. It is a conductive organic molecule due to delocalized π conjugation interactions, providing a good pathway for electron conduction and served as the base for a member of molecular dyads and triads used for solar cells.[36-38]

To measure its molecular photoconductivity, **MPEA** molecules were inserted into a **C12** SAM on Au{111}/Al_2O_3(0001) (Figure 2.8A). In topographic STM images, these inserted molecules protrude from the surrounding **C12** SAM matrix (Figure 2.8C), because they are both longer than the matrix molecules and conductive due to π conjugation.[37] Isolated **MPEA** molecules within a **C12** matrix respond to 405 nm illumination (Figure 2.8D).[39] The photocurrent originates from electron transfer from singlet excited **MPEA** to the tip. The non-zero LIA signal from the surrounding matrix is due to photo-induced tunneling of hot-electrons in gold and instrumental electronic noise. More frequent absorption of **MPEA** molecules was observed along step edges rather than around vacancy islands or domain boundaries. Photon STM enables chemical identification of optically sensitive molecules based on their energy selectivity.

2.3.4 Single-Molecule Photoconductance Measurement

The current-voltage (I-V) response of an isolated **MPEA** molecule with and without illumination indicates that the molecule is optically active; producing higher tunneling currents while irradiated (Figure 2.8B). The current collected without illumination appears flat when plotted on the same vertical axis scale as photocurrent. No corresponding current increase was observed for the illuminated **C12** monolayer. Evanescent field at **MPEA** is considered to be the driving force of increased charge flux. Current through the ground state is blocked by the filled electron reservoir on one side of the junction, however, optical excitation effectively transfers electrons in **MPEA** from ground to excited state, leading to a higher total current through the junction.[40] In addition, hot electrons excited in the metal leads can tunnel into the unoccupied states of **MPEA** and contribute to the light-induced current.[41]

2.4 Conclusions and Prospects

The photon STM presented here is designed to measure the intrinsic photocurrent or photoconductance of single molecules, and enables local probes of excited state photochromic and photoreactive molecules. It also enables us to conduct photochemical reactions of organic molecules in controlled, stable environments. The system can resolve the photoinduced effects of single molecules with spectral and temporal selectivity. Improvements in Au{111} substrate quality offer better imaging characteristics, enabling long-duration monitoring even under ambient environmental conditions.

This microscope can be easily modified to add further capabilities. For example, it is possible to study the surface plasmon resonances of individual particles including nanoclusters,[42,43] nanoprisms,[44,45] and nanocages.[46,47] The photon STM can detect local details of topographic and optoelectronic differences with sub-nanometer precision. It can also be applied to liquid systems to study biological specimens under illumination. Photon STM measurements do not require fluorescent tags, and the technique can be applied to measure photoinduced charge transport within single biomolecules, such as DNA.[48,49]

Most importantly, photon STM can serve as a diagnostic tool to measure the intrinsic photovoltaic efficiency of single organic molecules for solar cell applications. By investigating candidate molecules with photon STM, we can obtain insight into the photovoltaic effect with molecular resolution and provide direct figures of merit for energy conversion. Specifically, details of the orientation and contacts can be extracted in a way inaccessible to ensemble measurements of organic photovoltaics. These studies will provide important design principles and feedback for synthetic chemists, and help to determine key components for efficient light conversion. Candidate molecules must first be objectively compared at the molecular level for photovoltaic efficiency prior to device fabrication, which will enable the interpretation of negative results of photovoltaic device candidates.

Multiple wavelengths of light can be introduced simultaneously to resolve samples that contain mixtures of molecules. Two-photon and time-resolved pulse-probe experiments are also accessible. Photon STM can thus be used to improve our understanding of a wide range of chemical systems. Our instrument configuration takes advantage of full access to the sample surface. Light illumination is isolated from the sample side. This facile access to the sample surface will enable us to characterize photothermal effects, fluorescence, and light scattering in the near field.[50-52]

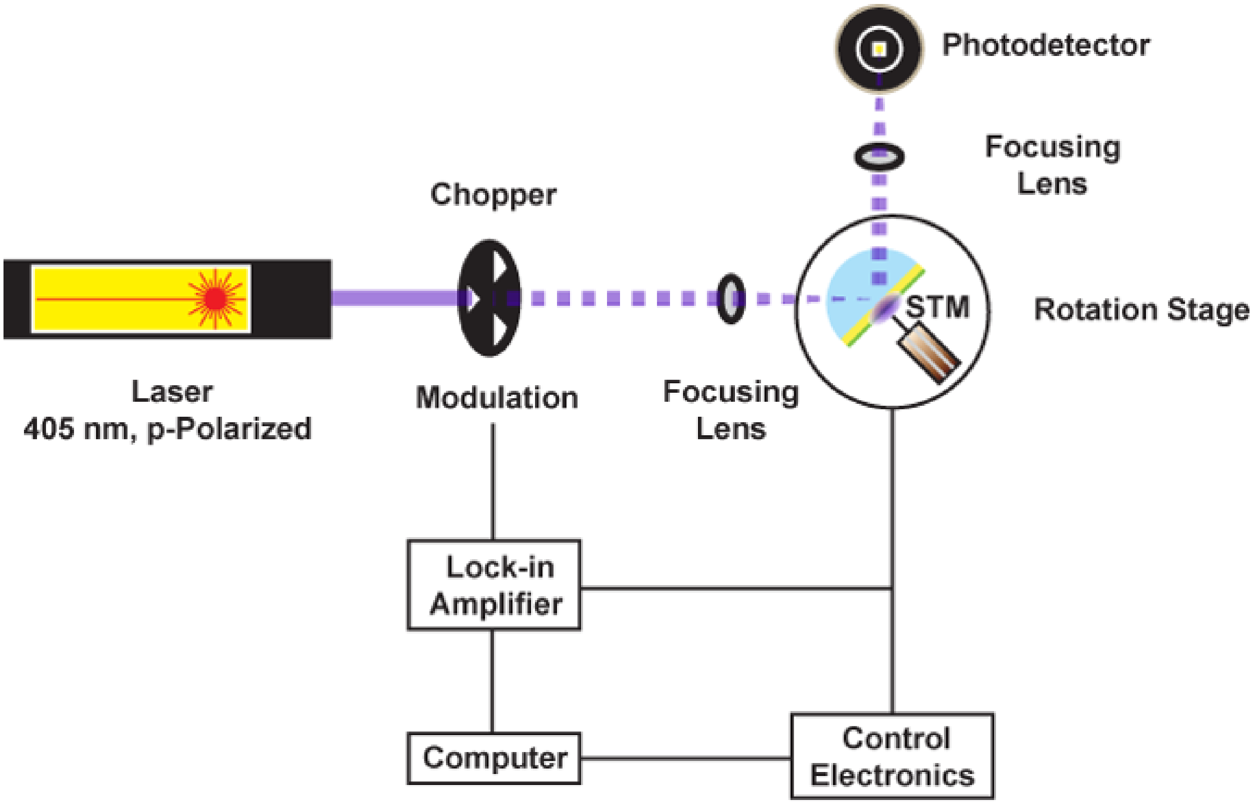

Figure 2.1 Schematic illustration of the experimental setup for the photon STM experiment.

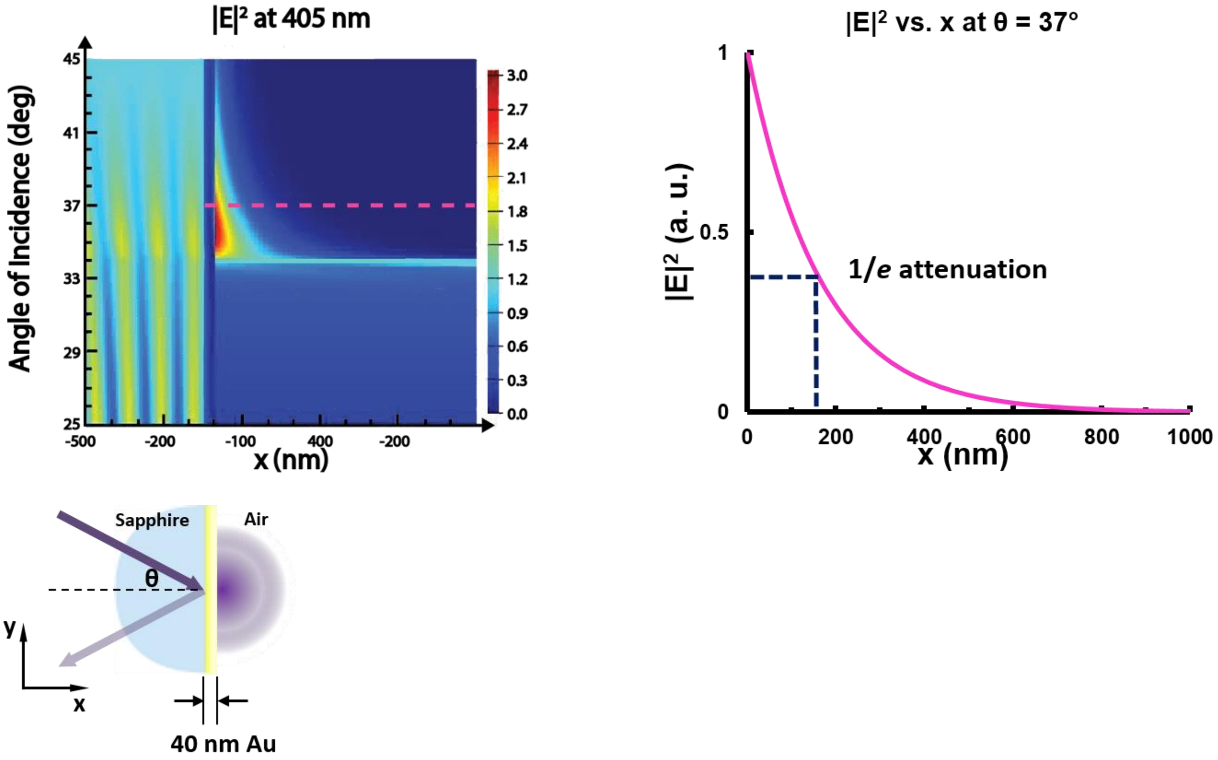

Figure 2.2 Left, electric field intensity ($|E|^2$) distribution at sapphire/Au/Air interface for different incident angles, simulated with finite-difference time-domain method. A *p*-polarized planewave, with a wavelength of 405 nm, propagates from the sapphire toward the interface. As the incident angle exceeds the critical angle for total internal reflection, an evanescent field penetrating the Au surface appears. Right, electric field intensity is plotted as a function of position x at 37° incidence angle. The depth of penetration, defined by the 1/*e* attenuation is approximately 160 nm. At this wavelength, the incident electromagnetic field excites an interband transition in the gold, instead of surface plasmons. The thickness of gold film is 40 nm.

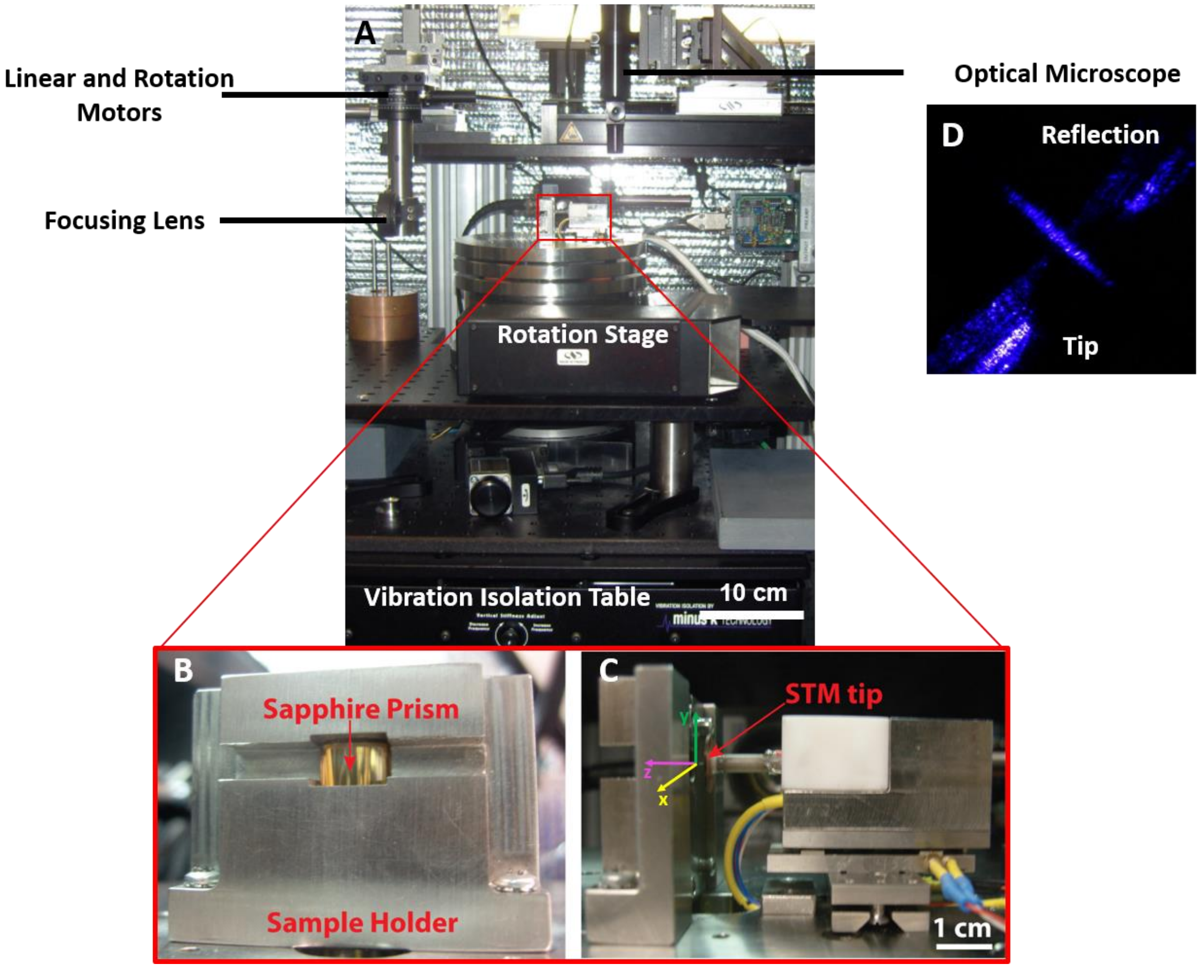

Figure 2.3 Photographs of **(A)** Photon STM setup, **(B)** sample holder, and **(C)** STM scanner. **(D)** Optical microscope image of the tunneling junction.

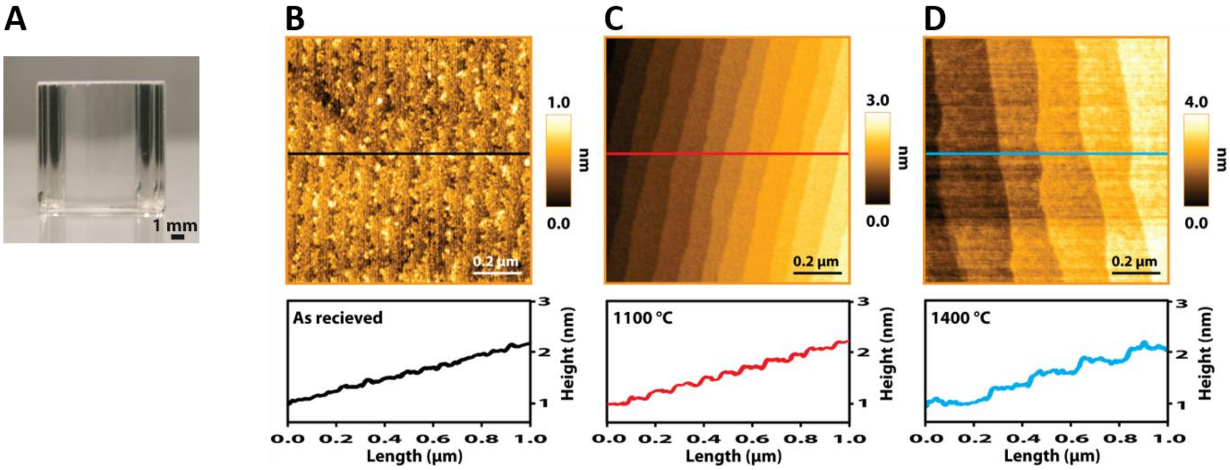

Figure 2.4 Thermal treatment of *c*-cut sapphire prisms for atomically flat substrates. **(A)** Photograph of a *c*-cut sapphire cylindrical prism. Atomic force microscopy images (top) and line profiles (bottom) of $Al_2O_3(0001)$ prisms, **(B)** as-supplied, **(C)** after annealing at 1100 °C for 24 h, and **(D)** after another subsequent annealing at 1400 °C for 18 h. Imaging parameters: amplitude set point: 200 mV; drive frequency: 270 kHz, scan rate: 2 Hz. A line profile was taken along the line indicated in the middle images. The as-received substrates contain grease contaminants due to *epi*-polishing and irregularly rough surface with hardly distinguishable steps. Thermal treatment at 1100 °C smooths the entire surface, producing atomically flat terraces with straight linear steps. Further heat treatment at 1400 °C doubles the terrace sizes.

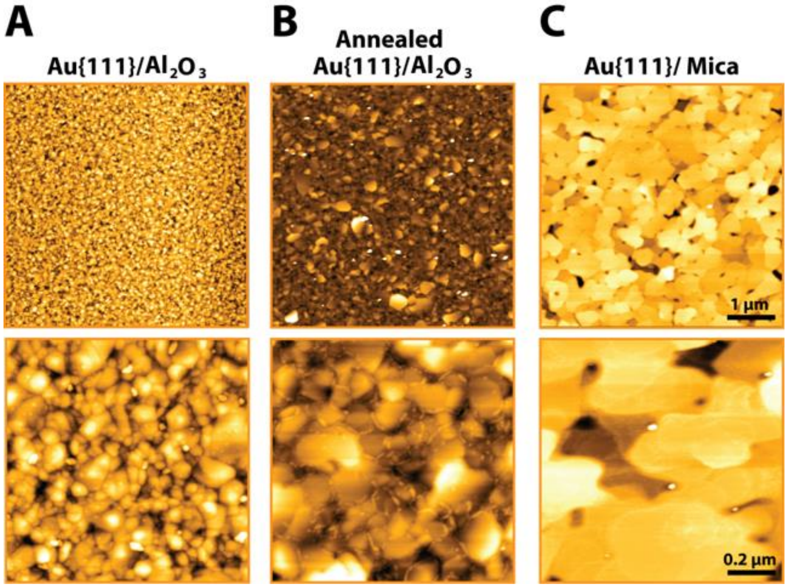

Figure 2.5 Au{111} film deposition and thermal annealing for high-quality substrates with large {111} terraces. Atomic force microscopy images of **(A)** a 45-nm-thick Au{111} film deposited on 2-nm-thick Nb on a $Al_2O_3(0001)$ prism, **(B)** after thermal annealing at 400 ºC for 24 h, and **(C)** a 150-nm-thick Au{111}/mica substrate (Agilent, Santa Clara, CA). Imaging parameters: amplitude set point: 200 mV; drive frequency: 270 kHz; scan rate: 2.5 Hz. Small grains and large gaps around grain boundaries observed before thermal annealing. Thermal annealing at 400 ºC increases the grain sizes and generates many large flat terraces. Small curved islands between grains are attributed to Au residue from migration during annealing (B, bottom). The grains of Au{111} on mica are much larger than those for Au films grown on $Al_2O_3(0001)$ substrates.

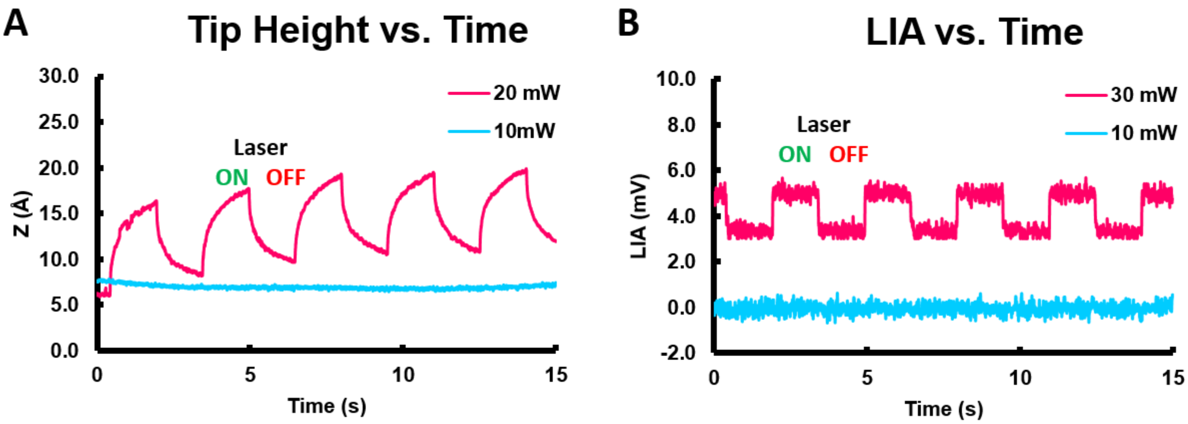

Figure 2.6 Scanning tunneling microscope tip length modulation depends on the laser power. Tip height **(A)** and laser induced signal **(B)** are plotted as a function of time. The laser is turned on and off at 2 s intervals; while on, the laser is modulated at 4.5 kHz by a mechanical chopper. At 10 mW, heat expansion of the probe tip is negligible, however, at 20 mW, the tip length variation is compensated by the distance feedback loop of the STM and reflected in the tip height (z), leading to a displacement current recorded by the lock-in amplifier.

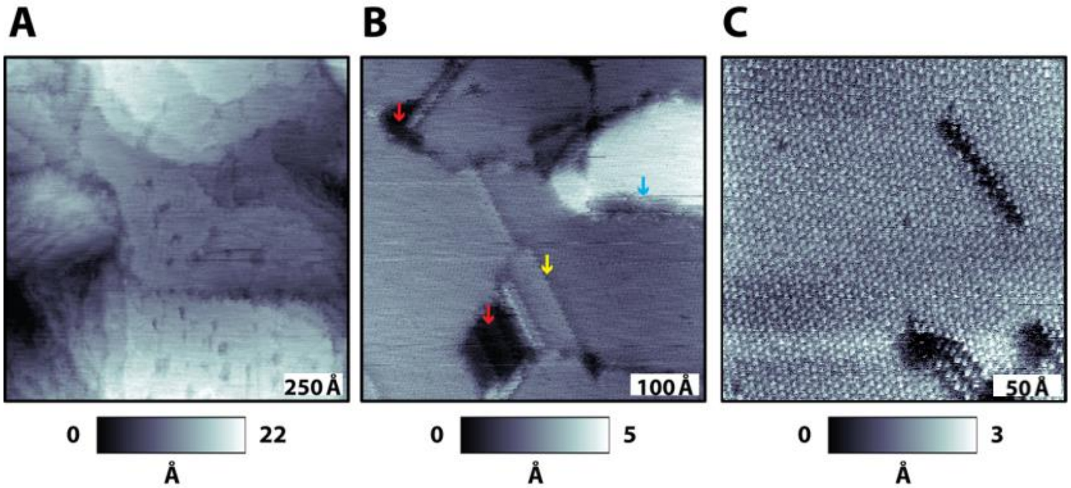

Figure 2.7 Scanning tunneling microscopy images of *n*-dodecanethiolate (**C12**) monolayers assembled on Au{111}/$Al_2O_3(0001)$ substrates, all obtained at a tunneling current of 1.0 pA and a sample bias voltage of -1.0 V. The average terrace size is smaller than for typical **C12** SAMs on Au/mica. **(A)** Terraces tilted in random orientations, and narrow terraces with many steps are often observed in large scan areas. (**B** and **C**) Hexagonal close packing and characteristic SAM features including vacancy islands (red arrow), domain boundaries (yellow arrow), and step edges (blue arrow) indicate that there are no systematic differences from **C12** SAMs on Au{111}/mica.

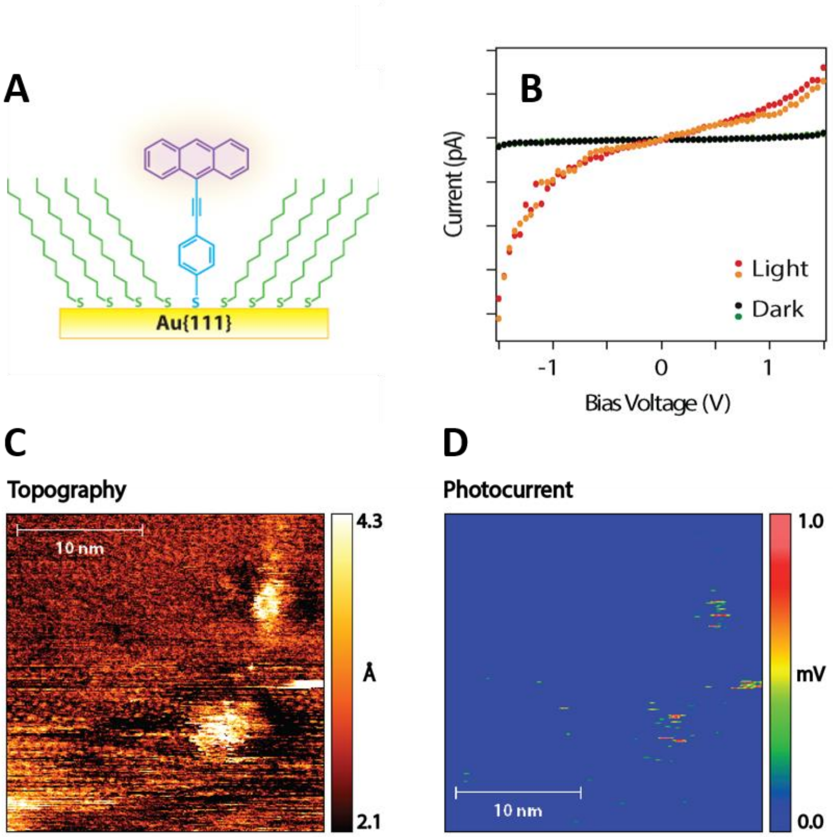

Figure 2.8 Photoconductance measurements of single organic molecules in a self-assembled monolayer with the photon STM. **(A)** Schematic illustration of 9-(4-mercaptophenylethynyl)anthracene (**MPEA)** molecules inserted into a **C12** monolayer assembled on a Au{111} film. **(B)** Scanning tunneling spectra of isolated single **MPEA** molecule in a **C12** monolayer with laser on (light, forward: red, reverse: orange circles) and off (dark, forward: black, reverse: green circles). Scanning tunneling microscopy images of simultaneously acquired topography **(C)**, photocurrent **(D)** of **MPEA**/**C12** molecular system. Upon evanescent field illumination with 405 nm incident light wavelength, **MPEA** molecules produce photocurrent while **C12** manifests little response to the radiation.

References

1. Schmid, T.; Opilik, L.; Blum, C.; Zenobi, R. Nanoscale chemical imaging using tip-enhanced raman spectroscopy: A critical review. *Angew. Chem. Int. Ed.* 2013, 52, 5940-5954.

2. Sonntag, M. D.; Pozzi, E. A.; Jiang, N.; Hersam, M. C.; Van Duyne, R. P. Recent advances in tip-enhanced raman spectroscopy. *J. Phys. Chem. Lett.* 2014, 5, 3125-3130.

3. Moore, A. M.; Weiss, P. S. Functional and spectroscopic measurements with scanning tunneling microscopy. *Annu. Rev. Anal. Chem.* 2008, 1, 857-882.

4. Gerstner, V.; Knoll, A.; Pfeiffer, W.; Thon, A.; Gerber, G. Femtosecond laser assisted scanning tunneling microscopy. *J. Appl. Phys.* 2000, 88, 4851-4859.

5. Wu, S. W.; Ho, W. Two-photon-induced hot-electron transfer to a single molecule in a scanning tunneling microscope. *Phys. Rev. B* 2010, 82, 085444.

6. Gaffney, K. J.; Miller, A. D.; Liu, S. H.; Harris, C. B. Femtosecond dynamics of electrons photoinjected into organic semiconductors at aromatic-metal interfaces. *J. Phys. Chem. B* 2001, 105, 9031-9039.

7. Pathem, B. K.; Claridge, S. A.; Zheng, Y. B.; Weiss, P. S. Molecular switches and motors on surfaces. *Annu. Rev. Phys. Chem.* 2013, 64, 605-630.

8. Kim, M.; Hohman, J. N.; Cao, Y.; Houk, K. N.; Ma, H.; Jen, A. K. Y.; Weiss, P. S. Creating favorable geometries for directing organic photoreactions in alkanethiolate monolayers. *Science* 2011, 331, 1312-1315.

9. Wiesendanger, R. *Scanning Probe Micoscopy and Spectroscopy*. Cambridge University Press: Cambridge, 1994.

10. Guhr, D. C.; Rettinger, D.; Boneberg, J.; Erbe, A.; Leiderer, P.; Scheer, E. Influence of laser light on electronic transport through atomic-size contacts. *Phys. Rev. Lett.* 2007, 99, 086801.

11. Gerstner, V.; Thon, A.; Pfeiffer, W. Thermal effects in pulsed laser assisted scanning tunneling microscopy. *J. Appl. Phys.* 2000, 87, 2574-2580.

12. Grafström, S. Photoassisted scanning tunneling microscopy. *J. Appl. Phys.* 2002, 91, 1717-1753.

13. Terada, Y.; Yoshida, S.; Takeuchi, O.; Shigekawa, H. Laser-combined scanning tunnelling microscopy for probing ultrafast transient dynamics. *J. Phys. Condens. Mat.* 2010, 22, 264008.

14. Bonnell, D. A.; Basov, D. N.; Bode, M.; Diebold, U.; Kalinin, S. V.; Madhavan, V.; Novotny, L.; Salmeron, M. B.; Schwartz, U. D.; Weiss, P. S. imaging physical phenomena with local probes: from electrons to photons. *Rev. Mod. Phys.* 2012, 84, 1343-1381.

15. Kretschmann, E. ATR method with focused light - application to guide waves on a grating. *Opt. Commun.* 1978, 26, 41-44.

16. Ballard, J. B.; Carmichael, E. S.; Shi, D. X.; Lyding, J. W.; Gruebele, M. Laser absorption scanning tunneling microscopy of carbon nanotubes. *Nano Lett.* 2006, 6, 45-49.

17. Bumm, L. A.; Arnold, J. J.; Cygan, M. T.; Dunbar, T. D.; Burgin, T. P.; Jones, L.; Allara, D. L.; Tour, J. M.; Weiss, P. S. Are single molecular wires conducting? *Science* 1996, 271, 1705-1707.

18. Cygan, M. T.; Dunbar, T. D.; Arnold, J. J.; Bumm, L. A.; Shedlock, N. F.; Burgin, T. P.; Jones, L.; Allara, D. L.; Tour, J. M.; Weiss, P. S. Insertion, conductivity, and structures of conjugated organic oligomers in self-assembled alkanethiol monolayers on Au{111}. *J. Am. Chem. Soc.* 1998, 120, 2721-2732.

19. Smith, D. A.; Owens, R. W. Laser-assisted scanning tunnelling microscope detection of a molecular adsorbate. *Appl. Phys. Lett.* 2000, 76, 3825-3827.

20. Feldstein, M. J.; Vohringer, P.; Wang, W.; Scherer, N. F. Femtosecond optical spectroscopy and scanning probe microscopy. *J. Phys. Chem.* 1996, 100, 4739-4748.

21. Knoll, W. optical characterization of organic thin-films and interfaces with evanescent waves. *MRS Bull.* 1991, 16, 29-39.

22. Kastle, G.; Boyen, H. G.; Koslowski, B.; Plettl, A.; Weigl, F.; Ziemann, P. Growth of thin, flat, epitaxial (111) oriented gold films on *c*-cut sapphire. *Surf. Sci.* 2002, 498, 168-174.

23. Wildes, A. R.; Mayer, J.; Theis-Brohl, K. The growth and structure of epitaxial niobium on sapphire. *Thin Solid Films* 2001, 401, 7-34.

24. Wagner, T. High temperature epitaxial growth and structure of Nb films on α-Al_2O_3(0001). *J. Mater. Res.* 1998, 13, 693-702.

25. Gutekunst, G.; Mayer, J.; Ruhle, M. Atomic structure of epitaxial Nb-Al_2O_3 interfaces. 1. Coherent regions. *Philos. Ma.g A, Phys. Condens. Matter Defects Mech. Prop.* 1997, 75, 1329-1355.

26. Wildes, A. R.; Cowley, R. A.; Ward, R. C. C.; Wells, M. R.; Jansen, C.; Wireen, L.; Hill, J. P. The structure of epitaxially grown thin films: a study of niobium on sapphire. *J. Phys. Condens. Mat.* 1998, 10, L631-L637.

27. Kitada, M. Reactions in Au/Nb bilayer thin-films. *Thin Solid Films* 1994, 250, 111-114.

28. Yoshimoto, M.; Maeda, T.; Ohnishi, T.; Koinuma, H.; Ishiyama, O.; Shinohara, M.; Kubo, M.; Miura, R.; Miyamoto, A. Atomic-scale formation of ultrasmooth surfaces on sapphire substrates for high-quality thin-film fabrication. *Appl. Phys. Lett.* 1995, 67, 2615-2617.

29. Nakamura, S.; Mukai, T.; Senoh, M. High-brightness InGaN/GaN double-heterostructure blue-green-light-emitting diodes. *J. Appl. Phys.* 1994, 76, 8189-8191.

30. Kawasaki, M.; Takahashi, K.; Maeda, T.; Tsuchiya, R.; Shinohara, M.; Ishiyama, O.; Yonezawa, T.; Yoshimoto, M.; Koinuma, H. Atomic control of the $SrTiO_3$ crystal-surface. *Science* 1994, 266, 1540-1542.

31. Cui, J.; Sun, A.; Reshichkov, M.; Yun, F.; Baski, A.; Morkoc, H. Preparation of sapphire for high quality III-nitride growth. *MRS Internet J. Nitride Semicond. Res.* 2000, 5, 1-6.

32. Porath, D.; Millo, O.; Gersten, J. I. Scanning tunneling microscopy studies and computer simulations of annealing of gold films. *J. Vac. Sci. Technol. B* 1996, 14, 30-37.

33. Adzic, R. R.; Hsiao, M. W.; Yeager, E. B.; Pruett, G. Scanning tunneling microscopy of stepped single-crystal surface of gold. *Surf. Sci.* 1992, 273, L425-L429.

34. Rundqvist, J.; Hoh, J. H.; Haviland, D. B. Substrate effects in poly(ethylene glycol) self-assembled monolayers on granular and flame-annealed gold. *J. Colloid Interface Sci.* 2006, 301, 337-341.

35. Dishner, M. H.; Ivey, M. M.; Gorer, S.; Hemminger, J. C.; Feher, F. J. Preparation of gold thin films by epitaxial growth on mica and the effect of flame annealing. *J. Vac. Sci. Technol. A* 1998, 16, 3295-3300.

36. Dou, R. F.; Ma, X. C.; Xi, L.; Yip, H. L.; Wong, K. Y.; Lau, W. M.; Jia, J. F.; Xue, Q. K.; Yang, W. S.; Ma, H.; Jen, A. K. Y. Self-assembled monolayers of aromatic thiols stabilized by parallel-displaced π-π stacking interactions. *Langmuir* 2006, 22, 3049-3056.

37. Zareie, M. H.; Ma, H.; Reed, B. W.; Jen, A. K. Y.; Sarikaya, M. Controlled assembly of conducting monomers for molecular electronics. *Nano Lett.* 2003, 3, 139-142.

38. Kang, M. S.; Kang, S. H.; Ma, H.; Kim, K. S.; Jen, A. K. Y. Efficient photocurrent generation through a self-assembled monolayer of C_{60}-mercaptophenylanthrylacetylene. *J. Power Sources* 2006, 160, 711-715.

39. Kim, M.; Hohman, J. N.; Cao, Y.; Houk, K. N.; Ma, H.; Jen, A. K.-Y.; Weiss, P. S. Creating favorable geometries for directing organic photoreactions in alkanethiolate monolayers. *Science* 2011, 331, 1312-1315.

40. Sukharev, M.; Galperin, M. Transport and optical response of molecular junctions driven by surface plasmon polaritons. *Phys. Rev. B* 2010, 81.

41. Wu, S. W.; Ogawa, N.; Ho, W. Atomic-scale coupling of photons to single-molecule junctions. *Science* 2006, 312, 1362-1365.

42. Smith, R. K.; Nanayakkara, S. U.; Woehrle, G. H.; Pearl, T. P.; Blake, M. M.; Hutchison, J. E.; Weiss, P. S. Spectral diffusion in the tunneling spectra of ligand-stabilized undecagold clusters. *J. Am. Chem. Soc.* 2006, 128, 9266-9267.

43. Claridge, S. A.; Castleman, A. W.; Khanna, S. N.; Murray, C. B.; Sen, A.; Weiss, P. S. Cluster-assembled materials. *ACS Nano* 2009, 3, 244-255.

44. Jin, R. C.; Cao, Y. W.; Mirkin, C. A.; Kelly, K. L.; Schatz, G. C.; Zheng, J. G. Photoinduced conversion of silver nanospheres to nanoprisms. *Science* 2001, 294, 1901-1903.

45. Sherry, L. J.; Jin, R. C.; Mirkin, C. A.; Schatz, G. C.; Van Duyne, R. P. Localized surface plasmon resonance spectroscopy of single silver triangular nanoprisms. *Nano Lett.* 2006, 6, 2060-2065.

46. Au, L.; Zheng, D. S.; Zhou, F.; Li, Z. Y.; Li, X. D.; Xia, Y. N. A quantitative study on the photothermal effect of immuno gold nanocages targeted to breast cancer cells. *ACS Nano* 2008, 2, 1645-1652.

47. Zeng, J.; Zhang, Q.; Chen, J. Y.; Xia, Y. N. A Comparison Study of the Catalytic Properties of Au-Based Nanocages, Nanoboxes, and Nanoparticles. *Nano Lett.* 2010, 10, 30-35.

48. Slinker, J. D.; Muren, N. B.; Renfrew, S. E.; Barton, J. K. DNA charge transport over 34 nm. *Nat. Chem.* 2011, 3, 228-233.

49. Genereux, J. C.; Barton, J. K. Mechanisms for DNA Charge Transport. *Chem. Rev.* 2010, 110, 1642-1662.

50. Harootunian, A.; Betzig, E.; Isaacson, M.; Lewis, A. Super resolution fluorescence near-field optical microscopy. *Appl. Phys. Lett.* 1986, 49, 674-676.

51. Lieberman, K.; Lewis, A. Simultaneous scanning tunneling and optical near-field imaging with a micropipette. *Appl. Phys. Lett.* 1993, 62, 1335-1357.

52. Formanek, F.; De Wilde, Y.; Aigouy, L.; Kwok, W. K.; Paulius, L.; Chen, Y. Nanometer-scale probing of optical and thermal near-fields with an apertureless NSOM. *Superlattices Microstruct.* 2004, 35, 315-323.

CHAPTER 3

Location-Controlled Incorporation of C_{60}-Donor-C_{60} Triad and Donor Derivative Molecules in the Same Matrix – Towards Molecular *p-n* Junctions Studies

3.1 Introduction

Donor-acceptor (D-A) heterojunctions (HJs) constitute the central components of organic solar cells. Better understandings into the generation and recombination processes of charge carriers at donor-acceptor and molecule-electrode interfaces will be crucial for further organic optoelectronics advances. Our photon STM offers the capability of identifying the involvement of electronic states, particular molecular orientations, and local environment that affect generation, transfer, and recombination at single molecule D-A HJs.

Due to their high degree of π-electron delocalization, fullerenes and their derivatives are studied extensively to understand and to utilize their interesting photochemical and photophysical properties.[1-4] Fullerene-based monolayers formed on metal oxides have been demonstrated to enhance electronic coupling between perovskites and polymer semiconductors and thus offers a promising route forward for hybrid photovoltaics.[5] C_{60}-tethered 2,5-dithienylpyrrole triad[6] has a C_{60} attached to both ends of an electron-rich chromophore and a rigid backbone providing a stable and conducting tether. This donor-acceptor triad structure increases the molecule's efficiency in light harvesting and results in large photocurrent generation in the triad SAMs based electrochemical cell measurements. Here, we attempt to determine the photo-induced charge generation and separation in single triad *via* photon STM. Compared with device-based measurement, the advantage of using photon STM is that the intrinsic molecular properties are determined without the complication from multiple interfaces. Since charges are directly extracted from the molecule, our approach also avoids disorder-induced relaxation that occurs in macroscopic device measurements.

We use well-ordered monolayers of alkanethiolates on gold as host matrices to isolate the molecules of interest. By employing SAM coadsorption, vapor-phase annealing, and solution-phase insertion,[7,8] photoactive molecules with and without C_{60} tethered to the donor (Figure 3.1) are deposited into a precisely controlled environment, which enables us to identify the photoactive molecules in topographic images according to their locations and to measure their response to illumination simultaneously. C_{60} triads are compared with internal controls on the same surface to avoid disparities introduced by different samples.

3.2 Experimental Session

3.2.1 Materials

C_{60}-tethered triads and control molecules were synthesized following previously reported procedures.[6] 1-Dodecanethiol, toluene, and absolute ethanol (non-denatured) were used as received from Sigma Aldrich.

3.2.2 Preparation of Gold Substrates

Gold on sapphire (preparation procedure is described in chapter 2) and gold on mica substrates (Agilent, Santa Clara, CA) are annealed by 10 passes of a hydrogen flame. The flame is struck from a quartz tip, which is held at a 45° angle while passed over the substrate. Substrates are used immediately after preparation.

3.2.3 Formation of Monolayers

The **C12** solution (1 mM) is prepared by transferring 2.4 μL of neat liquid substance to a 10 mL volumetric flask, the mass confirmed gravimetrically. Flasks are then filled to the appropriate volume with ethanol. Vapor-deposited **C12** SAMs are obtained by placing the gold substrates in the airspace in a vial over a small volume of **C12** solution. The vial is capped and placed in a furnace set to 78 °C for 24 h. The sample is then washed with ethanol and blown dry with a nitrogen stream.

With ultrasonication to speed up the dissolution, the solution of 2,5-dithienylpyrrole with conjugated tether (**DTP**, Figure 3.1, 0.05 mM, 10 mL) in toluene (HPLC purity) is prepared and purged with dry nitrogen. Ammonium hydroxide (28.0-30.0% NH_3, 5 μL) is added to 1 mL of the solution. The aqueous ammonia hydrolyzes the thioacetyl protecting group, generating the thiolate *in situ*. After 2-min ultrasonication to mix ammonium hydroxide with toluene solution, the mixture stands for 30 min for deprotection before use. Monolayer with **DTP**s inserted is prepared by submerging the gold substrate with vapor-deposited **C12** SAM into solution of deprotected **DTP** molecules overnight at room temperature. 1-Dodecanethiol and **DTP** coadsorbed monolayers are formed by immersing the flame-annealed gold substrates into 1:4 **DTP**/**C12** solution overnight at room temperature. During the vapor annealing step, the substrate is hold above the liquid in a sealed v-vial containing 10-20 μL of **C12** solution. The vial is kept at 80 °C for 2 h, exposing the monolayer to vapor-phase **C12**.

The solution of C_{60} triad (0.05 mM, 10 mL) in toluene (HPLC purity) is ultrasonicated and bubbled with dry nitrogen. The partial solution (2 mL) are transferred into a vial and diluted with 0.25 mL of ethanol to ease the dissolution of ammonium hydroxide. Two doses of ammonium hydroxide (28.0-30.0% NH_3, 25 μL) are added with 3 min sonication in between. After the solution is stirred for 0.5 h, the Au substrates are immersed into the solution for 24 h, followed by rinsing with toluene and ethanol, and drying with a nitrogen stream. The color of the solution turning to light brown indicates that the acetate protecting group has been removed. The solution of C_{60} triads is purged with dry nitrogen gas weekly to stabilize this thioester molecule in solution.

3.2.4 Scanning Tunneling Microscope Measurements

All topographic images were collected in atmospheric air and at room temperature with constant tunneling current mode, as described previously.[9] The Pt/Ir 80:20 tip wire was supplied by Alfa Aesar (Ward Hill, MA). The gain of the piezoelectric scanners was calibrated by comparison of a **C12** monolayer on Au{111} to its known lattice constant of 4.99 Å and Au{111} monoatomic step height of 2.34 Å. Photocurrent images are collected with the custom-built photon STM. The 405-nm diode laser, modulated by a mechanical chopper, illuminates the tunneling junction from the rear sapphire at an incident angle of 37°. The optically modulated current is recorded phase sensitively.

3.3 Results and Discussion

3.3.1 Incorporation of C_{60} Triads and Control into the Same 2D Matrix

To study the light-induced effects in the C_{60} triad and the chromophore, these molecules are incorporated into the **C12** film. Figure 3.2 are STM topographic images of films containing **DTP** deposited by successive, simultaneous depositions and postadsorption processing, respectively. Figure 3.3 are images of the C_{60} triad inserted into a **C12** SAM without and with **DTP** mixed in the domain. These images are characteristic of a large number of measurements.

The co-assembled method results in monolayers distinct from those have **DTP** inserted. Figure 3.3 shows representative constant-current STM images of **C12** monolayer containing

DTP. Vacancy islands and terrace domain boundaries are visible in the film as for pure alkanethiolate films.[10] Protrusions from the film are features assigned as **DTP**, which are located at step edges and terrace domain boundaries in samples deposited with both methods. These are the locations where the alkanethiolate film density is lower, thus, offer increased access to the gold substrate, resulting in lower barriers to chemisorption. Mixed composition monolayers of **C12** and **DTP** prepared with simultaneous deposition have alkanethiolate domains incorporated with **DTP** (Figure 3.2 B, yellow boxes), which is not seen in **C12** monolayers with inserted **DTP**s (Figure 3.1A). The differences in the apparent feature sizes of **DTP** between locations indicate that access to single and multimolecular bundles are both possible. Dodecanethiol is adsorbed preferentially over **DTP** due to the strong intermolecular-interaction of the former and the solubility of the latter in ethanol. However, **DTP** interacts with **C12** strongly enough to mix into the alkanethiolate 2D lattice during its formation. In the annealing step, we use **C12** vapor to replace molecules of **DTP** at defect sites and step edges with matrix molecules. The thermal processing induces desorption of weakly bound **DTP**s and improvement of the host matrix order (Figure 3.1C).[11,12] Although the surface coverage of **DTP** has reduced, those guest molecules located within the **C12** domains are preserved, since their exchange with vapor-phase **C12**s is restricted by the reinforced host matrix. This enables us to differentiate protrusions of C_{60} triads from those of **DTP**s, once the triads are inserted to the defect sites of the film.

We have engineered molecular assemblies to isolate and to immobilize the organic molecules for single-molecule optical measurements. The C_{60} triad and **DTP** molecules are placed within domains and at defect sites of the same **C12** matrix. Figure 3.3 typifies the surface topography of films resulting from insertion of triads to vapor-annealed **DTP**/**C12** co-assembled monolayers. The protrusions with full-width-half-maximum (FWHM) of approximately 25 Å are assigned to triads, and they are all present at domain boundaries and step edges. Tethered chromophores are those protrusions mixed in the terrace domains with FWHM of about 14 Å. In this way, molecules of interest can be identified in STM topographic images based on their locations.

3.3.2 Photo-Response of the C_{60} Triad

The study of molecular junctions interacting with the radiation field has attracted considerable theoretical and experimental effort.[13,14] At the tunneling junction of photon STM, the molecule is in a non-equilibrium state caused by two different driving processes – an electron flux induced by the tip-sample bias and a photon flux associated with optical field. Thus, the electronic current may appear as a response to optical pumping. From the experiment perspective, interpreting with physical integrity is critical in observing a meaningful signal in a system of uncertain structure and competing response and relaxation pathways. In this section, the possible origins and amplitudes of the photo-induced current will be discussed.

The frequency of the input laser beam is in resonance with the molecular electronic transitions of the C_{60} triads. When the triads undergo charge transfer upon excitation, the charge distribution of the molecules changes considerably. This indicates that the highest occupied molecular orbitals (HOMO) are localized spatially on the chromophore (donor) moiety, while the lowest unoccupied molecular orbitals (LUMO) are on the C_{60} moieties. The asymmetry creates a molecular photovoltage that drives charge flow between the metallic tip and gold surface. Increased carrier density in previously unpopulated orbitals leads to larger tunneling currents under bias voltage. Galperin and Nitzan[13] have modeled this non-adiabatic physical process and predicted that, with sufficient electron transfer coupling and local field intensity at the junction, the steady current resulted from molecule-radiation field interaction should be measurable. The nonradiative damping leads to a current that would reach ~1 nA, with an assumed reasonable life time of ~6 fs for an excited molecule to relax via the electron-hole pair mechanism, and incident radiation intensity of ~10^8 W/cm^2.[15]

The photocurrent amplitude of C_{60} triad is estimated in the following way. We start with calculating photocurrent density by this equation: $i = I(1-10^{-A})\varphi \cdot e$, where $I = \frac{W\lambda}{hc}$ is the flux of photons per unit area per unit time, W is the light input power , λ is the wavelength of incident light (405 nm), A is absorbance of the chromophores (C_{60} triad here), h is Planck's constant, c is the light velocity, and e is elementary charge. Jen and coworkers have reckoned that the quantum efficiency (φ) of C_{60} triad SAMs formed on gold electrodes in electrochemical cells is 51%.[6] With the assumption that the absorption coefficient of triads on gold substrate is the same as that in solution, A was estimated to be 0.0097. The photocurrent occurred in a single molecular junction can be derived by dividing the current density with the number of the molecules in unit area. C_{60} triads occupy an area of approximately 234 Å^2 per molecule, based on density functional theory calculations and estimates from charge integration within known area in an electrochemical cell. Although the intensity of the 405-nm *cw* laser in our laser-assisted STM can only be up to a few Watts per unit area, the photocurrent from individual molecule is still a realistic possibility. (Figure 3.4)

We use laser-assisted scanning tunneling microscopy to study the interaction of the triads with light. Laser illumination (*p*-polarized, 405 nm in wavelength) is introduced into the tunneling junction via total internal reflection. An evanescent wave containing the same energy with the incident light propagates through the gold film and gold-supported organic monolayer. The STM probe tip is positioned over the illumination spot and is used to image the local environment, and to probe the optical response of photoactive molecules.[16] The topography and light-induced current were obtained simultaneously (Figure 3.5). The amplitude of the photocurrent signal is close to the background noise of the lock-in amplifier. Features in alkanethiolate SAMs, i.e., domain boundary, adatom island, terraces with monoatomic gold step height differences and resolved molecular lattices, present in the topographic image are absent in the photocurrent image. This is consistent with the HOMO-LUMO gap in **C12** being larger than the energy of incident photon, leading to no detectable current corresponding to the excitation. The fact that the light-induced signal is lower where C_{60} triads are located is different from our expectation (Figure 3.5B, yellow and green boxes). Our explanation is that the sudden tip height change and surge of photocurrent at the triad protrusion needs several LIA time-constants to be reflected in the LIA output, and the STM tip only lingers at each pixel point for one time-constant, which means that LIA cannot respond fast enough to the current, giving rise to null signal. Similar phenomena are observed at those bright and dark lines where a tip change occurs as the tip moves from one scanning line to the next. This problem can be solved by reducing the LIA time constant and slowing down the STM scan speed, which requires high stability at the tunneling junction. Revised experiments are ongoing and results will be reported elsewhere.

3.4 Conclusions and Prospects

In summary, we presented an approach to incorporate C_{60}-donor-C_{60} triads and their chromophore derivatives into the same 2D matrices, where their photo-activity and quantum efficiency will be determined in parallel. These two photoactive molecules can be identified according to their local environments, providing a platform to test the chemical specificity from photoconductance mapping with our custom-built photon STM. Molecular sizes measured from line profiles confirm that the chromophores are embedded in terrace domains while the triads in defect sites of the SAM. Beyond characterizing optical processes experimentally, theory computation to model the response of the tunneling junction to incident light is crucial as well. Fundamental understanding of our well-controlled model system could help us infer how electrons cross the metal-molecule interface upon irradiation. It also provides us with insights into tailoring the chemical composition and structure of molecules used as electronic components.

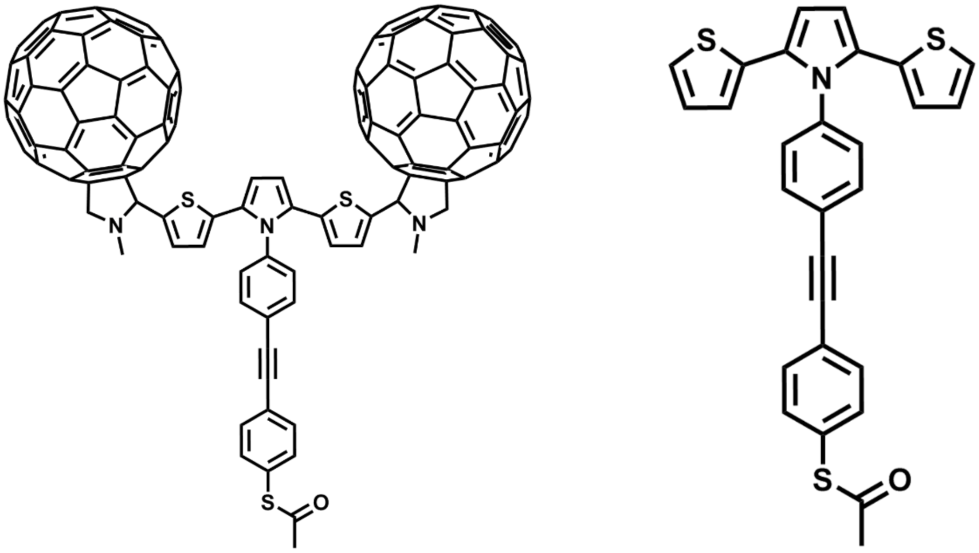

Figure 3.1 Chemical structure of C_{60}-tethered 2,5-dithienylpyrrole triad **(Left)** and the control that has no C_{60} attached **(DTP**, **Right)**.

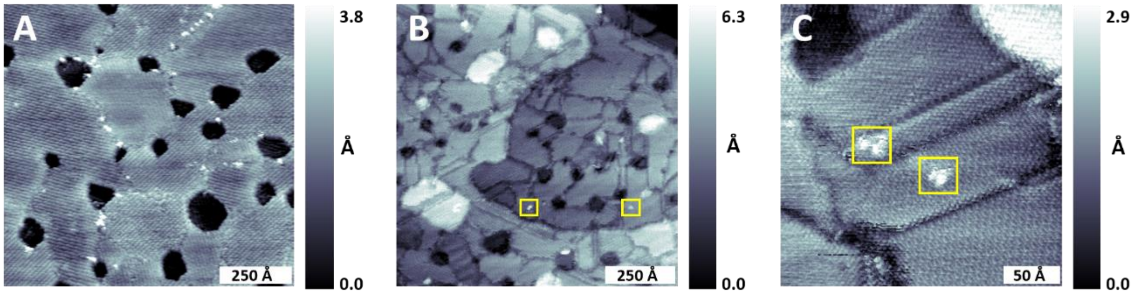

Figure 3.2 Scanning tunneling microscope topographic images of 2,5-dithienylpyrrole derivative (**DTP**) incorporated into the dodecanethiolate (**C12**) monolayer by insertion **(A)** and coadsorption **(B)** methods and the co-assembled film after vapor annealing process **(C)**. The **DTP** molecules appear as protrusions in topography (displayed as bright) and are indicated by yellow boxes. They are predominantly located at structural domain boundaries, terrace step edges and other defect sites in the films prepared by both methods. However, some are mixed into **C12** SAM domains and they remain in their locations after the rest are displaced by matrix molecule during vapor annealing. These images are obtained at a sample bias voltage of -1 V and a constant tunneling current of 1.0 pA in **(A)** and 5.0 pA in **(B)** and **(C)**.

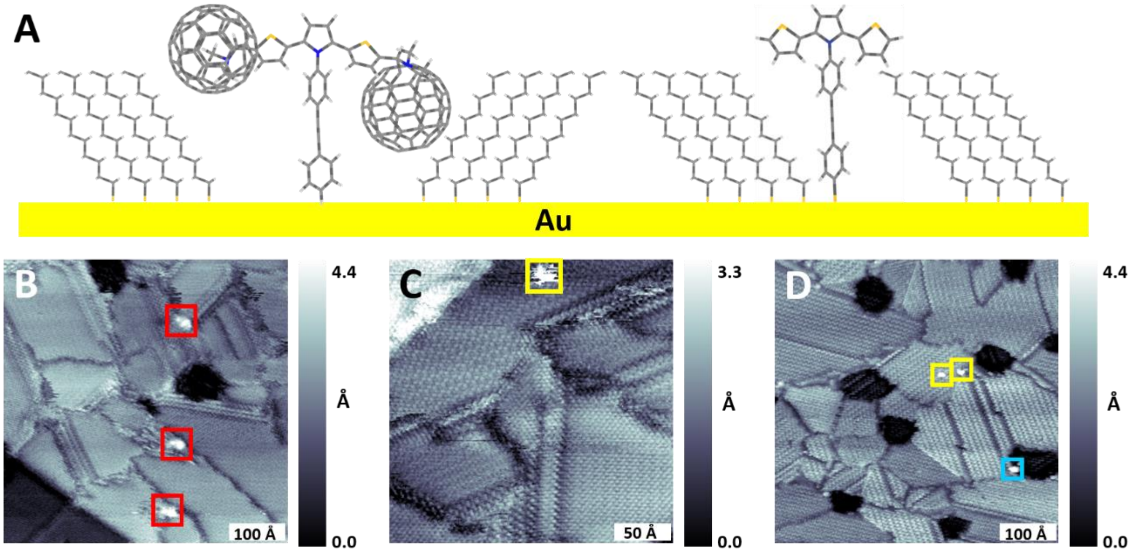

Figure 3.3 Incorporating C_{60} triads and **DTP** molecules into the same **C12** self-assembled monolayer. Schematic illustration **(A)** and scanning tunneling microscope images (**B**-**D**) of triads inserted into the defect sites of a **C12** monolayer while **DTP** molecules embedded in **C12** domains: **(B)** inserted C_{60} triads (red boxes) within a **C12** monolayer; (**C**, **D**) **DTP**s mixed within **C12** domains (yellow boxes) and step edges around the vacancy islands (blue box). Line profiles show that C_{60} triads has a full-width-half-maximum of ~25 Å and **DTP** of ~14 Å**.** These images are acquired at a sample bias voltage of -1.0 V and a constant tunneling current of 5.0 pA.

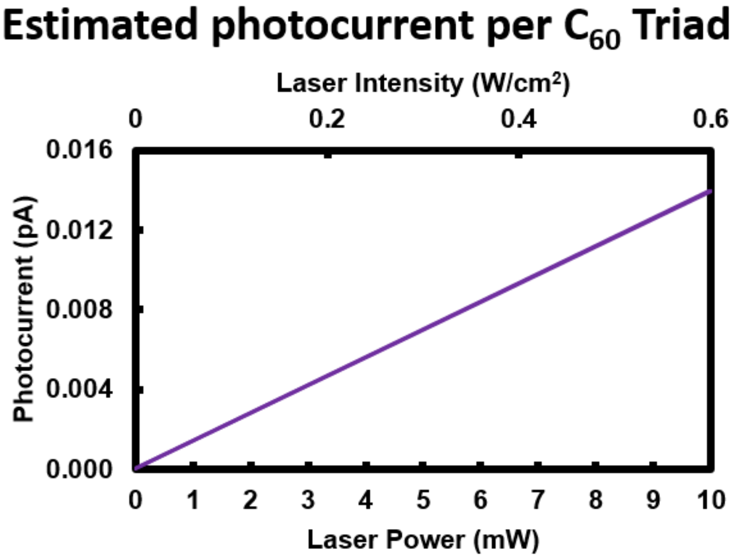

Figure 3.4 Estimated photocurrent generated from single C60 triad as a function of laser power and laser density. The method for numerical estimation is explained in the text. Theoretical results predict that light-induced current on the order of 0.01 to 0.1 pA should be generated by illuminating the triads with the laser used in our system. The laser power is limited by laser-induced heating.

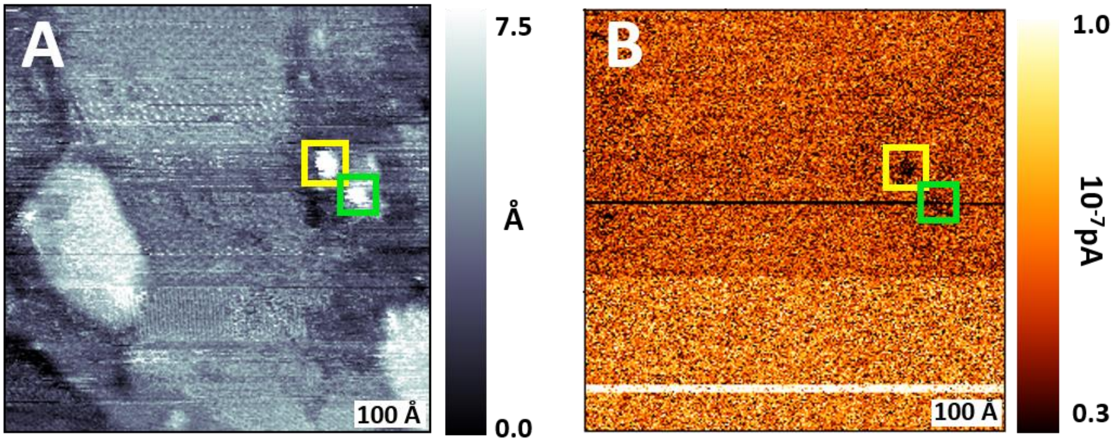

Figure 3.5 Scanning tunneling microscopy images of inserted C_{60} triads (yellow and green box) within a **C12** monolayer. Topography **(A)** and photocurrent **(B)** are simultaneously acquired at a sample bias voltage of -1.0 V and a constant tunneling current of 1.0 pA. The laser irradiation is modulated with a mechanical chopper at 4.8 kHz. The topography of the **C12** monolayer appears the same as for a typical alkanethiolate film without illumination. There is no light-absorption signal for **C12** in the photocurrent map except the background noise from the lock-in amplifier. Photocurrent at C_{60} triads is suppressed because the time constant of the lock-in amplifier is too long for it to respond to the signal change.

References

1. Prato, M. Fullerene materials. *Top Curr. Chem.* 1999, 199, 173-187.

2. Yu, G.; Gao, J.; Hummelen, J. C.; Wudl, F.; Heeger, A. J. Polymer photovoltaic cells - enhanced efficiencies via a network of internal donor-acceptor heterojunctions. *Science* 1995, 270, 1789-1791.

3. Shi, X. B.; Caldwell, W. B.; Chen, K. M.; Mirkin, C. A. A Well-defined surface-confinable fullerene - monolayer self-assembly on Au(111). *J. Am. Chem. Soc.* 1994, 116, 11598-11599.

4. Guldi, D. M.; Prato, M. Excited-state properties of C_{60} fullerene derivatives. *Acc. Chem. Res.* 2000, 33, 695-703.

5. Abrusci, A.; Stranks, S. D.; Docampo, P.; Yip, H. L.; Jen, A. K. Y.; Snaith, H. J. High-performance perovskite-polymer hybrid solar cells via electronic coupling with fullerene monolayers. *Nano Lett.* 2013, 13, 3124-3128.

6. Kim, K. S.; Kang, M. S.; Ma, H.; Jen, A. K. Y. Highly efficient photocurrent generation from a self-assembled monolayer film of a novel C_{60}-tethered 2,5-dithienylpyrrole triad. *Chem. Mater.* 2004, 16, 5058-5062.

7. Donhauser, Z. J.; Price, D. W.; Tour, J. M.; Weiss, P. S. Control of alkanethiolate monolayer structure using vapor-phase annealing. *J. Am. Chem. Soc.* 2003, 125, 11462-11463.

8. Mullen, T. J.; Dameron, A. A.; Andrews, A. M.; Weiss, P. S. Selecting and driving monolayer structures through tailored intermolecular interactions. *Aldrichim Acta* 2007, 40, 21-31.

9. Bumm, L. A.; Arnold, J. J.; Charles, L. F.; Dunbar, T. D.; Allara, D. L.; Weiss, P. S. Directed self-assembly to create molecular terraces with molecularly sharp boundaries in organic monolayers. *J. Am. Chem. Soc.* 1999, 121, 8017-8021.

10. Poirier, G. E. Characterization of organosulfur molecular monolayers on Au(111) using scanning tunneling microscopy. *Chem. Rev.* 1997, 97, 1117-1127.

11. Smith, R. K.; Lewis, P. A.; Weiss, P. S. Patterning self-assembled monolayers. *Prog. Surf. Sci.* 2004, 75, 1-68.

12. Donhauser, Z. J.; Mantooth, B. A.; Pearl, T. P.; Kelly, K. F.; Nanayakkara, S. U.; Weiss, P. S. Matrix-mediated control of stochastic single molecule conductance switching. *Jpn. J. Appl. Phys., Part 1* 2002, 41, 4871-4877.

13. Galperin, M.; Nitzan, A. Current-induced light emission and light-induced current in molecular-tunneling junctions. *Phys. Rev. Lett.* 2005, 95, 206802

14. Galperin, M.; Nitzan, A. Molecular optoelectronics: the interaction of molecular conduction junctions with light. *Phys. Chem. Chem. Phys.* 2012, 14, 9421-9438.

15. Galperin, M.; Nitzan, A. Optical properties of current carrying molecular wires. *J. Chem. Phys.* 2006, 124.

16. Feldstein, M. J.; Vohringer, P.; Wang, W.; Scherer, N. F. Femtosecond optical spectroscopy and scanning probe microscopy. *J. Phys. Chem.* 1996, 100, 4739-4748.

CHAPTER 4

Exchange Reactions between Alkanethiolates and Alkaneselenols on Au{111}

4.1 Introduction

Self-assembled monolayers are test beds for two-dimensional assembly and control. Despite 30 years of study and myriad applications, the well-known covalent gold-sulfur bond between alkanethiol and the gold surface remains imcompletely understood. A confluence of studies employing methodologies ranging from scanning probe microscopy, X-ray diffraction, computation, and others now support the generally accepted model of a S/Au-adatom complex.[1-6] Consensus has emerged that this energetically stable gold adatom complex exists, which has sulfur atoms bound to gold atoms or on opposite sides of the gold adatom in a barbell configuration.[2-4,6-15] We have observed the important roles of gold adatoms in motion of Au-thiolate complexes[1] and in conformational changes of molecular switches.[16] Assuming the existence of an adatom complex, critical unresolved questions remain. Is the adatom layer ordered, disordered, or can it transition from one to the other? Are gold adatoms derived from the initial lift of the herringbone reconstruction,[17-19] or are they abstracted from the unreconstructed surface leaving behind vacancy sites?[5,7] What is the significance of a proposed barbell motif relative to other binding models in the context of molecular exchange and place-exchange reactions?[20-25] Towards answering such questions, we have explored exchange reactions between alkaneselenols and alkanethiolate monolayers. The exchange reaction of an alkaneselenol molecule into a preformed alkanethiolate SAM occurs at a substrate presenting nominally complete Au-thiolate complex coverage. We investigate the reaction products of this reaction in the context of a mobile, labile adatom complex. The Au{111} herringbone reconstruction[17] is already lifted by thiolate deposition, so Au-S/Se exchange reactions provide an opportunity to examine reaction products in the context of the Au-adatom complex.[1]

Replacing thiols with selenols has attracted interest for improving the overall oxidative and thermal stability of SAMs, and (in some cases) electronic coupling of molecules to the substrate.[26-37] Selenium tends to outcompete sulfur for binding sites on the gold substrate.[38,39] Studies of likely binding sites for the selenium atoms are in their relative infancy, with models not yet taking into account discoveries in the chemistry of sulfur-gold adatom complexes. Of primary interest is the configuration of the selenolate attachment: by observing coexisting structures of the two chalcogenolates, we may obtain insight into whether or not selenium is attached to the substrate in a manner similar to sulfur.

In this Chapter, we compare and contrast the structures formed by single-component alkanethiolate and alkaneselenolate films on Au{111}, and then report the structures formed by and the kinetics of the rapid molecular exchange reaction between gold-bound alkanethiolates and alkaneselenols. Additionally, we observe 2D place-exchange reactions between adsorbed thiolates and selenolates induced by STM tip. This chemical system provides a basis for investigating both gold-thiolate and gold-selenolate attachment chemistry. Our observations suggest that, initially, the gold-selenolate structure occupies the same binding structure and configuration as the gold-thiolate complex, but as selenolate coverage increases, there is a transition to a new interface structure.

4.2 Results and Discussion

4.2.1 Morphological Comparisons of Alkanethiolate and Alkaneselenolate Monolayer Structures

The scanning tunneling microscope is capable of exquisite molecular- and atomic-scale resolution, but does not intrinsically provide a means for chemical identification beyond the relative sizes and conductance of the molecules measured.[40-42] To investigate alkanethiolates and alkaneselenolates in mixed, ordered systems, we chose to employ different alkyl chain lengths for the two species; a shorter alkyl chain for the thiolate matrix 1-decanethiolate (**C10**), as opposed to the slightly longer 1-dodecaneselenolate (**C12Se**). The difference in height enables the identification of the two molecular species at various stages of their exchange reaction.[27,43] Figure 4.1 details a morphological comparison of single-component **C10** and **C12Se** SAMs on Au{111}.

Imaging an annealed **C10** SAM (Figure 4.1A-C) reveals the expected well-ordered hexagonal lattice of molecules in the $(\sqrt{3} \times \sqrt{3})R30°$ configuration. There are two important classes of defects: domain boundaries and gold substrate step edges (of which the circular depressions in Figure 4.1A, substrate vacancy islands, are a subclass).[36,44-47] Ordered molecular domains having different alkyl chain azimuthal orientations are typically separated by domain boundaries.[46,48-50] Domain boundaries appear either more or less protruding than the surrounding domains, depending on the configuration of molecules at that interface.[46] In highly ordered films, such as the annealed film shown in Figure 4.1A-C, domain boundaries tend to align with the close-packed substrate lattice directions, with different boundaries oriented 60° with respect to another. Molecular vacancies are defined as one or more molecules missing from an otherwise well-ordered lattice, a rare monolayer defect in well-ordered alkanethiolate films. Substrate step edges are a single-gold-atom-high transition from one atomically flat terrace to the next. Gold terrace step edges and the step edges at substrate vacancy islands are functionally identical in structure and behavior.

The **C12Se** films[26,27,51] are strikingly dissimilar from the alkanethiolate films, as reported previously, despite the identical geometries of the alkyl chains (Figure 4.1D and 4.1E). Absent are the characteristic alkanethiolate domain boundary structures,[46,52] such as those observed in the **C10** SAM images. Instead, the Moiré patterns of topographic differences are readily apparent in the STM images of the **C12Se** film (Figure 4.1D). These patterns originate from differences in the lattice constants of the gold substrate and the overlying molecular layer and result in a smooth, continuous variation of molecular apparent height by ~1 Å. These features generally align with the substrate, rotated with respect to one another by multiples of 30°, as seen previously in annealed monolayers of 1-adamantaneselenolate.[32]

The substrate step edges tend to align along the close-packed directions of the gold substrate after **C12Se** adsorption. Additionally, high-resolution STM imaging enables us to report the presence of narrow 'vacancy trenches' in the single-component **C12Se** SAMs. These configurations are consistent structurally with the round vacancy islands found in **C12** SAMs. Each trench shows a median apparent height that is ~2.3 Å lower than the median apparent height of the surrounding terrace, indicative of a gold substrate monatomic step. The trenches tend to elongate along the crystallographic close-packed direction of the gold substrate. The missing row of the vacancy trench is often accompanied by parallel **C12Se** molecular rows that are dissimilar from the surrounding lattice. A typical image at high resolution is shown in

Figure 4.1F. The row adjacent to the trench is less protruding than the median height of the surrounding terrace, while the next row is more protruding by the same value of 1 Å. These features highlight the variability of bonding configurations available for the Au-Se interactions, depending on the immediate local environment.

The **C12Se** SAM structure reflects the underlying crystallographic structure of the gold substrate, and the differences in apparent height of various features implies with several binding configurations with the gold substrate coexisting, a feature we previously reported in our study of the 1-adamantaneselenolate system on Au{111}.[32] From our observations, we can confirm that the **C12Se** SAM formation lifts the gold herringbone reconstruction and spawns vacancy islands. Additionally, the selenolate-gold interaction results in straightened substrate step edge features, and produces only small vacancy trenches (compared to the large vacancy islands produced after alkanethiolate deposition). The straightening and existence of multiple binding sites are consistent with our previous suggestions of gold-selenolate bond promiscuity,[26,27] and with more recent examples suggesting a number of acceptable binding configurations for selenium to gold.[32,53] Rapid straightening of gold substrate features also suggests that the gold-selenolate complex is more mobile than its sulfur counterpart. We will return to discuss the mobility of the selenolate and the hypothesized gold-selenolate complex below.

4.2.2 Molecular-Exchange and Place-Exchange Reactions of Self-Assembled Monolayers

We will now introduce and define terms that are important for understanding the phenomena and associated timescales of reactions that occur between molecules in self-assembled monolayers. There are two distinct types of exchange reactions described in this article. These two reactions are related, but are treated separately here. First, we define a molecular exchange (or displacement) reaction as the replacement of an adsorbed molecule by a second species, typically accomplished by immersion of a preformed SAM-coated substrate into a solution or vapor of the replacing chemical.[54-56] The term "insertion" refers to the initial stage of a molecular exchange reaction, where molecules of the second species can be found decorating the defect sites of the preformed film.[54,57] Such sites are well known to provide access to the substrate for other species and for chemical reactions,[24,26,45,48,56,58-67] and are the first to be occupied. Defects are critical to both insertion and displacement.

Second, we define a place-exchange reaction as a position swap between proximate molecules in a 2D lattice, without desorption of either molecule. For our investigations of place-exchange reactions, **C12Se** is incorporated into the **C10** SAM by a molecular exchange reaction that is arrested before a large fraction of the initial monolayer is displaced. Place-exchange reactions are mediated by defects.[22,68]

Exchange between adsorbed molecular assemblies and molecules in solution is mediated by four primary factors: the chemistry of the molecule/substrate attachment, molecular geometries, intermolecular forces, and the type and density of defects (of both the supramolecular assembly and the substrate, i.e., by access to the substrate). In the case of molecular self-exchange (e.g., the exchange between a 1-dodecanethiolate monolayer and 1-dodecanethiol), most molecules are kinetically trapped in domains and exchange occurs primarily at defect sites.[20] The constituent molecules can be tailored to engineer molecular exchange reactions. For instance, a combination of weak intermolecular interactions and low surface density make 1-adamantanethiolate SAMs susceptible to molecular exchange by *n*-alkanethiols.[54,57,69] Also, monolayer defects and disorder can be induced by exothermic reactions.[70,71] The attachment chemistry also plays an important role. Selenols have previously been shown to outcompete sulfur for binding sites on Au{111}. Packing densities of **C12** and **C12Se** are similar,[26,72] so a thermodynamic drive towards increased coverage is absent.[57] The Se-Au bond is stronger than the S-Au bond;[73] we have shown that the Se-Au bond is more promiscuous in terms of binding sites.[26] Garrell and coworkers[38] showed a strong surface preference for benzeneselenolates over benzenethiolates, a phenomenon attributed to the higher acidity of the selenol group relative to the thiol. Similar experiments on copper-supported monolayers of thiolates and selenolates did not show strong preferences for either chalcogen.[74,75] Substrates can also be engineered to promote exchange.[76,77]

Place-exchange between adsorbed thiolates is generally slow in full coverage monolayers.[20,21,24,57,78-80] Most monolayer dynamics within crystalline domains of nearly complete SAMs occur over short distances and over time scales of hours or longer. There is a notable difference at defect sites, where dynamics are relatively fast, but there is little precedent for covalently bound molecules to transit long distances.[59] We have previously observed apparent site-hopping of adamantaneselenolates on Au{111}, although these motions are thought to occur between adjacent sites separated by only a few Ångströms.[32] The even greater promiscuity of amine-Au bonds might be expected to lead to enhanced mobility of these species.[81]

4.2.3 Determination of Exchange Kinetics by Infrared Spectroscopy

We employ infrared reflectance absorption spectroscopy (IRRAS) to measure the exchange kinetics of SAM exchange/replacement. This method has several advantages for tracking changes in monolayers: gold reflectivity is high, the carbon-hydrogen bonds absorb strongly between 2800 and 3000 cm^{-1}, coverage down to a few percent of a monolayer can be detected, and the resulting spectra provide both coverage and structural information.

A typical spectrum for a **C12Se** SAM, shown as the top spectrum in Figure 4.2A, is analogous to that of most alkanethiolates on gold. There are five dominant spectral features: methylene symmetric and asymmetric stretches at 2850 and 2918 cm^{-1}, respectively, methyl symmetric and asymmetric stretches at 2877 and 2963 cm^{-1}, and a weak band associated with a Fermi resonance of the symmetric methyl stretch with a methyl deformation mode, presented as a shoulder of the methylene asymmetric stretch.[82-84] The intensity and position of the methylene asymmetric stretch correlate to monolayer order. The peak position at 2918 cm^{-1} is consistent with a highly ordered, solid-like film. The intensity of the methylene symmetric stretch relative to the other peaks is lower than those reported for selenolate monolayers deposited from dialkyldiselenide.[72] We note that the microscopic structure we have observed for monolayers fabricated from alkaneselenol appears topographically dissimilar to monolayers deposited from dialkyl diselenide (a surface that has been reported to show a substantially larger number of gold substrate defects as compared to our observations for alkaneselenol films).[85] A thorough comparison of alkaneselenol versus dialkyl diselenide self-assembly characterization is warranted.

For determining partial coverage of alkanethiolate monolayers, the methyl symmetric stretch (2877 cm^{-1}) is an important spectral feature; taking the ratio of the peak area at each time point to the peak area after 24 h displacement yields fractional coverage. The symmetry of the group gives it a largely uniform intensity over a range of possible standing-up configurations, making it a useful metric for coverage in mixed systems of standing-up phase alkanethiolate SAMs.[57,84] In the case of **C10** exchange by **C12Se**, the intensity of the 2877 cm^{-1} peak is nominally constant throughout the experiment, as the overall coverage and orientation of the terminal methyl groups remain static. Spectral interference is too high for accurate observation of the exchange reaction, and monitoring intensity changes of the methylene asymmetric 2919 cm^{-1} peak is unreliable. We remove spectral interference of the base monolayer by depositing a perdeuterated dodecanethiolate (**D12**) monolayer, with the assumption that the chemistry of **D12** film exchange is the same as that of a **C12** monolayer. Unlike our STM measurements, alkyl chains of identical length are employed to simplify interpretation of the kinetics. The infrared spectrum of a **D12** monolayer can be found in Figure 4.7.

Figures 4.2A and 4.2B show the progression of the exchange reaction between a spectroscopically transparent **D12** monolayer exposed to an ethanolic solution of **C12Se**. The C-H peaks of the **C12Se** film emerge with increasing exposure time, and the reaction terminates after complete **D12** monolayer displacement. The relative ratio of peak intensities remains largely static throughout the displacement process, which implies that there is little reorganization during displacement (for example, we see no evidence of a transition between lying-down and standing-up phases,[86] as might be observed for deposition onto a bare substrate). Molecules are thus found in their near-final orientations shortly after incorporation into the film. Figure 4.2B shows the fractional coverage of **C12Se** monolayers versus immersion time. As seen in the STM images in Figure 4.3, there is an initial phase of slower adsorption dominated by insertion at defect sites, followed by a period of more rapid replacement, and the rate ultimately slows as the reaction approaches completion. The predominant source of error is sample-to-sample variability. Each gold substrate has a characteristic (and unquantified) fraction of steps and defects.[57,87] As the exchange reaction is initiated by insertion at defect sites, subtle differences in sample defect density can have large cumulative effects on the final rate of exchange. These differences are reflected in the standard deviation of fractional coverage at each time point.

The Johnson, Mehl, Avrami, and Kolmogorov (JMAK) model was devised originally to describe phase transitions in metal alloys.[88-90] We have previously used the site-saturated nucleation JMAK2 model to describe perimeter-dependent island growth of 1-adamantanethiolate exchange by **C12**, and given as:

$$\theta(t) = 1 - e^{(\kappa t)^2}$$

where κ is the rate constant.[57] Recent reports suggest that this model can be used generally to describe 2D film exchange.[91] For comparison, the kinetic data are fit to a variety of other models, including pure diffusion, first-, second-, and diffusion-limited Langmuir models, and the constant nucleation-rate JMAK3 model. The JMAK2 model, used to fit the kinetic data in Figure 4.2B, best represents the data and is consistent with our observations of the reaction progression (a slower initial rate followed by a more rapid rate as coverage increased). As shown in Figure 4.2C, plotting the displacement rate versus the concentration of **C12Se** on a logarithmic scale gives a slope of ~1, implying that the rate is directly proportional to the concentration of **C12Se**.

At nearly all conditions investigated, we observe that alkanethiolate monolayers are unstable in the presence of alkaneselenols. Codeposition results in single-component **C12Se** monolayers, until the molar ratio approaches 100:1 in favor of the **C12**. Figure 4.2D shows the sharp transition between full-coverage **C12Se** and **D12** monolayers as a function of mole fraction. In their work on benzenethiolates and selenolates, Huang et al. linked the faster kinetic exchange of benzenethiol and benzeneselenol to the pK_a of the selenol, suggesting that the deprotonated forms of the selenols were responsible for the faster exchange kinetics.[38] Our results examining the effect of solution pH on alkanethiolate displacement by selenol corroborate this finding: **C12Se** exchange with **C10** SAMs was faster after addition of aqueous sodium hydroxide to the ethanolic selenolate solution. It remains unclear whether this increase in exchange rate is due primarily to deprotonation of the replacing species, or whether the hydroxide is facilitating abstraction of molecules from the preexisting monolayer. In all cases of hydroxide-catalyzed exchange, the methylene asymmetric stretch (~2918 cm^{-1}) is observed to increase in intensity by a factor of two to three and shift to ~2930 cm^{-1}, indicative of poor order in the resulting film.[57,84] Annealing the film in the same solution at elevated temperature for 24 h and then repeating the spectroscopic analysis reveals a monolayer film indistinguishable from one deposited at room temperature, evidence of poor ordering after base-catalyzed displacement of thiolate by selenolate. Spectra and kinetic results are collected in the Figure 4.8.

4.2.4 Molecular Exchange of Decanethiolate by Dodecaneselenol

A preformed **C10** SAM is exposed to 10 mM ethanolic **C12Se** for 1 min. The STM micrographs in Figure 4.3A and 4.3A' reveal rapid insertion of **C12Se** into the **C10** lattice, notably at domain boundaries and at step edges. The selenolates appear to occupy hexagonal lattices and to incorporate commensurately to the lattices of the surrounding thiolates (Figure 4.3A’). Insertion has also been noted at isolated locations within ordered domains, likely a result of **C12Se** insertion at molecular vacancy defect sites (an example image is shown in Figure 4.6).

In these and most STM images, **C12Se** molecules appear somewhat more protruding, here ~0.7 Å, than the neighboring **C10** molecules. The measured apparent height is related to the configuration of the STM tip, through which the tunneling current passes. We note that changes in the tip state result in variations of the observed relative apparent height. In some cases, inversion of the relative selenolate and thiolate conductance occurs after a change in the electronic properties of the probe. This tendency for tip-dependent conductance changes must be carefully monitored to ensure that probe variations are distinguished from changes in molecular binding site. Examples of conductance reversal on tip state changes are shown in Figure 4.6.

Additional exposure to solution results in rapid increases in the relative **C12Se** coverages, with each site of **C12Se** insertion becoming a nucleation site for **C12Se** island growth.[57] After 4 min of **C12Se** exposure, **C12Se** is no longer confined to the regions in close proximity to **C10** defect sites, and occupies a substantial fraction of the surface. The relative apparent heights have inverted, with **C12Se** now appearing less protruding. Ordered islands are the dominant configuration of the residual **C10**. Such large thiolate islands (appearing as the protruding features shown in Figure 4.3B and 3B') have edge lengths of 100-500 Å. The largest, most ordered SAM domains are similarly most resistant to molecular exchange, as there are few internal defects to provide initiation sites for selenolate displacement, requiring molecular exchange to occur from the domain edges inwards.

The displacement reaction does not appear to be a smooth progression between continuous domains of **C10** to **C12Se**. The images in Figure 4.3C and 4.3C' reveal striped features of high- and low-conductance rows. Comparing apparent heights of the striped regions, it is composed of features that match the relative height of thiolate islands separated by less-protruding features. We attribute the more protruding of the features to structures at least partially composed of residual **C10**. We use apparent height as the marker for chemical identification. Low-coverage, inserted **C12Se** appears more protruding than **C10** in STM images, while the striped features are at equal or lower apparent height than **C10**. As the infrared analysis suggests no change in absolute molecular coverage, these lower-height features are consistent with a different bonding configuration of the **C12Se** as relative coverage increases. The reaction progresses with incoming selenolates dismantling the organized domains of the **C10** film, making coalescence into a single-component **C12Se** film rapid. This process appears to be anisotropic, with displacement favoring the direction along the rows rather than perpendicular to them.

Unlike the low-coverage example, the **C12Se**-dominated regions now appear less protruding than the **C10** matrix. Figure 4.3B' provides further evidence that the relative conductance of thiolates and selenolates is strongly influenced by the underlying substrate binding site. The image shows selenolates in two distinct conductance configurations: at the top left are selenolates that appear to protrude and are lattice matched to the **C10**, and on the right is the striped selenolate domain, which appears less protruding than the **C10** island.

The apparent height of **C12Se** is observed to depend on the binding site. As mentioned previously, selenolates inserted at defects appear protruding from and lattice matched to the **C10** lattice, which adopts a $(\sqrt{3} \times \sqrt{3})R30°$ lattice (and related superstructures). After the selenolates collapse into their own preferred bonding configuration, the alkanethiolate islands appear to protrude in STM images from the surrounding alkaneselenolate lattice by ~ 0.7 Å (for the conditions shown), despite the longer chain length of the **C12Se** molecules. This measurement is in close agreement with our previously reported value for **C12** inserted into a **C12Se** SAM, wherein **C12** molecules in STM images appeared to protrude from preformed **C12Se** SAMs.[27]

After 7 min exposure to a **C12Se** solution, all **C10** molecules were replaced by **C12Se**. The monolayer is configured differently than the directly deposited **C12Se** SAM, but the variations in apparent height in STM images remain. The structure is primarily striped, as shown in Figure 4.3C and 3C', reflecting the linear propagation of the displacement reaction. Like the single-component **C12Se** film, the difference between the most and least protruding molecules in STM images on single terraces is approximately 1 Å.

The integrity of the top layer of the gold substrate is preserved by the displacement reaction. No aforementioned "trench" vacancy islands are observed after the alkaneselenolates have occupied the substrate surface, and the vacancy islands that form after thiolate SAM assembly are preserved by the new monolayer. This observation provides evidence that vacancy island formation is tied directly to lifting the Au herringbone reconstruction at the initial stage of SAM formation, and thus no new vacancy islands can form after thiolate replacement by selenolate. Likewise, we do not observe adatom islands, as would be expected if thiolates were abstracted and gold adatoms left behind.[8,10] At the early stages of the displacement reaction, the longer **C12Se** molecules appear lattice matched to the **C10**. In such cases, they are trapped in the same binding configuration as the sulfur in the **C10** SAM. Later, as coverage increases, the selenolates are no longer confined to thiolate-like configurations and adopt their own preferred binding configurations.

4.2.5 Bias-Induced Place exchange of Selenolates with Thiolates

Local SAM coverage, structure, and composition can be used to tailor physical and chemical properties at interfaces. Phase-separated molecules can be selectively moved and removed *via* electrochemistry, where domains having weaker intermolecular interactions desorb at lower potential.[92,93] The STM probe has long been used to manipulate atoms and molecules directly, and to perform nanoscale lithographic patterning.[94-99] At relatively high voltages (sample bias of +3 V), the STM tip can be used to pattern alkanethiolate monolayers.[100-102] We have observed that the threshold for induced motion of the selenolates is lower, with motion observed at low sample biases, e.g., +1 V, and that we are able to manipulate alkaneselenolates selectively. This may be related to the promiscuous binding of selenolates to Au (relative to thiolates).[26]

For imaging without perturbing the SAM, we use a sample bias of -1 V at a tunneling current of 3 pA. Imaging at a sample bias of +1 V induces physical reorganization of thiolate/selenolate mixed monolayers. After reorganization, the overall film order is retained. At high selenolate coverage, the effect becomes more dramatic: both thiolate and selenolate domains become disordered, and a mottled configuration of high and low conductance domains are observed (images can be found in Figure 4.9).

In Figures 4.4A and 4.4A', **C12Se** molecules appear protruding relative to the **C10** lattice in STM images. Upon bias polarity reversal (to +1 V sample bias), the positions of individual **C12Se** molecules are no longer well defined, as shown in Figure 4.4B. We attribute this "noise" to molecular place-exchange reactions and motion occurring at timescales faster than imaging.[103-106] Each image is recorded over ~4 min by moving the tip in a raster pattern over the interface, with the tip encountering individual protruding molecules at many positions, rather than over a single, well-defined binding site. In image 4.4C, a return to -1 V sample bias halts the place-exchange reactions, and the selenolates are again at well-defined sites. There are approximately the same numbers of molecules visible in the recorded area before and after bias-induced shuffling. A change in the tip geometry after bias reversal resulted in faint "double tip" artifacts to the lower right of all high-aspect-ratio protrusions, giving the false impression that more **C12Se** molecules are present in the images in Figure 4.4C, C'. Selenolates are then observed incorporated into the centers of ordered domains. While the overall domain structures before and after place-exchange reactions are nominally the same, the movement of molecules to the new sites results in increased disorder. Protruding **C12Se** molecules are thus accompanied by depressions in the **C10** lattice that arise from the additional free space created by decreases in the local alkyl chain crystallinity. The structures of the **C10** domain boundaries have likewise been reconfigured.

While bias-induced place-exchange reactions are localized, the reactions are not limited to the specific position of the tunneling junction. Figure 4.4C' shows that the monolayer was reconfigured as far as 50 nm from the region imaged at +1 V substrate bias. The tip scanned only over a 250 Å × 250 Å region, but molecules have been shuffled over the 500 Å × 500 Å terrace. Additional images recorded at distances greater than 500 Å from the region of induced motion reveal no apparent molecular place exchange (Figure 4.10).

We demonstrated the ability to manipulate small groups of molecules with localized, short-duration voltage pulses, although the 500 Å range over which motion can be induced made directed assembly of individual molecules into specific patterns impractical. Figure 4.5 shows a small cluster of protruding **C12Se** molecules at which the STM tip is positioned. The sample bias is set to +1 V at 3 pA tunneling current for 5 sec. Subsequent imaging at -1 V sample bias revealed substantial rearrangement of the local structure that continued long after the initial pulse. In many cases, however, short pulses had no obvious effects on the local structure at the scale imaged, but responses at distances larger than the imaging window could not be excluded. Evolution of the structure is observed to continue at faster than the minute timescale.

4.2.6 Implications for the Gold-Adatom Complex

There is no evidence for the restructuring of the gold substrate during complete exchange reactions. **C12Se** SAMs deposited by displacement of **C10** show evidence of the topographic variations characteristic of the selenolate system, but show vacancy islands characteristic of the **C10** system (Figure 4.3C, 4.3C'). These features add to the existing evidence that the formation of vacancy islands is due to dynamics between the substrate and binding chalcogen as the herringbone reconstruction of the gold is lifted.[2,18,19,107] We conclude that the configuration of the gold-thiolate association is conserved after the initial molecular exchange reaction, and additional reconfiguration that does not involve loss of gold atoms occurs as alkaneselenolate coverage increases.

Our observations support two distinct binding modes for selenolate on gold. In the early stages of the displacement reaction, **C12Se** molecules appear more protruding from the **C10** lattice, and the apparent heights of the inserted **C12Se** are similar to the expected heights for **C12** molecules inserted into **C10** lattices. We postulate that the selenolates occupy the binding sites previously occupied by thiolates. Exchange at this early stage of the reaction is slow, and **C12Se** molecules are predominantly found at defects in the **C10** SAM. In the later stages of the replacement reaction, the **C12Se** molecules appear lower than the **C10** domains, and propagation of **C12Se** appears to occur in bands several molecules wide, with stripes of **C10** remaining. We postulate that the gold-thiolate complexes exhibit long-range order in highly annealed films, thus enabling linear stripes of selenolates to propagate over long distances (hundreds of Ångströms).

A barbell configuration of the gold adatom-thiolate complex has been proposed separately by several groups.[4,13,32,108,109] Several of our observations mesh well with this concept for the gold-adatom complex. The early, high conductance stage of **C12Se** insertion can be seen as an alkaneselenolate binding to and displacing the alkanethiolate from this complex, conserving the structure (Figures 4.3A, 4.3A'). As the coverage of selenolates increases, we note a change in structure and observed apparent heights of the selenolates (Figures 4.3B, 4.3B'). There are a number of mechanistic pathways that can explain the progression of the displacement mechanism. Thiolate desorption at SAM and substrate domain boundaries frees binding sites for selenol insertion from solution,[110] but does not account for the observed accelerated displacement after insertion.[20,57] A ligand exchange model provides a mechanistic pathway for displacement, in which a selenolate binds at the thiolate-occupied complex adjacent to a defect site, and the thiolate is subsequently induced to desorb. This mechanism would require formation of a transient $Au(SeR)(SR)_2$ complex prior to desorption, which would likely not be observable at room temperature or at the slow experimental imaging timescales used in this study.

It is less clear how to reconcile the barbell model with the mobility of the gold-selenolate complex and the patterns formed by the progression of the selenol-thiolate exchange reaction. Gold-thiolate complex mobility has long been an important concept for explaining the order and dynamics of alkanethiolate monolayers; however, the mobility we observe in the bias-induced reactions (as shown in Figure 4.4, above) are unprecedented. During the tip-induced place-exchange reactions, there are translation distances on the order of 5 nm (corresponding to a minimum of 10 molecular lattice site hops to reach the new location) for both individual and grouped **C12Se**. A turnstile mechanism relying on the transient trichalcogen gold complex described above provides a possible mechanism. If the selenolate dissociates from a complex and can hop to an adjacent complex after bias induced activation, then the thiolate on the destination complex could in turn step back to effectively switch sites with the selenolate. Within the alkyl backbone superlattice and in the absence of available solution phase interactions favoring abstraction, subsequent transfer of a thiolate to the site vacated by the selenolate would be likely. The packing of the alkyl chains would be expected to deteriorate after repeated place exchanges by this mechanism, and this is observed as an increase in depressions in the monolayer (e.g., in comparison of Figures 4.5A' and 4.5C'). As described above, at higher selenolate coverage, the mixed monolayer system becomes randomly mixed and order is lost after imaging at +1 V sample bias. Conversely, the gold adatom complexes may instead be swapping sites with neighbors, consistent with the observed mobility of the complex. Additional experiments and theoretical modeling will be required to address the question of the buried structure and mechanism of both molecular and place-exchange reactions between thiolate/selenolate gold complexes.

4.3 Conclusions and Prospects

Examining SAM molecular exchange reactions through the lens of a gold adatom complex provides a variety of insights for interpreting the structural evolution from one complex supramolecular system to another, significantly less studied system. The atomic-scale configurations of gold-chalcogen bonds are deceptively complex problems. There are numerous phases of even simple alkanethiolates and alkaneselenolates on Au{111}.[26,86,111] We observed a monolayer transition from a full-coverage sulfur-bound **C10** SAM to a full-coverage selenium-bound **C12Se**, taking note of how the gold substrate directs the progression of the reaction, and the structures of the products.

In comparing single-component **C10** and **C12Se** SAMs, there are numerous structural differences. We reported substrate vacancy trenches in single-component **C12Se** SAMs, which become visible as narrow, linear vacancy islands. These trenches are aligned with the close-packed substrate lattice directions. Likewise, the ±1 Å apparent height variations of highly ordered **C12Se** are grouped in similarly aligned substrate-matched patches and rows. The boundaries between groups of different apparent heights are less stark than the domain boundaries in ordered **C10** domains. These observations are consistent with the viewpoint that there are both more varied binding sites available for selenolates and associated adatom complexes, and that apparent height is highly dependent on the Au-Se attachment geometry.

The replacement of **C10** by **C12Se** does not generate new vacancy trench features or adatom islands, suggesting that there is no ejection or reconstruction on thiolate replacement by selenium, pointing to conservation of the adatom complex (or of any other hypothesized motif) immediately following the exchange reaction. The contrast between the linear propagation of the thiolate/selenol displacement versus the more radial growth mechanism of 1-adamantanethiolate displacement by alkanethiols may provide insight into the stoichiometry of the complexes involved and into mechanistic details of exchange at adatom complexes. The displacement reaction follows the JMAK2 site-saturated island growth mechanism, consistent with similar monolayer exchange reactions.

We have observed that access to the substrate is required to initiate the exchange reaction, since insertion is observed predominantly at monolayer and substrate defect sites, and the insertion of a single molecule creates an adjacent molecular defect site. Also, inserted **C12Se** molecules appear lattice matched to adjacent **C10** molecules due to molecule-molecule interactions. For low fraction **C12Se** monolayers, we conclude that the selenolates have adopted thiolate-like binding configurations with the gold substrate, and as coverage is increased, the disruption of ordered alkanethiolate domains appears to occur directionally. From this result, we infer that the adatom layer is ordered in the highly annealed **C10** films we employ. Multiple binding configurations have been shown previously to be close energetically, and indicate that there are multiple stable possibilities for substrate attachment. The low energy barbell configuration may be consistent with these results, however, future experiments with grazing angle X-ray diffraction and local barrier height imaging[50] will be necessary to elucidate the binding configurations of **C12Se** and **C12**S. Data shown will have implications not only for the Au-S bond complexes, but also in the field of chemical patterning down to the single-molecule scale.[87]

Finally, we also observed a low (≤1 eV) barrier to induced motion of **C12Se** by the STM tip at positive sample bias, where electrons injected into empty states of the mixed monolayer film induce place-exchange reactions between the selenolates and thiolates. During motion, adjacent sites seem to have equal probability of providing a new attachment site, assuming the substrate bond configuration is the same. The atomistic nature of this reaction remains an open question. We postulate that application of positive sample bias induces a local thiolate to selenolate ligand exchange metathesis reaction between adjacent gold-adatom complexes. A turnstile adatom trichalcogen transitional state would account for the capacity of isolated selenolates to move through an ordered lattice without inducing extensive monolayer order.

4.4 Materials and Methods

4.4.1 Materials

1-Dodecanselenol was prepared by reduction of di(dodecyl)diselenide with $LiAlH_4$ in diethylether. After an acidic work-up, the product was purified by distillation over a 30 cm Vigreux column at a pressure of 20 hPa. It is vital to strictly exclude oxygen throughout each preparation step. 1-Decanethiol, 1-dodecanethiol, and absolute ethanol (nondenatured) were used as received from Sigma Aldrich (St. Louis, MO). Perdeuterated 1-dodecanethiol (**D12**) is used as received from CDN Isotopes (Canada). For air-sensitive work, ethanol is degassed via freeze-pump-thawing cycles as described previously[32] and is subsequently transferred to a sealed, gasketed bottle stored inside an oxygen-free (<1 ppm) glovebox. All glassware was cleaned by immersion in fresh piranha solution (1:3 H_2O_2 and concentrated sulfuric acid; *safety warning: solutions are strongly acidic and oxidizing, reactions are energetic and improper use or disposal could result in explosion or severe burns.*) and thorough rinsing in deionized water supplied by a Milli-Q system from Millipore (Billerica, MA).

4.4.2 Preparation of Substrates and Self-Assembled Monolayers

Gold on mica substrates (Agilent, Santa Clara, CA) and gold on silicon (prepared by electron beam evaporation of 1000 Å Au on a 50 Å Cr adhesion layer, without breaking vacuum, at a rate of 1 Å s^{-1} onto a *p*-type silicon wafer supplied by Silicon Quest International (Santa Clara, CA)) are annealed by 40 passes of a hydrogen flame (*safety warning: use appropriate engineering controls when striking a flame from a compressed fuel cylinder*) at an approximate rate of 0.5 Hz. The flame is struck from a quartz tip, which is held at a 45° angle while passed over the substrate. Substrates for **C12** SAM fabrication are used immediately after preparation, and the time between annealing and **C12Se** fabrication is minimized. Titanium adhesion layers for gold substrates are not recommended as the metal can peel from the substrate in response to flame exposure.

Preparation of exceptionally well-ordered, stable self-assembled monolayers is achieved through control of deposition conditions. The **C10**, **C12**, and **D12** solutions are prepared by transferring the appropriate volume of neat liquid substance to a volumetric flask, the mass confirmed gravimetrically. Flasks are then filled to the appropriate volume with ethanol. A freshly flame-annealed substrate is quickly immersed in the solution. Since full monolayer coverage is achieved within milliseconds of solution contact, excess volume is withdrawn. The gold substrate is left exposed to the airspace in the vial over a small volume of residual solution. The vial is capped and placed in a furnace set to 78 °C for a minimum of 24 h and up to 5 days. Under these vapor annealing conditions, SAM domain sizes grow exceptionally large and the SAM is well ordered, conditions conducive to imaging substrate-linked structures through minimization of alkyl backbone orientational defects. Any oxidative degradation of the film is immediately healed, maintaining film quality indefinitely until just before imaging or further modification. These well-ordered films resist oxidative degradation better than films deposited rapidly or at room temperature, and thus support stable continuous imaging for several days.

Ethanolic solutions of **C12Se** are prepared in an oxygen- and water-free glovebox. Organic thiols and selenols can contaminate a glovebox environment, so care is taken to minimize clean substrate exposure to the glovebox environment. Sample transfer operations are thus conducted rapidly, typically less than 3 s. Two vials are each filled with 1 mL of ethanol degassed via freeze-pump-thaw cycles. The first vial is kept sealed, and is held in reserve for a later rinsing step. One μL of **C12Se** is added to the first vial. A 5-min purge procedure is then performed on the glovebox environment. A freshly annealed substrate is placed in a gasketed vial, which has been briefly purged with a stream of nitrogen prior to sealing. The sample is then transferred to the glovebox, removed from the vial, and quickly immersed in the **C12Se** solution for 24 h. At the end of the immersion, the sample is removed from **C12Se** solution and placed immediately into the vial of neat ethanol, which is removed from the glovebox. The film is not air sensitive, and is then rinsed with neat ethanol and dried with nitrogen.

For molecular exchange experiments, the prefabricated initial sample is placed in a solution of the specified concentration for the specified time. Exchange by **C12Se** is performed inside the environmental glovebox, and exchange by **C10**, **C12**, or **D12** is performed under atmospheric conditions.

4.4.3 Scanning Tunneling Microscopy Measurements

All images were collected on a custom-built beetle-style STM in atmospheric air and at room temperature, as described previously.[112] The Pt/Ir 90:10 tip wire was supplied by Alfa Aesar (Ward Hill, MA). The gain of the piezoelectric scanners was calibrated by comparison of a **C10** monolayer on Au{111} to its known lattice constant of 4.99 Å. To ensure low drift, the STM tip is held in tunneling for as long as several days. Imaging of **C12Se** films is highly dependent on the state of the tip, which can change during imaging. Values reported were for stable and reproducible tips that could generally persist for several days. If a tip changed states frequently, a new tip was either cut immediately, or the instrument was left in tunneling for a period of several hours.

4.4.4 Infrared Reflectance Absorption Spectroscopy Measurements

All infrared spectra were collected on a Nicolet 8700 equipped with a Seagull variable angle reflection accessory, supplied by Harrick Scientific, Inc. (Ossining, NY). The spectrometer was purged by an FTIR Purge Gas Generator supplied by Parker-Balston (Cleveland, OH). Each spectrum was the result of between 512 and 1024 multiplexed scans, obtained at the grazing incidence angle of 84° relative to sample normal, and at a resolution of 4 cm^{-1}. For fractional coverage determination, samples were held in 1 mM exchange solution (typically ethanolic **C12SeH**) for 24 h to provide a 100% selenolate coverage substrate having identical reflective properties as those used for the kinetic experiment. Consequently, absolute coverage in the kinetic experiment increases slightly in that time. This small source of systematic error results in the observed kinetic trend of sub-100% maximum within the kinetic experimental timescale.

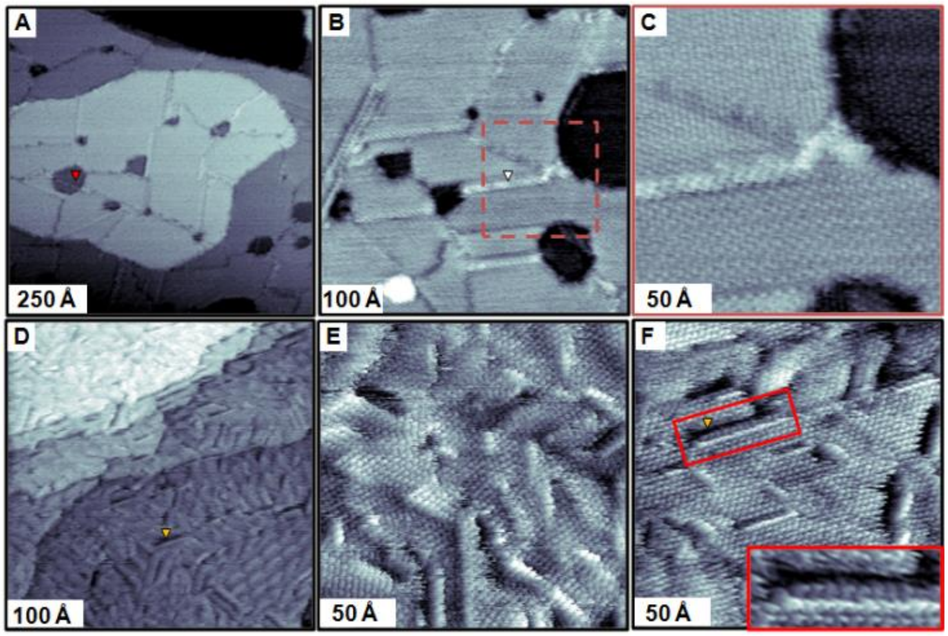

Figure 4.1 Comparison of scanning tunneling microscope images of single-component 1-decanethiolate (**C10**, top) and 1-dodecaneselenolate (**C12Se**, bottom) self-assembled monolayers on Au{111} obtained at a tunneling current of 3 pA and a sample bias voltage of -1 V. **(A-C)** The annealed **C10** monolayer is highly ordered, with large domains. The image shows important defect sites, including roughly circular vacancy island substrate defects (red arrow, **(A)** and linear domain boundaries SAM defects (white arrow, B) that appear either more or less protruding than the surrounding lattice. **(C)** A high-resolution image of the enclosed region in B. **(D-F)** The **C12Se** monolayer is ordered locally, but shows local variations in apparent height. The periodicity of the variation gives rise to the apparent Moiré pattern (visible in the lower right section of D).[26] The features align with the underlying substrate, with linear features rotated with respect to one another in integer multiples of 30°. **(F)** Vacancy islands in single-component **C12Se** SAMs are observed, hereafter described as vacancy trenches, presenting as narrow, linear depressions aligned with the close-packed direction of the substrate (examples denoted with the yellow arrows, D and F). Vacancy trenches are often accompanied

by a pair of **C12Se** molecular rows, which appear to be depressed or protruding from the median terrace height by -1 or +1 Å, respectively. The inset shows an expanded view of the region bounded by the red box. The median trench apparent height is ~2.3 Å lower than the median terrace apparent height, reflecting a monatomic step of the gold substrate surface.

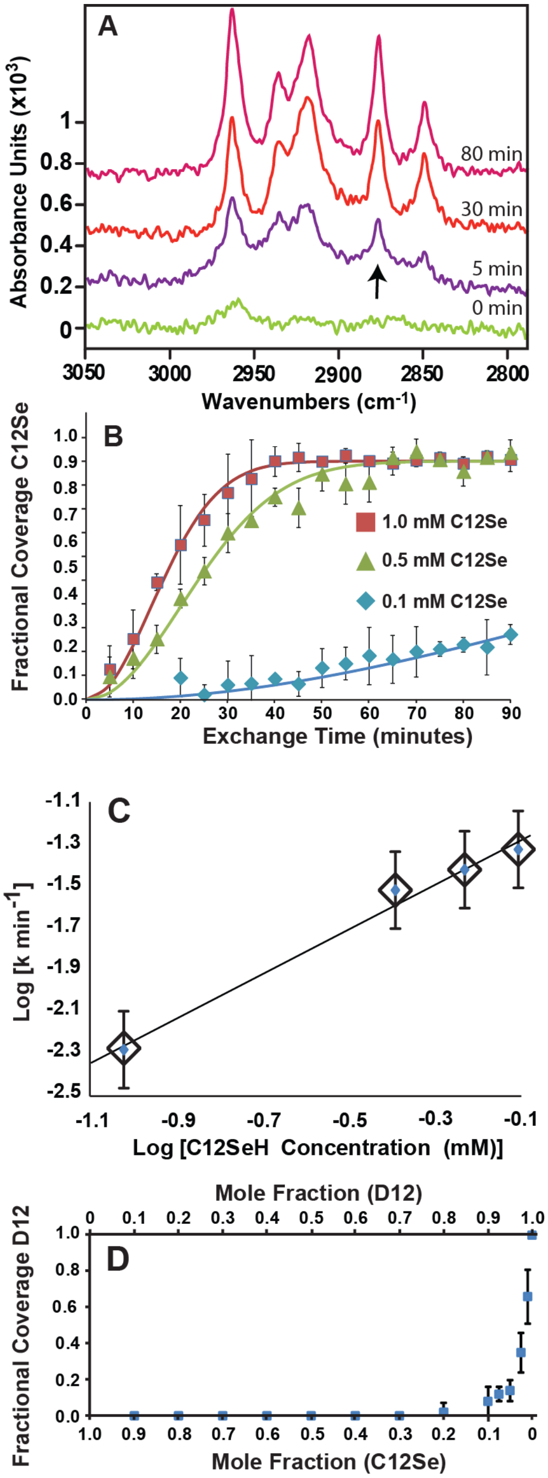

Figure 4.2 Tracking the exchange of perdeuterated 1-dodecanethiol (**D12**) by 1-dodecaneselenol (**C12Se**) via infrared reflectance absorption spectroscopy (IRRAS). **(A)** Evolution of the **C12Se** spectrum as it displaces the **D12** film. Spectral interference over the range shown was eliminated

by employing the deuterated species. The coverage indicator is the 2877 cm^{-1} methyl symmetric stretch, denoted by the black arrow. After 90 min, the reaction has reached completion and no further exchange occurs. **(B)** Examples of kinetic experiments tracking the progression of the exchange reaction between a preformed **D12** film and **C12Se** in solution. The data are fit to a site-saturated JMAK2 (Johnson, Mehl, Avrami, and Kolmogorov) model for perimeter dependent island growth.[57] **(C)** Rate constant of displacement versus **C12Se** concentration on a logarithmic scale has a slope of ~1, implying that the rate constant is directly proportional to the concentration of **C12Se**. **(D)** Codeposition studies of **D12** with **C12Se** demonstrating the preference for **C12Se** in mixed monolayers. **C12Se** dominates the coverage of a film until the mole fraction approaches 100:1 in favor of **D12**.

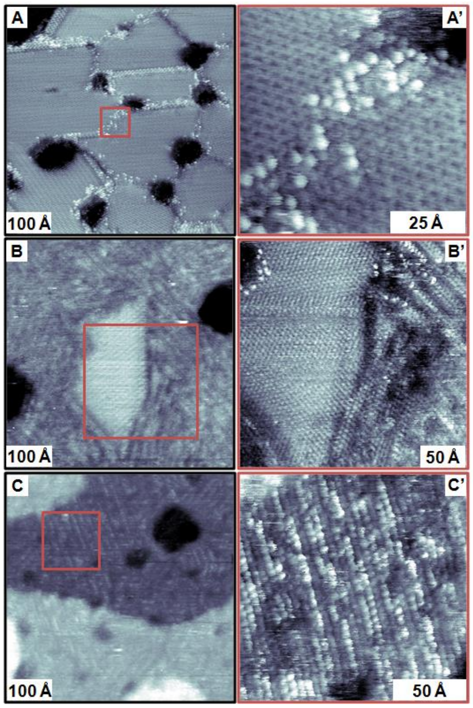

Figure 4.3 Scanning tunneling micrographs of mixed thiolate/selenolate self-assembled monolayers (SAMs) on Au{111}, all obtained at -1 V sample bias and 1 pA tunneling current. **(A, A')** Brief exposure (1 min) of a **C10** SAM to an ethanolic solution of 10 mM 1-dodecaneselenol (**C12Se**) results in adsorption at defect sites (step edges and domain boundaries). The **C12Se** molecules appear to protrude from the **C10** lattice by approximately ~0.7 Å in STM images under these conditions. **(B, B')** Longer exposures (4 min) resulted in substantial molecular exchange with **C12Se**, replacing **C10** under these conditions. The relative apparent heights of the two species have reversed; the thiolates appear to protrude from the predominantly **C12Se** lattice by ~0.7 Å in STM images. In B', features at three different apparent heights can be observed in a single image; **C12Se** molecules (top left) appear to protrude from the **C10** island by ~0.7 Å, while the island appears ~0.7 Å more protruding than nearby striped **C12Se**. Some intercalation of **C10** within the **C12Se** striped phase cannot be excluded. (**C, C'**) After 10 min of exposure, no **C10** molecules are observed, leaving only a striped phase of single-component **C12Se**.

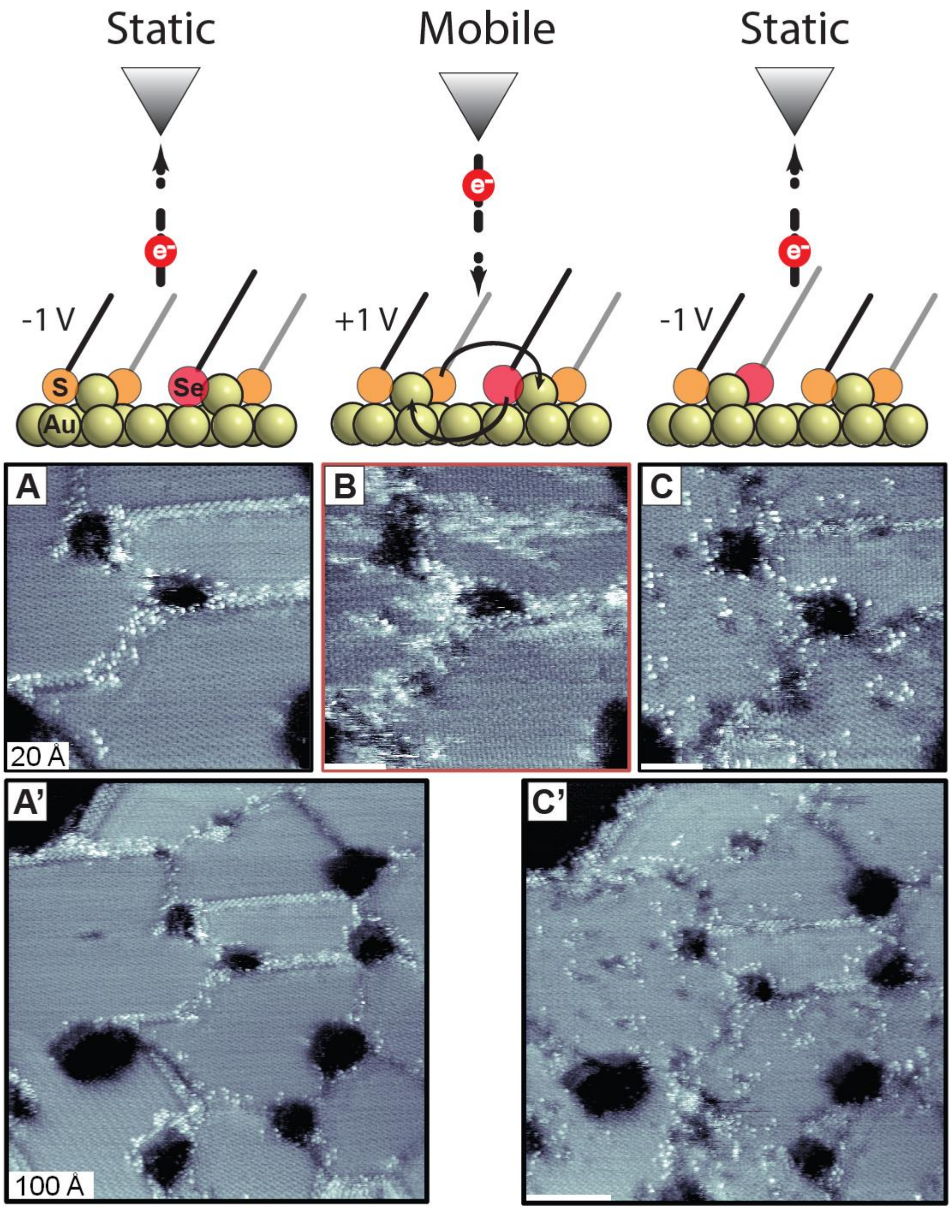

Figure 4.4 (Top) Schematic depicting direction of electron flow, sample bias, and reaction occurring between the gold (yellow circles) complex of selenolates (red circles), and thiolates (orange circles). Alkyl chains are denoted by black or grey lines. (Bottom) Sequence of images showing the effect of induced motion of 1-dodecaneselenolate (**C12Se**) in a 1-decanethiolate (**C10**) self-assembled monolayer. **(A and A')** Scanning tunneling micrographs of **C12Se** molecules (appear protruding) inserted predominantly at step edges and domain boundaries. Images collected at -1 V sample bias and 3 pA tunneling current. **(B)** Image of the same region

after reversal of the sample bias to +1 V. The reversal of bias polarity induces motion that enables **C12Se** to exchange positions with neighboring **C10**. The place-exchange reaction occurs faster than image acquisition, so the STM probe is no longer able to record the precise position of the selenolates.[103,104] (**C** and **C'**) Returning to -1 V sample bias halts the tip-induced motion of selenolates. Protruding molecules are observed in ordered **C10** domains, having diffused several nanometers while the region was imaged at +1 V sample bias. The larger scan area, image C', reveals that the motion of **C12Se** is induced at distances up to 50 nm from the tip position.

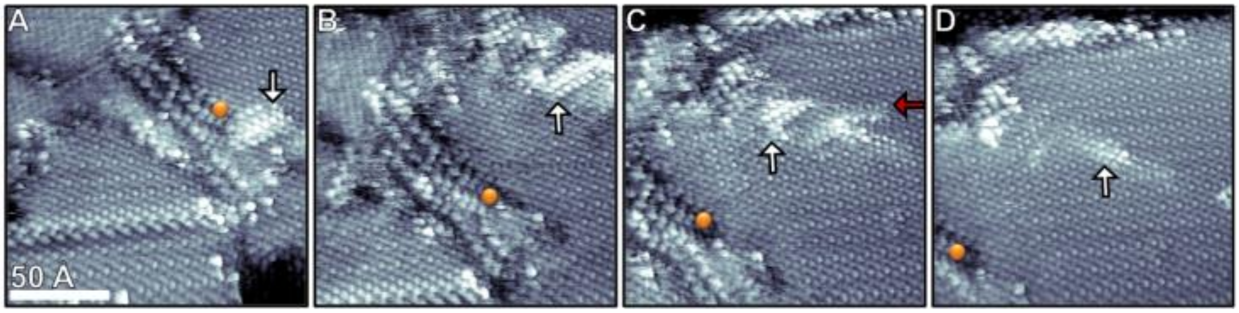

Figure 4.5 Application of a short voltage pulse over a **C12Se** cluster (+1 V sample bias, 3 pA, 5 s) induces 2D place-exchange reactions. Molecules that appear to protrude are attributed to 1-dodecaneselenolates in a 1-dodecanethiolate matrix. The pulse target, denoted by the orange circle, is labeled to account for drift over image acquisition times in excess of 5 min. The cluster denoted by the white arrow was the target of the voltage pulse. **(B)** In subsequent images, the cluster is displaced as a group and evolves over time. **(C)** The feature appears stable, and is then suddenly truncated at image line denoted in the red arrow, evidence of motion faster than the imaging timescale. **(D)** Subsequent images reveal continued changes in relative heights, with molecules likely drawn out of the field of view. The shift in image frame is because of drift over long image acquisition times (~5 min/frame).

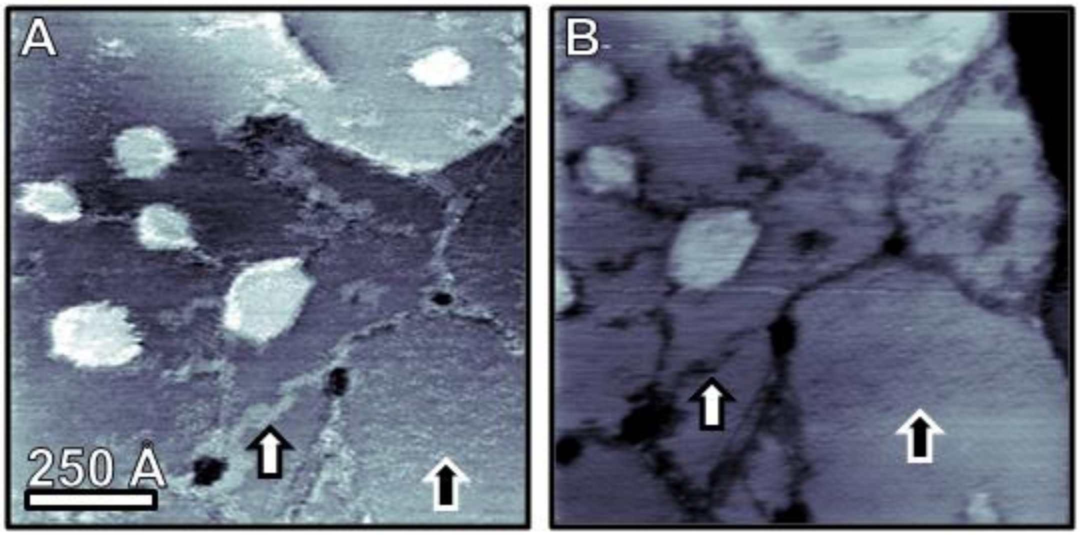

Figure 4.6 Distribution of selenolate exchange and tip dependence of apparent height. **(A)** Dodecaneselenolates inserted predominantly at decanethiolate SAM matrix defects appear protruding relative to the surrounding thiolates. In this example, insertion occurs at domain boundaries (white arrow), step edges, and within ordered domains, attributed to insertion at molecular vacancies (black arrow). **(B)** A tip state change after continuous imaging resulted in inverted contrast for the two molecular species. Both insertion at domain boundaries and within the domain now appear less protruding than the surrounding decanethiolate matrix. Such tip state changes occur randomly, but are more common as SAM order declines and after repeated sample bias reversal experiments. It is important to attribute molecular identity carefully as such tip changes can give a false representation of molecular motion and SAM dynamics.

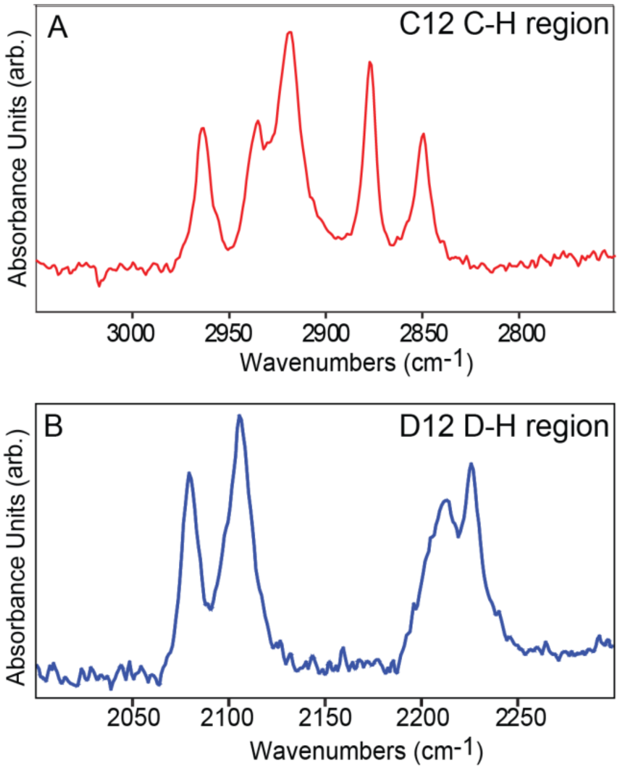

Figure 4.7 Carbon-hydrogen and carbon-deuterium stretches for 1-dodecanethiolate **(C12, A)** and perdeuterated 1-dodecanethiolate **(D12, B)** respectively.

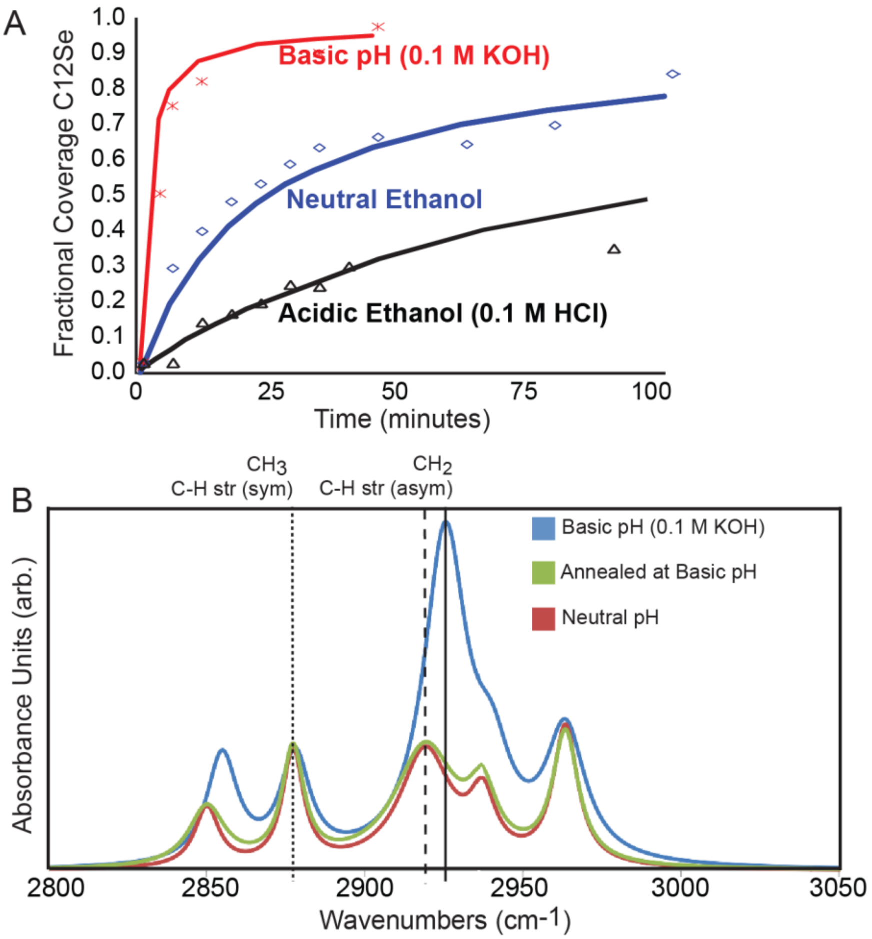

Figure 4.8 Effect of solution pH on perdeuterated 1-dodecanethiolate SAM exchange by 1-dodecaneselenol (**C12Se**) at 1 mM. **(A)** Addition of aqueous KOH to 1 mM ethanolic **C12Se** markedly increases displacement rate, while similar addition of aqueous hydrochloric acid reduces the rate of exchange. **(B)** Infrared reflectance spectra of the C-H region after 1 h base-catalyzed **C12Se** displacement (blue trace) compared to 24-h displacement at neutral pH. The methyl symmetric stretch at 2871 cm^{-1} has similar intensity, attributed to similar absolute coverage. Annealing in basic solution for 24 h at elevated temperature results in a **C12Se** film largely indistinguishable from the neutral pH control sample. This is additional evidence that base-catalyzed exchange is disruptive to film structure but does not appreciably affect the underlying gold substrate.

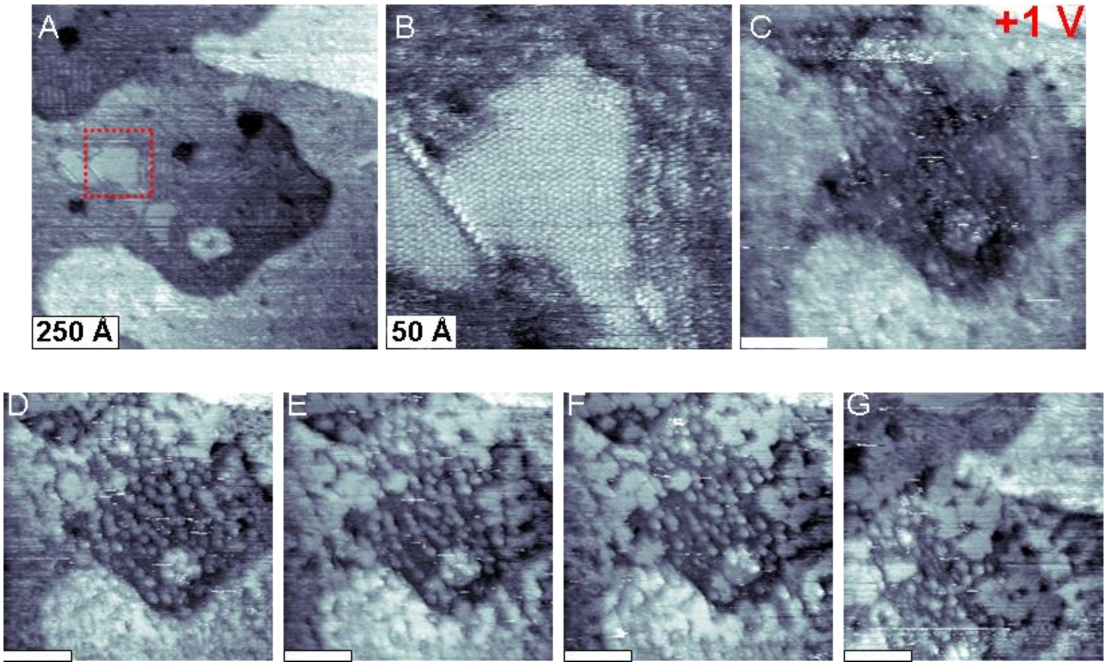

Figure 4.9 Imaging at positive bias at high relative 1-dodecaneselenol (**C12Se**) coverage (>25%) results in large-area reconfiguration of the monolayer structure. **(A)** Islands of pristine 1-decanethiolate (**C10**) remaining after significant **C12Se** displacement, an example is enclosed in a red square. **(B)** A high-resolution view of the **C10** island in A. **(C)** Imaging at +1 V sample bias results in a decrease in image resolution, consistent with molecular motion and place exchange between alkanethiolate and alkaneselenolate. **(D)** Returning to -1 V sample bias reveals a scrambled interface. The discrete **C10** islands and striped features have been replaced with a mottled structure. **(E-G)** Continued imaging reveals motion and reconfiguration of the domains in the image. With the exception of C, images were collected at -1 V sample bias, and all images at 3 pA tunneling current. Images C-G shares the scale of image A.

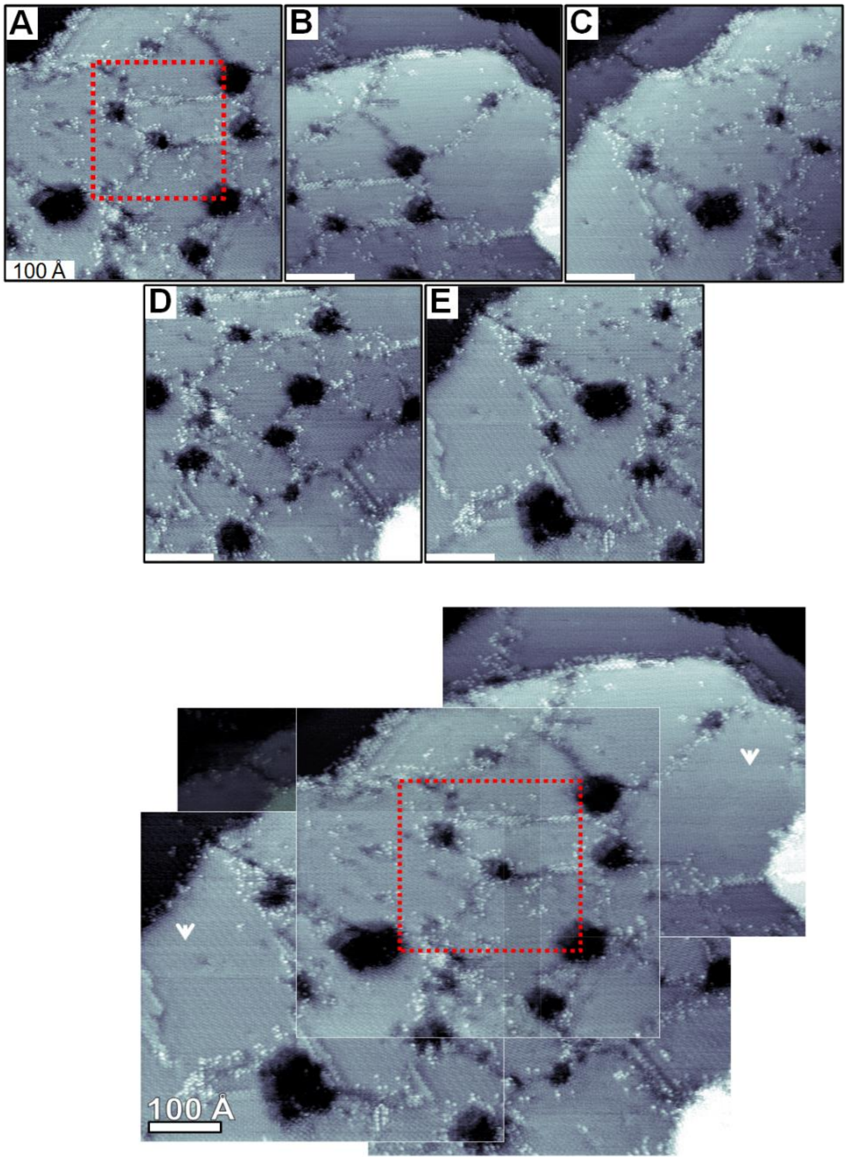

Figure 4.10 Images and aligned composite revealing the spatial distribution of molecules induced to move via tip-induced place-exchange reactions. **(A)** The region highlighted by the red square at image center is the region scanned at +1 V sample bias for a full image acquisition time (~5 min). The protruding **C12Se** molecules are found in different positions after imaging at this potential. Domains in excess of 250 Å from the center of the imaged area are largely undisturbed by positive bias imaging, as indicated by the white arrows denoting pristine domains in the composite image (left and right).

References

1. Stranick, S. J.; Parikh, A. N.; Allara, D. L.; Weiss, P. S. A new mechanism for surface diffusion: motion of a substrate-adsorbate complex. *J. Phys. Chem.* 1994, 98, 11136-11142.

2. Maksymovych, P.; Sorescu, D. C.; Yates, J. T. Gold-adatom-mediated bonding in self-assembled short-chain alkanethiolate species on the Au(111) surface. *Phys. Rev. Lett.* 2006, 97, 146103.

3. Yu, M.; Bovet, N.; Satterley, C. J.; Bengio, S.; Lovelock, K. R. J.; Milligan, P. K.; Jones, R. G.; Woodruff, D. P.; Dhanak, V. True nature of an archetypal self-assembly system: Mobile Au-thiolate species on Au(111). *Phys. Rev. Lett.* 2006, 97, 166102.

4. Jadzinsky, P. D.; Calero, G.; Ackerson, C. J.; Bushnell, D. A.; Kornberg, R. D. Structure of a thiol monolayer-protected gold nanoparticle at 1.1 Å resolution. *Science* 2007, 318, 430-433.

5. Mazzarello, R.; Cossaro, A.; Verdini, A.; Rousseau, R.; Casalis, L.; Danisman, M. F.; Floreano, L.; Scandolo, S.; Morgante, A.; Scoles, G. Structure of a CH_3S monolayer on Au(111) solved by the interplay between molecular dynamics calculations and diffraction measurements. *Phys. Rev. Lett.* 2007, 98, 4.

6. Maksymovych, P.; Yates, J. T. Au adatoms in self-assembly of benzenethiol on the Au(111) surface. *J. Am. Chem. Soc.* 2008, 130, 7518-7519.

7. Cossaro, A.; Mazzarello, R.; Rousseau, R.; Casalis, L.; Verdini, A.; Kohlmeyer, A.; Floreano, L.; Scandolo, S.; Morgante, A.; Klein, M. L.; Scoles, G. X-ray diffraction and computation yield the structure of alkanethiols on gold(111). *Science* 2008, 321, 943-946.

8. Kautz, N. A.; Kandel, S. A. Alkanethiol/Au(111) Self-assembled monolayers contain gold adatoms: scanning tunneling microscopy before and after reaction with atomic hydrogen. *J. Am. Chem. Soc.* 2008, 130, 6908-6909.

9. Voznyy, O.; Dubowski, J. J.; Yates, J. T.; Maksymovych, P. The role of gold adatoms and stereochemistry in self-assembly of methylthiolate on Au(111). *J. Am. Chem. Soc.* 2009, 131, 12989-12993.

10. Kautz, N. A.; Kandel, S. A. Alkanethiol monolayers contain gold adatoms, and adatom coverage is independent of chain length. *J. Phys. Chem. C* 2009, 113, 19286-19291.

11. Qian, H.; Eckenhoff, W. T.; Zhu, Y.; Pintauer, T.; Jin, R. Total structure determination of thiolate-protected Au_{38} nanoparticles. *J. Am. Chem. Soc.* 2010, 132, 8280-8281.

12. Liu, Y.; Ozolins, V. Self-assembled monolayers on Au(111): structure, energetics, and mechanism of reconstruction lifting. *J. Phys. Chem. C* 2012, 116, 4738-4747.

13. Hakkinen, H. The gold-sulfur interface at the nanoscale. *Nat. Chem.* 2012, 4, 443-455.

14. Knoppe, S.; Dolamic, I.; Bürgi, T. Racemization of a chiral nanoparticle evidences the flexibility of the gold-thiolate interface. *J. Am. Chem. Soc.* 2012, 134, 13114-13120.

15. Fan, X.; Zhang, C.; Liu, Y.; Lau, W. M. Effects of intrinsic surface defects on thiophenol self-assembly on au(111): surface structures and reaction mechanisms. *J. Phys. Chem. C* 2012, 116, 19909-19917.

16. Moore, A. M.; Mantooth, B. A.; Donhauser, Z. J.; Yao, Y. X.; Tour, J. M.; Weiss, P. S. Real-time measurements of conductance switching and motion of single oligo(phenylene ethynylene) molecules. *J. Am. Chem. Soc.* 2007, 129, 10352-10353.

17. Poirier, G. E. Mechanism of formation of Au vacancy islands in alkanethiol monolayers on Au(111). *Langmuir* 1997, 13, 2019-2026.

18. Akihiro, N.; Yoshitada, M. Adsorption states of methylthiolate on the Au(111) surface. *J. Phys.: Condens. Matter* 2007, 19, 365245.

19. Jewell, A. D.; Tierney, H. L.; Sykes, E. C. H. Gently lifting gold's herringbone reconstruction: Trimethylphosphine on Au(111). *Phys. Rev. B* 2010, 82, 205401.

20. Schlenoff, J. B.; Li, M.; Ly, H. Stability and self-exchange in alkanethiol monolayers. *J. Am. Chem. Soc.* 1995, 117, 12528-12536.

21. Shon, Y. S.; Lee, T. R. Desorption and exchange of self-assembled monolayers (SAMs) on gold generated from chelating alkanedithiols. *J. Phys. Chem. B* 2000, 104, 8192-8200.

22. Moore, A. M.; Mantooth, B. A.; Donhauser, Z. J.; Maya, F.; Price, D. W.; Yao, Y. X.; Tour, J. M.; Weiss, P. S. Cross-step place-exchange of oligo(phenylene-ethynylene) molecules. *Nano Lett.* 2005, 5, 2292-2297.

23. Kassam, A.; Bremner, G.; Clark, B.; Ulibarri, G.; Lennox, R. B. Place exchange reactions of alkyl thiols on gold nanoparticles. *J. Am. Chem. Soc.* 2006, 128, 3476-3477.

24. Patole, S. N.; Baddeley, C. J.; O'Hagan, D.; Richardson, N. V. Reversible exchange of self-assembled monolayers of semifluorinated *n*-alkanethiols and *n*-alkanethiols on Au/mica surfaces. *J. Phys. Chem. C* 2008, 112, 13997-14000.

25. Ballav, N.; Terfort, A.; Zharnikov, M. Mixing of nonsubstituted and partly fluorinated alkanethiols in a binary self-assembled monolayer. *J. Phys. Chem. C* 2009, 113, 3697-3706.

26. Monnell, J. D.; Stapleton, J. J.; Jackiw, J. J.; Dunbar, T.; Reinerth, W. A.; Dirk, S. M.; Tour, J. M.; Allara, D. L.; Weiss, P. S. Ordered local domain structures of decaneselenolate and dodecaneselenolate monolayers on Au{111}. *J. Phys. Chem. B* 2004, 108, 9834-9841.

27. Monnell, J. D.; Stapleton, J. J.; Dirk, S. M.; Reinerth, W. A.; Tour, J. M.; Allara, D. L.; Weiss, P. S. Relative conductances of alkaneselenolate and alkanethiolate monolayers on Au{111}. *J. Phys. Chem. B* 2005, 109, 20343-20349.

28. Bashir, A.; Käfer, D.; Müller, J.; Wöll, C.; Terfort, A.; Witte, G. Selenium as a key element for highly ordered aromatic self-assembled monolayers. *Angew. Chem., Int. Ed.* 2008, 47, 5250-5252.

29. Cyganik, P.; Szelagowska-Kunstman, K.; Terfort, A.; Zharnikov, M. Odd-even effect in molecular packing of biphenyl-substituted alkaneselenolate self-assembled monolayers on Au(111): Scanning tunneling microscopy study. *J. Phys. Chem. C* 2008, 112, 15466-15473.

30. Track, A. M.; Rissner, F.; Heimel, G.; Romaner, L.; Käfer, D.; Bashir, A.; Rangger, G. M.; Hofmann, O. T.; Bucko, T.; Witte, G.; Zojer, E. Simultaneously understanding the geometric and electronic structure of anthraceneselenolate on Au(111): A combined theoretical and experimental study. *J. Phys. Chem. C* 2010, 114, 2677-2684.

31. Weidner, T.; Ballav, N.; Grunze, M.; Terfort, A.; Zharnikov, M. Modification of biphenylselenolate monolayers by low-energy electrons. *Phys. Status Solidi B* 2009, 246, 1519-1528.

32. Hohman, J. N.; Kim, M.; Schüpbach, B.; Kind, M.; Thomas, J. C.; Terfort, A.; Weiss, P. S. Dynamic double lattice of 1-adamantaneselenolate self-assembled monolayers on Au{111}. *J. Am. Chem. Soc.* 2011, 133, 19422-19431.

33. Yokota, K.; Taniguchi, M.; Tsutsui, M.; Kawai, T. Molecule-electrode bonding design for high single-molecule conductance. *J. Am. Chem. Soc.* 2011, 132, 17364-17365.

34. Cometto, F. P.; Patrito, E. M.; Paredes Olivera, P.; Zampieri, G.; Ascolani, H. Electrochemical, high-resolution photoemission spectroscopy and vdW-DFT study of the thermal stability of benzenethiol and benzeneselenol monolayers on Au(111). *Langmuir* 2012, 28, 13624-13635.

35. Kurashige, W.; Yamaguchi, M.; Nobusada, K.; Negishi, Y. Ligand-induced stability of gold nanoclusters: thiolate versus selenolate. *J. Phys. Chem. Lett.* 2012, 3, 2649-2652.

36. Pathem, B. K.; Claridge, S. A.; Zheng, Y. B.; Weiss, P. S. Molecular switches and motors on surfaces. *Annu. Rev. Phys. Chem.* 2013, 64, 605-630.

37. Romashov, L. V.; Ananikov, V. P. Self-assembled selenium monolayers: from nanotechnology to materials science and adaptive catalysis. *Chem. Eur. J.* 2013, 19, 17640-17660.

38. Huang, F. K.; Horton, R. C.; Myles, D. C.; Garrell, R. L. Selenolates as alternatives to thiolates for self-assembled monolayers: A SERS study. *Langmuir* 1998, 14, 4802-4808.

39. Szelągowska-Kunstman, K.; Cyganik, P.; Schupbach, B.; Terfort, A. Relative stability of thiol and selenol based SAMs on Au(111) - exchange experiments. *Phys. Chem. Chem. Phys.* 2010, 12, 4400-4406.

40. Stipe, B. C.; Rezaei, M. A.; Ho, W. Single-molecule vibrational spectroscopy and microscopy. *Science* 1998, 280, 1732-1735.

41. Bumm, L. A.; Arnold, J. J.; Dunbar, T. D.; Allara, D. L.; Weiss, P. S. Electron transfer through organic molecules. *J. Phys. Chem. B* 1999, 103, 8122-8127.

42. Weiss, P. S.; Eigler, D. M. Site dependence of the apparent shape of a molecule in scanning tunneling micoscope images: Benzene on Pt{111}. *Phys. Rev. Lett.* 1993, 71, 3139-3142.

43. Donhauser, Z. J.; Mantooth, B. A.; Kelly, K. F.; Bumm, L. A.; Monnell, J. D.; Stapleton, J. J.; Price, D. W.; Rawlett, A. M.; Allara, D. L.; Tour, J. M.; Weiss, P. S. Conductance switching in single molecules through conformational changes. *Science* 2001, 292, 2303-2307.

44. Camillone, N.; Eisenberger, P.; Leung, T. Y. B.; Schwartz, P.; Scoles, G.; Poirier, G. E.; Tarlov, M. J. New monolayer phases of *n*-alkanethiols self-assembled on Au(111) – preparation, surface characterization, and imaging. *J. Chem. Phys.* 1994, 101, 11031-11036.

45. Poirier, G. E.; Tarlov, M. J. The *c*(4 × 2) superlattice of *n*-alkanethiol monolayers self-assembled on Au(111). *Langmuir* 1994, 10, 2853-2856.

46. Poirier, G. E. Characterization of organosulfur molecular monolayers on Au(111) using scanning tunneling microscopy. *Chem. Rev.* 1997, 97, 1117-1127.

47. Weiss, P. S. Functional molecules and assemblies in controlled environments: formation and measurements. *Acc. Chem. Res.* 2008, 41, 1772-1781.

48. Love, J. C.; Estroff, L. A.; Kriebel, J. K.; Nuzzo, R. G.; Whitesides, G. M. Self-assembled monolayers of thiolates on metals as a form of nanotechnology. *Chem. Rev.* 2005, 105, 1103-1169.

49. Bent, S. F. Heads or tails: Which is more important in molecular self-assembly? *ACS Nano* 2007, 1, 10-12.

50. Han, P.; Kurland, A. R.; Giordano, A. N.; Nanayakkara, S. U.; Blake, M. M.; Pochas, C. M.; Weiss, P. S. Heads and tails: simultaneous exposed and buried interface imaging of monolayers. *ACS Nano* 2009, 3, 3115-3121.

51. Choi, J.; Lee, Y. J.; Kang, H.; Han, J. W.; Noh, J. Self-assembled monolayers of dioctyl diselenides on au(111). *Bull. Korean Chem. Soc.* 2008, 29, 1229-1232.

52. Yang, G.; Liu, G.-y. New insights for self-assembled monolayers of organothiols on Au(111) revealed by scanning tunneling microscopy. *J. Phys. Chem. B* 2003, 107, 8746-8759.

53. de la Llave, E.; Scherlis, D. A. Selenium-based self-assembled monolayers: The nature of adsorbate-surface interactions. *Langmuir* 2010, 26, 173-178.

54. Dameron, A. A.; Charles, L. F.; Weiss, P. S. Structures and displacement of 1-adamantanethiol self-assembled monolayers on Au{111}. *J. Am. Chem. Soc.* 2005, 127, 8697-8704.

55. Dameron, A. A.; Mullen, T. J.; Hengstebeck, R. W.; Saavedra, H. M.; Weiss, P. S. Origins of displacement in 1-adamantanethiolate self-assembled monolayers. *J. Phys. Chem. C* 2007, 111, 6747-6752.

56. Mullen, T. J.; Dameron, A. A.; Saavedra, H. M.; Williams, M. E.; Weiss, P. S. Dynamics of solution displacement in 1-adamantanethiolate self-assembled monolayers. *J. Phys. Chem. C* 2007, 111, 6740-6746.

57. Saavedra, H. M.; Barbu, C. M.; Dameron, A. A.; Mullen, T. J.; Crespi, V. H.; Weiss, P. S. 1-adamantanethiolate monolayer displacement kinetics follow a universal form. *J. Am. Chem. Soc.* 2007, 129, 10741-10746.

58. Bumm, L. A.; Arnold, J. J.; Cygan, M. T.; Dunbar, T. D.; Burgin, T. P.; Jones, L.; Allara, D. L.; Tour, J. M.; Weiss, P. S. Are single molecular wires conducting? *Science* 1996, 271, 1705-1707.

59. Cygan, M. T.; Dunbar, T. D.; Arnold, J. J.; Bumm, L. A.; Shedlock, N. F.; Burgin, T. P.; Jones, L.; Allara, D. L.; Tour, J. M.; Weiss, P. S. Insertion, conductivity, and structures of conjugated organic oligomers in self-assembled alkanethiol monolayers on Au{111}. *J. Am. Chem. Soc.* 1998, 120, 2721-2732.

60. Donhauser, Z. J.; Price, D. W.; Tour, J. M.; Weiss, P. S. Control of alkanethiolate monolayer structure using vapor-phase annealing. *J. Am. Chem. Soc.* 2003, 125, 11462-11463.

61. Weck, M.; Jackiw, J. J.; Rossi, R. R.; Weiss, P. S.; Grubbs, R. H. Ring-opening metathesis polymerization from surfaces. *J. Am. Chem. Soc.* 1999, 121, 4088-4089.

62. Kim, M.; Hohman, J. N.; Cao, Y.; Houk, K. N.; Ma, H.; Jen, A. K.-Y.; Weiss, P. S. Creating favorable geometries for directing organic photoreactions in alkanethiolate monolayers. *Science* 2011, 331, 1312-1315.

63. Zheng, Y. B.; Pathem, B. K.; Hohman, J. N.; Thomas, J. C.; Kim, M.; Weiss, P. S. Photoresponsive molecules: photoresponsive molecules in well-defined nanoscale environments. *Adv. Mater.* 2013, 25, 293-293.

64. Poirier, G. E.; Tarlov, M. J.; Rushmeier, H. E. 2-Dimensional liquid-phase and the $p \times \sqrt{3}$ phase of alkanethiol self-assembled monolayers on Au(111). *Langmuir* 1994, 10, 3383-3386.

65. Dishner, M. H.; Feher, F. J.; Hemminger, J. C. Formation and photooxidation of *n*-dodecanethiol self-assembled monolayers on Au(111): 'Pits' formed during chemisorption disappear upon oxidation. *Chem. Commun.* 1996, 1971-1972.

66. Smith, R. K.; Lewis, P. A.; Weiss, P. S. Patterning self-assembled monolayers. *Prog. Surf. Sci.* 2004, 75, 1-68.

67. Yang, G.; Amro, N. A.; Starkewolfe, Z. B.; Liu, G.-Y. Molecular-level approach to inhibit degradations of alkanethiol self-assembled monolayers in aqueous media. *Langmuir* 2004, 20, 3995-4003.

68. Stranick, S. J.; Parikh, A. N.; Allara, D. L.; Weiss, P. S. A new mechanism for surface-diffusion - motion of a substrate-adsorbate complex. *J. Phys. Chem.* 1994, 98, 11136-11142.

69. Kim, M.; Hohman, J. N.; Morin, E. I.; Daniel, T. A.; Weiss, P. S. Self-assembled monolayers of 2-adamantanethiol on Au{111}: Control of structure and displacement. *J. Phys. Chem. A* 2009, 113, 3895-3903.

70. Saavedra, H. M.; Thompson, C. M.; Hohman, J. N.; Crespi, V. H.; Weiss, P. S. Reversible lability by in situ reaction of self-assembled monolayers. *J. Am. Chem. Soc.* 2009, 131, 2252-2259.

71. Saavedra, H. M.; Mullen, T. J.; Zhang, P. P.; Dewey, D. C.; Claridge, S. A.; Weiss, P. S. Hybrid strategies in nanolithography. *Rep. Prog. Phys.* 2010, 73, 036501.

72. Shaporenko, A.; Ulman, A.; Terfort, A.; Zharnikov, M. Self-assembled monolayers of alkaneselenolates on (111) gold and silver. *J. Phys. Chem. B* 2005, 109, 3898-3906.

73. Yee, C. K.; Ulman, A.; Ruiz, J. D.; Parikh, A.; White, H.; Rafailovich, M. Alkyl selenide- and alkyl thiolate-functionalized gold nanoparticles: chain packing and bond nature. *Langmuir* 2003, 19, 9450-9458.

74. Fonder, G.; Cecchet, F.; Peremans, A.; Thiry, P. A.; Delhalle, J.; Mekhalif, Z. Conformational order of n-dodecanethiol and n-dodecaneselenol monolayers on polycrystalline copper investigated by PM-IRRAS and SFG spectroscopy. *Surf. Sci.* 2009, 603, 2276-2282.

75. Fonder, G.; Delhalle, J.; Mekhalif, Z. Exchange versus intercalation of *n*-dodecanethiol monolayers on copper in the presence of n-dodecaneselenol and *vice versa*. *Appl. Surf. Sci.* 2011, 256, 2968-2973.

76. Aizenberg, J.; Black, A. J.; Whitesides, G. M. Controlling local disorder in self-assembled monolayers by patterning the topography of their metallic supports. *Nature* 1998, 394, 868.

77. Black, A. J.; Paul, K. E.; Aizenberg, J.; Whitesides, G. M. Patterning disorder in monolayer resists for the fabrication of sub-100-nm structures in silver, gold, silicon, and aluminum. *J. Am. Chem. Soc.* 1999, 121, 8356-8365.

78. Collard, D. M.; Fox, M. A. Use of electroactive thiols to study the formation and exchange of alkanethiol monolayers on gold. *Langmuir* 1991, 7, 1192-1197.

79. Baralia, G. G.; Duwez, A.-S.; Nysten, B.; Jonas, A. M. Kinetics of exchange of alkanethiol monolayers self-assembled on polycrystalline gold. *Langmuir* 2005, 21, 6825-6829.

80. Hohman, J. N.; Claridge, S. A.; Kim, M.; Weiss, P. S. Cage molecules for self-assembly. *Mater. Sci. Eng., R* 2010, 70, 188-208.

81. Kamenetska, M.; Quek, S. Y.; Whalley, A. C.; Steigerwald, M. L.; Choi, H. J.; Louie, S. G.; Nuckolls, C.; Hybertsen, M. S.; Neaton, J. B.; Venkataraman, L. Conductance and geometry of pyridine-linked single-molecule junctions. *J. Am. Chem. Soc.* 2010, 132, 6817-6821.

82. Hill, I. R.; Levin, I. W. Vibrational spectra and carbon--hydrogen stretching mode assignments for a series of *n*-alkyl carboxylic acids. *J. Chem. Phys* 1979, 70, 842-851.

83. Porter, M. D.; Bright, T. B.; Allara, D. L.; Chidsey, C. E. D. Spontaneously organized molecular assemblies. 4. Structural characterization of *n*-alkyl thiol monolayers on gold by optical ellipsometry, infrared spectroscopy, and electrochemistry. *J. Am. Chem. Soc.* 1987, 109, 3559-3568.

84. Nuzzo, R. G.; Dubois, L. H.; Allara, D. L. Fundamental-studies of microscopic wetting on organic-surfaces. 1. Formation and structural characterization of a self-consistent series of polyfunctional organic monolayers. *J. Am. Chem. Soc.* 1990, 112, 558-569.

85. Choi, J.; Kang, H.; Ito, E.; Hara, M.; Noh, J. Phase transition of octaneselenolate self-assembled monolayers on Au(111) studied by scanning tunneling microscopy. *Bull. Korean Chem. Soc.* 2011, 32, 2623-2627.

86. Vericat, C.; Vela, M. E.; Salvarezza, R. C. Self-assembled monolayers of alkanethiols on Au(111): surface structures, defects and dynamics. *Phys. Chem. Chem. Phys.* 2005, 7, 3258-3268.

87. Claridge, S. A.; Liao, W.-S.; Thomas, J. C.; Zhao, Y.; Cao, H. H.; Cheunkar, S.; Serino, A. C.; Andrews, A. M.; Weiss, P. S. From the bottom up: Dimensional control and characterization in molecular monolayers. *Chem. Soc. Rev.* 2012, 42, 2725-2745.

88. Avrami, M. Kinetics of phase change I - General theory. *J. Chem. Phys.* 1939, 7, 1103-1112.

89. Avrami, M. Kinetics of phase change. II transformation-time relations for random distribution of nuclei. *J. Chem. Phys.* 1940, 8, 212-224.

90. Avrami, M. Kinetics of phase change. III granulation, phase change, and microstructure *J. Chem. Phys.* 1941, 9, 177-184.

91. Wang, Y.; Zeiri, O.; Neyman, A.; Stellacci, F.; Weinstock, I. A. Nucleation and island growth of alkanethiolate ligand domains on gold nanoparticles. *ACS Nano* 2012, 6, 629-640.

92. Hobara, D.; Sasaki, T.; Imabayashi, S.-I.; Kakiuchi, T. Surface structure of binary self-assembled monolayers formed by electrochemical selective replacement of adsorbed thiols. *Langmuir* 1999, 15, 5073-5078.

93. Mullen, T. J.; Dameron, A. A.; Weiss, P. S. Directed assembly and separation of self-assembled monolayers *via* electrochemical processing. *J. Phys. Chem. B* 2006, 110, 14410-14417.

94. Eigler, D. M.; Schweizer, E. K. Positioning single atoms with a scanning tunnelling microscope. *Nature* 1990, 344, 524-526.

95. Avouris, P.; Lyo, I.-W.; Bozso, F. Atom-resolved surface chemistry: The early steps of Si(111)-7×7 oxidation. *J. Vac. Sci. Technol. B* 1991, 9, 424-430.

96. Weiss, P. S.; Eigler, D. M. Adsorption and accommodation of Xe on Pt{111}. *Phys. Rev. Lett.* 1992, 69, 2240-2243.

97. Lyding, J. W.; Hess, K.; Abeln, G. C.; Thompson, D. S.; Moore, J. S.; Hersam, M. C.; Foley, E. T.; Lee, J.; Chen, Z.; Hwang, S. T.; Choi, H.; Avouris, P.; Kizilyalli, I. C. Ultrahigh vacuum scanning tunneling microscopy nanofabrication and hydrogen/deuterium desorption from silicon surfaces: implications for complementary metal oxide semiconductor technology. *Appl. Surf. Sci.* 1998, 130-132, 221-230.

98. Liu, M.; Amro, N. A.; Liu, G.-Y. Nanografting for surface physical chemistry. *Annu. Rev. Phys. Chem.* 2008, 59, 367-386.

99. Luis, G. R.; Jian, L. Atomic force microscope nanolithography: dip-pen, nanoshaving, nanografting, tapping mode, electrochemical and thermal nanolithography. *J. Phys.: Condens. Matter* 2009, 21, 483001.

100. Liu, G.-Y.; Xu, S.; Qian, Y. Nanofabrication of self-assembled monolayers using scanning probe lithography. *Acc. Chem. Res.* 2000, 33, 457-466.

101. Cheung, C. L.; Camarero, J. A.; Woods, B. W.; Lin, T. W.; Johnson, J. E.; De Yoreo, J. J. Fabrication of assembled virus nanostructures on templates of chemoselective linkers formed by scanning probe nanolithography. *J. Am. Chem. Soc.* 2003, 125, 6848-6849.

102. Kramer, S.; Fuierer, R. R.; Gorman, C. B. Scanning probe lithography using self-assembled monolayers. *Chem. Rev.* 2003, 103, 4367-4418.

103. Stranick, S. J.; Kamna, M. M.; Weiss, P. S. Atomic-scale dynamics of a two-dimensional gas-solid interface. *Science* 1994, 266, 99-102.

104. Mantooth, B. A.; Sykes, E. C. H.; Han, P.; Moore, A. M.; Donhauser, Z. J.; Crespi, V. H.; Weiss, P. S. Analyzing the motion of benzene on Au{111}: single molecule statistics from scanning probe images. *J. Phys. Chem. C* 2007, 111, 6167-6182.

105. Claridge, S. A.; Schwartz, J. J.; Weiss, P. S. Electrons, photons, and force: Quantitative single-molecule measurements from physics to biology. *ACS Nano* 2011, 5, 693-729.

106. Tarr, S.; Weiss, P. S. Very small horses: visualizing motion at the nanoscale. *Leonardo* 2012, 45, 439-445.

107. Nenchev, G.; Diaconescu, B.; Hagelberg, F.; Pohl, K. Self-assembly of methanethiol on the reconstructed Au(111) surface. *Phys. Rev. B* 2009, 80, 081401.

108. Zhu, M.; Aikens, C. M.; Hollander, F. J.; Schatz, G. C.; Jin, R. Correlating the crystal structure of a thiol-protected Au_{25} cluster and optical properties. *J. Am. Chem. Soc.* 2008, 130, 5883-5885.

109. Maksymovych, P.; Voznyy, O.; Dougherty, D. B.; Sorescu, D. C.; Yates, J. T. Gold adatom as a key structural component in self-assembled monolayers of organosulfur molecules on Au(111). *Prog. Surf. Sci.* 2010, 85, 206-240.

110. Lewis, P. A.; Donhauser, Z. J.; Mantooth, B. A.; Smith, R. K.; Bumm, L. A.; Kelly, K. F.; Weiss, P. S. Control and placement of molecules *via* self-assembly. *Nanotechnology* 2001, 12, 231-237.

111. Qian, Y.; Yang, G.; Yu, J.; Jung, T. A.; Liu, G.-Y. Structures of annealed decanethiol self-assembled monolayers on Au(111): An ultrahigh vacuum scanning tunneling microscopy study. *Langmuir* 2003, 19, 6056-6065.

112. Bumm, L. A.; Arnold, J. J.; Charles, L. F.; Dunbar, T. D.; Allara, D. L.; Weiss, P. S. Directed self-assembly to create molecular terraces with molecularly sharp boundaries in organic monolayers. *J. Am. Chem. Soc.* 1999, 121, 8017-8021.

CHAPTER 5

Summary and Outlook

5.1 Expanding the Capability of Laser-Assisted Scanning Tunneling Microscope

Chapter 2 explains the design of our custom-built laser-assisted STM that combines sub-nanometer spatial resolution with laser excitation. The current, originating from amplitude-modulated light interacting with a tip-molecule-metal contact interface, is detected under ambient condition using phase-sensitive detection technique. We use rear illumination in a total internal reflection geometry to reduce the thermal effects at the tunneling junction,[1,2] which contaminates current intrinsic to the molecule with those generated from thermal voltage, heat-induced expansion and vibration. The detection of photo-induced tunneling current opens new venues for investigating photochemical and photophysical phenomena in systems such as organic molecules, noble metal nanoplates, semiconductor nanoparticles, and quantum dots *via* the nanoscale analytical measurements with the photon STM.[3-6] For example, the photocurrent originating from the excitation of different chemical species on the surface can be measured concurrently with absorption spectroscopy measurements with tunable lasers.[7] We can infer the contributions to the photocurrent and their dynamics from the relationship of the photoinduced current with amplitude-modulation of the incident light and external bias.[4] By studying the luminescence from excited molecular states, we can determine the electronic states involved in the photocarrier transfer and the relaxation processes.[8,9] A confluence of experimental analyses with the photon STM and theoretical modeling will lead to unprecedented knowledge of intrinsic optical and electronic characteristics of nanomaterials. This information will guide the rational design and engineering of photoactive materials at the interface of optimized optoelectronic devices.

5.2 The Dependence of Single Molecule Photocurrent on Local Environment

The photocurrent probed by the STM tip above single **MPEA** molecules is a proof of principle. It shows that a standing evanescent wave penetrating the sapphire excites the gold and the adsorbates on it. A theoretical description of light-induced increases in tunneling current over molecular junctions is ongoing. Laser radiation triggers Au interband transition and generates hot electrons, followed by nonradiative processes, such as formation of an anion radical state after injection of a substrate electron into **MPEA**.[10] Preliminary data indicate that the photocurrent amplitude of **MPEA** molecules located at step edges is higher than those at domain boundaries and fluctuates between images. These images were recorded continuously and each took 2-3 min. There are several hypotheses that need to be tested. One is that **MPEA** molecules undergo conductance switching through conformational changes.[11,12] The electronic coupling between the LUMO levels and the gold substrate is strongly affected by the molecular orientation, giving rise to variations of the photocurrent. A second explanation is that intramolecular repulsive Coulomb interaction increase the energy required to inject more electrons, especially in the case that the coupling between **MPEA** and a Pt/Ir tip is weak and electrons cannot be removed from the molecule instantaneously. The last possibility is related with the image potential surface states of the gold induced by the photocarrier that **MPEA** molecule bears. Theoretical modeling predicts that electrons in the image potential surface states move perpendicular to step edges and parallel to terraces.[13] Taking into account that evanescent wave propagates parallel to the surface, this may explain the discrepancy of photocurrent amplitude of **MPEA** at different locations.

5.3 Photoinduced Charge Transfer in Donor-Acceptor Triads

Chapter 3 presents our successfully incorporation of C_{60} triads and its chromophore derivative into the same 2D matrix, and hence we can use local optical spectroscopy as a measure for distinguishing between different chemical species on a surface with laser-assisted STM, information difficult or impossible to obtain solely by STM. The molecular states to which the photons are coupled are revealed using differential conductance spectra of charged triads under irradiation. Electronic chemical potentials of metals are voltage dependent. Thus, the bias shift would affect energy alignment and lead to photocurrent suppression under certain bias and coupling conditions.[14] Demonstrating the interplay of optical transition and bias is one of the goals of future research. Additionally, the light-to-current efficiency may be affected by the energy transfer from the molecule to gold substrate *via* the conjugated tether.[15] Comparing the performance of photoactive functional groups attached to the metal contact with tethers of different conductivity will elucidate how to optimize the organic material for photovoltaic application by design. The realization of photon coupling at the molecular level provides a versatile and less destructive way to study fields such as surface reaction dynamics, photocatalysis and organic optoelectronics.

5.4 Exchange Reactions between Thiolates and Selenols

In Chapter 4, we illustrate the structural differences in SAMs formed by single-component alkanethiolate and alkaneselenolate molecules on Au{111} and report the molecular and place-exchange reaction between gold-bound thiolates and selenols/selenolates in detail. Alkaneselenolates have multiple stable Au-Se binding configurations, and they adopt the barbell binding configuration of the gold adatom-sulfur complex while replacing the thiolates. Further insights regarding the nature of the gold-chalcogenate bond can be obtained by investigating molecular exchange between adamantaneselenolate (**ADSe**) SAMs and alkaneselenolates/alkanethiolates. With their rigid and symmetric 10-carbon cage, **ADSe** produces SAMs with weaker van der Waals interactions. These cage molecules assume low- and high-conductance modes when adsorbed to the gold surface.[16] After annealing the monolayer, the high-conductance molecules form dimers with long-range order, implying that the displacement reactions at these sites may be distinct from those occur at sites where their more labile low-conductance counterparts are located. Due to the different molecule-substrate and intermolecular interactions of the chemical species involved in the exchange reactions, there is an opportunity for new mechanisms and transient gold-adsorbate complexes to be discovered.

References

1. Grafstrom, S. Photoassisted scanning tunneling microscopy. *J. Appl. Phys.* 2002, 91, 1717-1753.

2. Smith, D. A.; Owens, R. W. Laser-assisted scanning tunnelling microscope detection of a molecular adsorbate. *Appl. Phys. Lett.* 2000, 76, 3825-3827.

3. Fujita, Y.; Horimoto, N. N.; Kajimoto, S.; Fukumura, H. Bias voltage-dependent STM-tip-enhanced Raman spectroscopy of benzenethiol-modified gold nanoplates. *Chem. Phys. Lett.* 2013, 582, 110-114.

4. Jacobsen, V.; Knoll, W.; Kreiter, M.; Durr, M.; Yasuda, A.; Nelles, G. Photoassisted spatially resolved STM measurements of dye-sensitized nanocrystalline TiO_2 films. *Phys. Rev. B* 2007, 75, 165325

5. Kano, S.; Tada, T.; Majima, Y. Nanoparticle characterization based on STM and STS. *Chem. Soc. Rev.* 2015.

6. Kroo, N.; Varro, S.; Racz, P. Hysteresis phenomena in electron tunnelling, induced by surface plasmons. *J. Mod. Optic.* 2013, 60, 79-85.

7. Carmichael, E. S.; Ballard, J. B.; Lyding, J. W.; Gruebele, M. Frequency-modulated, single-molecule absorption detected by scanning tunneling microscopy. *J. Phys. Chem. C* 2007, 111, 3314-3321.

8. Berndt, R.; Schlittler, R. R.; Gimzewski, J. K. Photon-emission scanning tunneling microscope. *J. Vac. Sci. Technol. B* 1991, 9, 573-577.

9. Wu, S. W.; Nazin, G. V.; Ho, W. Intramolecular photon emission from a single molecule in a scanning tunneling microscope. *Phys. Rev. B* 2008, 77, 205430

10. Gaffney, K. J.; Miller, A. D.; Liu, S. H.; Harris, C. B. Femtosecond dynamics of electrons photoinjected into organic semiconductors at aromatic-metal interfaces. *J. Phys. Chem. B* 2001, 105, 9031-9039.

11. Donhauser, Z. J.; Mantooth, B. A.; Kelly, K. F.; Bumm, L. A.; Monnell, J. D.; Stapleton, J. J.; Price, D. W.; Rawlett, A. M.; Allara, D. L.; Tour, J. M.; Weiss, P. S. Conductance switching in single molecules through conformational changes. *Science* 2001, 292, 2303-2307.

12. Kim, M.; Hohman, J. N.; Cao, Y.; Houk, K. N.; Ma, H.; Jen, A. K. Y.; Weiss, P. S. Creating favorable geometries for directing organic photoreactions in alkanethiolate monolayers. *Science* 2011, 331, 1312-1315.

13. Clark, B. K.; Standard, J. M.; Gregory, B. W.; Hall, A. D. Modeling image potential surface states on silver and gold surfaces covered with self-assembled monolayers of alkanethiols and alkaneselenols. *Surf. Sci.* 2002, 498, 285-292.

14. Sukharev, M.; Galperin, M. Transport and optical response of molecular junctions driven by surface plasmon polaritons. *Phys. Rev. B* 2010, 81.

15. Pathem, B. K.; Zheng, Y. B.; Payton, J. L.; Song, T. B.; Yu, B. C.; Tour, J. M.; Yang, Y.; Jensen, L.; Weiss, P. S. Effect of tether conductivity on the efficiency of photoisomerization of azobenzene-functionalized molecules on Au{111}. *J. Phys. Chem. Lett.* 2012, 3, 2388-2394.

16. Hohman, J. N.; Kim, M.; Schupbach, B.; Kind, M.; Thomas, J. C.; Terfort, A.; Weiss, P. S. Dynamic double lattice of 1-adamantaneselenolate self-assembled monolayers on Au{111}. *J. Am. Chem. Soc.* 2011, 133, 19422-19431.